Higher-order motion processing in the ferret and its development

by

Augusto Abel Lempel

A dissertation submitted to Johns Hopkins University

In conformity with the requirements for the Doctor of Philosophy

Baltimore, Maryland

May, 2019

Abstract

Studying the functional development of brain structures is essential for understanding the mechanisms behind neurodevelopmental and psychiatric disorders. In addition, this knowledge could shed light on the principles underlying how neuronal networks are wired and the information processes that they implement. The ferret has for many years been a successful animal model for studying the functional development of the visual system due to its immature state at birth. In addition, information processing in lower-order visual structures in ferrets parallels that in primates. These similarities motivated extensive research in the ferret that characterized the development of tuning properties across lower-order visual areas such as the lateral geniculate nucleus (LGN) and primary visual cortex (V1). As of yet, studies have not targeted higher-order cortex. This is due to the lack of a functionally characterized higher-order visual area in this animal model.

In Chapter 2 of this thesis, I describe complex tuning properties in area PSS, a higher-order visual area in the ferret, and compare them to motion representation in V1. In addition, I present a computational model that can explain the range of motion responses in PSS using similar mechanisms as those used to explain motion responses in primate higher-order area MT. I then discuss how these results establish PSS, and therefore the ferret, as a viable model to study higher-order motion processing.

In Chapter 3, I characterize the development of the complex motion responses described in PSS in Chapter 2. Then, I apply a modified version of the computational model developed in Chapter 2 to PSS responses across development. Based on the results from

implementing this model, I propose potential neuronal mechanisms behind the development of complex motion tuning in PSS. I also discuss the possible contribution of V1 changes to this process. Moreover, I measure changes in V1 responses to complex motion stimuli that are temporally correlated to the emergence of complex motion responses in PSS, and compare these changes with model predictions. Finally, by performing inactivation experiments in PSS, I test the potential contributions of feedback to changes in motion responses in V1.

The body of work presented in this thesis was done with the goal of establishing the ferret as a model for visual system development beyond V1. I hope the addition of higher-order areas in the study of visual system development will bring about a more complete and fundamental understanding of how such a complex system is formed. By studying the functional development of different brain structures that implement distinct information processing steps, we can learn general rules about the logic governing how these complex circuits are wired.

Thesis readers

Kristina J. Nielsen, Ph.D. (Advisor).

Charles E. Connor, Ph.D. (Secondary reader).

Acknowledgments

First and foremost, I want to thank my parents, Nora Medicina and Mario Lempel. Without their guidance and unconditional love and support, I couldn't have found the courage and strength to embark in this fulfilling adventure that has been my Ph.D. I know it has not been easy for them to adjust to the long distance that this venture of mine has put between us. And so I want to thank their partners in life, Cecilia Botey and Julio Marino for supporting them as well as me in those times when thing are not so easy. I want to thank my sister Anabel and my brother Ariel for all the special moments we have shared over the last years. I thank them both for the fun vacations we have shared, either by ourselves or with their families, as well as those hard moments that have always found us together in spirit if not in person. I also want to thank my nieces: Jazmin Kozuch, Isabella and Clara Gastaldi, and Paloma and Esmeralda Lempel. Seeing them grow has amazed me more than anything in science ever could. Sharing so many moments with them as they grew has been my most treasured privilege. In addition, I want to give a special thanks to my godfather Norverto "Nujem" Schnayman, who from a very young age encouraged my scientific curiosity and sense of wonder.

I want to thank all those older friends that have remained close to me despite not only the physical distance but also the other kind of distance that becomes longer as we grow and our time is taken over by things other than friendship. I want to thank my oldest friend, Alan Dinovitzer, who always supported me since we were little kids; My cousin, and also one of my most supportive friends, Julieta Martori; My high-school friends with whom I

have shared precious moments both back home and from a distance and on whom I can always rely for anything: Valeria Abelof, Daniela Lin, Ilean Saragovi, Guido Duer, Dan Szczapowy and Facundo Castro; My college friends with whom I first embarked on this journey called science and with whom I still share that journey today: Ariel Nagel, Paula Lopez, Julia Busso, Nicolas Molina, Nicolas Lois, Martin Brioso and Ayelen Nally; And also those friends that I made out of sharing nothing more than some of the best moments of my college life: Andres Enriquez, Guido Caceres, Tomas Olmos, Federico Avaca, Agustin Soula and Matias Camino.

Despite the support of my family and older friends, this adventure would have been a joyless one without the new friends I have made along the way: Aneesh Donde, Gabrielle Sell, Richard Sima, Chanel Matney, Vijay Mohan and the late Nathan Johnson. This is especially the case for those new friends with whom I also shared my work-life: Ramanujan Srinath, Erika Dunn-Weiss, Alexandriya Emonds, Joshua Ross, Andrew Daniels, and Andrew Cheng. In addition to their friendship and support, they have offered their help at every turn to aid me and my research. Through countless hours of intellectual discussion they provided vital insight that has shaped my research and has made me grow as a professional. Special thanks go to Alexandriya Emonds for her most needed help in the writing of this dissertation. I also want to thank the undergrad students that have worked by my side: Jody Law, Amey Siddharth Kavuturu, and Marlynn Lopez. Mentoring them has been an honor and a unique learning experience. I am grateful to Ofelia Garalde, Justin Killebrew, William Nash and William Quinlan for all their help. Without them, none of the work presented here would be possible. I also thank Rita Ragan, Beth Wood Roig,

Susan Soohoo, Eric Potter and Charlie Meyers for all their support during my graduate school.

I want to thank my undergraduate mentors, Osvaldo Utchitel and Joaquin Piriz. If not for them, I would not have had the chance of joining this program nor the intellectual tools I needed to do this work. I am also thankful to the many professors that, over the course of my Ph.D., have provided me with indispensable mentorship. I am especially thankful to the late Steve Hsiao who served as my advisor during my first year and welcomed me so warmly to the program. I am grateful to my thesis committee members James Knierim, Charles E. Connor, and Solange Brown for their teachings and support. Special thanks go to James Knierim and Geeta Rao who provided me with essential training to make the tetrodes that provided much of the data presented here.

Of all the professors that have contributed to my professional training, I am most grateful to my mentor and thesis advisor Kristina Nielsen. Working by her side, I have grown and achieved more than I could have ever expected. She has taught me invaluable lessons on how to make good science that I can be proud of. It would be impossible to convey with words the extent to which her mentorship has enriched me as scientist. And yet, her professional contributions during my Ph.D. are dwarfed by the tremendous amount of support she has provided me over the past years. While overall enjoyable and always enriching, this journey has not been without tough moments, some of which have tested my resolve to an extent I wasn't sure it would prevail. This adventure has also been one of self-discovery, and I do not think it would have taken me where it did if she had not been supportive when I needed it the most.

Last, but certainly not least, I want to thank someone who has been alongside me most of the time during this journey. If it were up to him, I am sure he would have been by my side quite literally all the time. I want to thank my dog, Wilfred, for a kind of unconditional love and support than can only be given by his kind.

Table of contents

List of tables

List of figures

Chapter 1: General introduction

My thesis work focuses on the development of higher-order motion processing. To this end, I first characterize complex motion processing in area PSS, a higher-order motion area in the ferret. Then, I make use of PSS as a model to study how complex motion processing develops in the visual system. In this chapter, I review our current knowledge of visual motion processing across species, with a focus on the analysis of motion signals. Then, I discuss computational models that propose mechanisms for the transformation of motion signals by the visual system. In addition, I review our current knowledge on the development of visual processing across species, with a focus on motion processing. Finally, I lay out my motivation for the work presented in this thesis in the context of the reviewed literature and briefly describe the contents of the following chapters.

1.1 - Visual motion processing across species.

Vision is central to our interaction with the world and therefore has been extensively studied. The ease with which complex stimuli are delivered using visual displays has made it possible to gain detailed insight into information processing in different visual areas. A vast body of knowledge has been accumulated over the years on the mechanisms behind visual processing; this section will focus on key aspects of motion processing that are most relevant for this thesis.

The analysis of motion signals is crucial for a number of cognitive and behavioral tasks such as recognition of moving stimuli, self-motion perception, smooth pursuit eye movements, and gaze stabilization. In accordance with such a prominent role in driving behavior, motion processing is a key feature of visual systems across diverse species, from flies (Silies et al., 2014) to monkeys (Born and Bradley, 2005; Orban, 2008). The representation of motion signals has been analyzed in many species, but is best understood in the primate. In this section I will review some of the most relevant studies that describe motion processing in primates across different hierarchical levels of the visual system. I will then review the existing literature on motion processing in mice, currently the most commonly used animal model in neuroscience, and in carnivores, which are the most relevant for the work presented in this thesis.

1.1.1 - Motion processing in primates.

In primates, the analysis of motion signals starts in V1, where neurons respond to the motion of local edges. These signals are then sent via feed-forward connections to a group of specialized higher-order areas, such as MT and MST, referred to as the dorsal pathway.

Neurons in these areas integrate these simple signals to represent more complex motion patterns. In the following paragraphs I will review and discuss some of the most relevant literature that describes motion processing across V1 and higher-order area MT. The former is most relevant to this thesis, which focuses on processing stages analogous to those implemented by this motion area.

The first step in primate cortical motion processing is believed to be the computation of direction selectivity in V1. This area receives feed-forward input from the LGN, where almost all neurons show no direction tuning (De Valois et al., 1982; Xu et al., 2002). In contrast, most V1 neurons show a direction preference, and some respond exclusively to one motion direction (Hubel and Wiesel, 1968; Orban et al., 1986). The neuronal mechanisms behind this response transformation have been the object of many studies (De Valois et al., 1982, 2000; Livingstone, 1998; Peterson et al., 2004; Saul et al., 2005). This work led to the theory that direction tuning is computed de-novo in V1 by integrating over non-selective LGN inputs with specific spatial and temporal shifts (see section 1.2.1).

Due to their small receptive fields, V1 neurons can only represent motion information from local edges. This leads to a limitation commonly referred to as the "aperture problem". Complex objects are made of many contours that are spatially segregated. Each of these contours, when observed locally and out of context, can only be seen as moving in one of the two directions perpendicular to its orientation (Fennema and Thompson, 1979). Therefore, acquiring tuning for the global motion of a complex stimulus requires the integration of motion signals across different contours at different locations, which is not implemented in V1.

Area MT, located in the posterior bank of the medial temporal sulcus (Figure 1.1), is thought to represent the next stage of motion processing after V1. This area receives feed-forward input directly from V1 and specifically from those neurons that show strong direction selectivity (Movshon and Newsome, 1996). Most cells in MT are highly direction selective (Dubner and Zeki, 1971), possibly a direct consequence of the aforementioned selective input (Movshon and Newsome, 1996).

In addition to the increased occurrence of direction-selective responses, probing MT neurons with more complex stimuli revealed a higher level of integration of motion signals when compared to V1. One manifestation of MT's increased degree of integration is the inhibition of neuronal responses when two opposing motion signals are superimposed, for example using two random dot kinematograms (RDKs, Snowden et al., 1991. Figure 1.2). This integration could play a role in resolving signal-to-noise problems when computing motion and may contribute to the static perception of flash stimuli and the perceptual transparency of moving surfaces (Andersen, 1997; Qian and Andersen, 1994; Snowden et al., 1991). Note that while suppression is prevalent in MT, it is also present - albeit to a much lesser degree - in V1 (Qian and Andersen, 1994; Snowden et al., 1991). Interestingly, suppression is correlated with direction selectivity in both areas. When suppression is considered as a function of direction selectivity, neurons in both V1 and MT fall along the same continuum. Considering the selective V1 input that MT receives (Movshon and Newsome, 1996), it is therefore unclear whether motion opponency is computed de-novo in the MT circuitry, or is inherited from the biased V1 input. In either way, these results indicate stronger interactions between multiple motion signals in MT than in V1.

A more complex manifestation of motion integration in MT is the analysis of pattern motion, which solves the aperture problem described in the previous section. This kind of integration is commonly studied using plaid stimuli. Plaids are constructed by combining two sinusoidal gratings moving in different, but not completely opposing, directions (Figure 1.3A). These stimuli appear to move in a direction intermediate between the directions of the two gratings (Adelson and Movshon, 1982; Movshon et al., 1985). Therefore, one can define two types of motion directions in plaids: the component motion directions of the two gratings and the resulting pattern motion direction. A neuron that only analyses local motion signals, such as those in V1, cannot solve the aperture problem and will only respond to the component motion. We refer to these neurons as component cells. A component cell will respond to a plaid stimulus whenever one of the two components move in its preferred direction. As a result, these neurons show preference for two plaid stimuli that have different pattern motion directions (Figure 1.3B). In contrast, if a neuron integrates over local signals, it can solve the aperture problem and respond according to the pattern motion of the plaid. This cell will respond strongly only when the plaid moves in its preferred direction. We refer to such neurons as pattern cells (Figure 1.3B).

In a seminal study, Movshon and collaborators measured responses to plaid stimuli in primate V1 and MT to investigate differences in motion integration across these areas (Movshon et al., 1985). In V1, they observed that all neurons behave like component cells, suggesting that the V1 circuitry is unable to integrate local motion signals to represent pattern motion. In contrast, a significant proportion of MT neurons (~25%; Movshon et al., 1985) behaved like pattern cells. This result has led the field to believe that one important aspect of the information processing implemented in MT is the integration of local motion

signals provided by V1 input into global motion signals. Since the first descriptions of these responses by Movshon and collaborators in the 1980s, the neuronal mechanisms behind pattern motion tuning in MT have been the object of several studies (Jazayeri et al., 2012; Majaj et al., 2007; Pack and Born, 2010, 2001; Rodman and Albright, 1989; Rust et al., 2006; Smith et al., 2005; Wang and Movshon, 2016). In addition, different computational models have been developed to explain how pattern responses are generated (see Section 1.2.2).

As explained above, one alternative strategy to solve the aperture problem is to observe the motion of certain local cues such as corners or contour endpoints. These cues are commonly referred to as "terminators" (Shimojo et al., 1989). Terminators provide veridical motion cues even on the small scale of V1 receptive fields. Terminator motion information could be provided by end-stopped, also called hypercomplex, cells in V1, which only respond when the endpoint of an edge is inside their receptive field (Jones et al., 2001; Pack et al., 2003; Sceniak et al., 2001). These cells provide the information required to compute pattern motion tuning without the need to integrate different motion directions (Pack and Born, 2010; Pack et al., 2003; Tsui et al., 2010; Zarei Eskikand et al., 2016). Therefore, hypercomplex V1 neurons could provide MT pattern cells with a signal that emphasizes pattern motion provided by the terminators.

1.1.2 - Motion processing in mice.

Mice are currently the most common animal model in neuroscience and have been used to study the visual system's physiology and development, with most studies focusing on retinal and thalamic circuits. In general, research has revealed that the distribution of

motion related tuning properties in the mouse visual system differs strongly from that of primates. Direction selectivity is found in a significant proportion of retinal ganglion cells (Sun et al., 2006) and LGN relay cells (Marshel et al., 2012; Piscopo et al., 2013; Zhao et al., 2013). Direction selectivity is also found strongly in mouse V1, but is organized very differently from that in carnivores and primates. While there is growing evidence for some organization of tuning properties in mouse V1 at least on small (<100μm) scales (Bonin et al., 2011; Ringach et al., 2016), no significant organization is detected when scales similar to those of functional maps in carnivores and primates are considered (Bonin et al., 2011).

Measuring pattern motion responses in mouse V1 using plaid stimuli revealed that most cells do not behave as component cells, as they would in primates. Instead, most cells fall in the intermediate unclassified category, meaning they do not faithfully represent either component or pattern motion (Juavinett and Callaway, 2015; Muir et al., 2015; Palagina et al., 2017). In addition, expanding these experiments into higher-order cortex did not reveal any particular area with a proportion of pattern cells similar to that of primate MT (Juavinett and Callaway, 2015).

1.1.3 - Motion processing in carnivores.

Many studies of the visual system, and in particular those focusing on functional development, have used cats and ferrets, both carnivore species, as model organisms. Motion processing in early stages of the visual system of these species is comparable to that of primates. While a small proportion of direction-selective retinal ganglion cells may be present in these species, neuronal responses in both the retina and LGN are largely insensitive to motion direction (Cleland and Levick, 1974; Thompson et al., 1994a, 1994b).

Instead, direction selectivity is believed to emerge de-novo in V1 (Priebe et al., 2010). In carnivore V1, direction selectivity is organized in an orderly map, that is coordinated with the orientation map by subdividing each orientation column into columns for the directions perpendicular to the column's preferred orientation (Bonhoeffer and Grinvald, 1991; Grinvald et al., 1986; Ohki et al., 2006; Weliky et al., 1996). In primate V1, orientation maps are well established (Blasdel and Salama, 1986; Hubel and Wiesel, 1968; Ts'o et al., 1990). Yet, it is unclear whether direction maps exist in primate V1.

The visual system of cats and ferrets includes a number of higher-order areas that receive input from V1 (Homman-Ludiye et al., 2010; Manger et al., 2004; Scannell et al., 1995; Sherk, 1986). Even though the physiology and tuning properties of these areas have not been investigated in as much detail as in primates, areas dedicated to motion processing have been identified. In the cat, one such area is PMLS (posteromedial lateral suprasylvian area), named after its anatomical position in the cat cerebral cortex (Figure 1.1). The discovery of PMLS, previously referred to as the Clare-Bishop area, predates that of MT. It has since been the target of several studies (Blakemore and Zumbroich, 1987; Gizzi et al., 1990; Hubel and Wiesel, 1969; Kiefer et al., 1989; Li et al., 2000, 2001; Lomber et al., 1994; Rauschecker et al., 1987; Wright, 1969). Consistent with a role as a specialized higher-order motion area, neurons in PMLS have larger receptive fields, show a stronger preference for moving over static stimuli, and are more direction selective than V1 neurons (Blakemore and Zumbroich, 1987; Hubel and Wiesel, 1969; Spear and Baumann, 1975; Wright, 1969). The behavioral significance of motion processing by PMLS was investigated using both lesion studies and reversible inactivation (Kiefer et al., 1989;

Lomber et al., 1994). Both studies confirmed that this higher-order area is required for cats to perform tasks that require processing of moving but not static stimuli.

Neurons in PMLS show signatures of motion integration such as a preference for optic flow patterns (Blakemore and Zumbroich, 1987; Li et al., 2000; Rauschecker et al., 1987; Spear and Baumann, 1975). Yet, whether cells in PMLS perform pattern motion integration like neurons in MT has been a matter of debate. While responses to plaid stimuli did not reveal a significant proportion of pattern cells (Gizzi et al., 1990; Movshon et al., 1985), testing pattern motion tuning with texture-like stimuli suggests that most cells in this area do respond according to some forms of pattern motion (Li et al., 2001). Whether tuning for the motion of these texture-like patterns emerges in PMLS or is already present in V1 has not been tested.

In ferrets, the animal model for this thesis, there have only been a few studies investigating tuning properties in higher-order cortex. One of these studies identified a potential higher-order area specialized for motion processing. This candidate area was found in the posterior bank of the suprasylvian sulcus (similar location to PMLS, Figure 1.1) and exhibited strong direction selectivity (Philipp et al., 2006). In the initial study by Philipp and collaborators, the area is referred to as PSS (posterior suprasylvian sulcus; Philipp et al., 2006), but anatomical studies have also defined it as PMLS (Dell et al. 2019; Homman-Ludiye et al., 2010). Throughout this thesis this area will be referred to as PSS. Later studies showed that PSS receives direct input from V1 that is functionally biased to favor motion processing. V1 neurons projecting to PSS are more direction selective, more end-stopped, and prefer lower spatial frequencies and higher temporal frequencies than those projecting to other

areas (Jarosiewicz et al., 2012). In addition, behavioral studies have demonstrated that PSS is required for a motion detection task (Hupfeld et al., 2007). These results would suggest that PSS is a higher-order motion area with a functional role analogous to that of MT in primates. However, tests with more complex stimuli that investigate motion integration are required to corroborate this hypothesis.

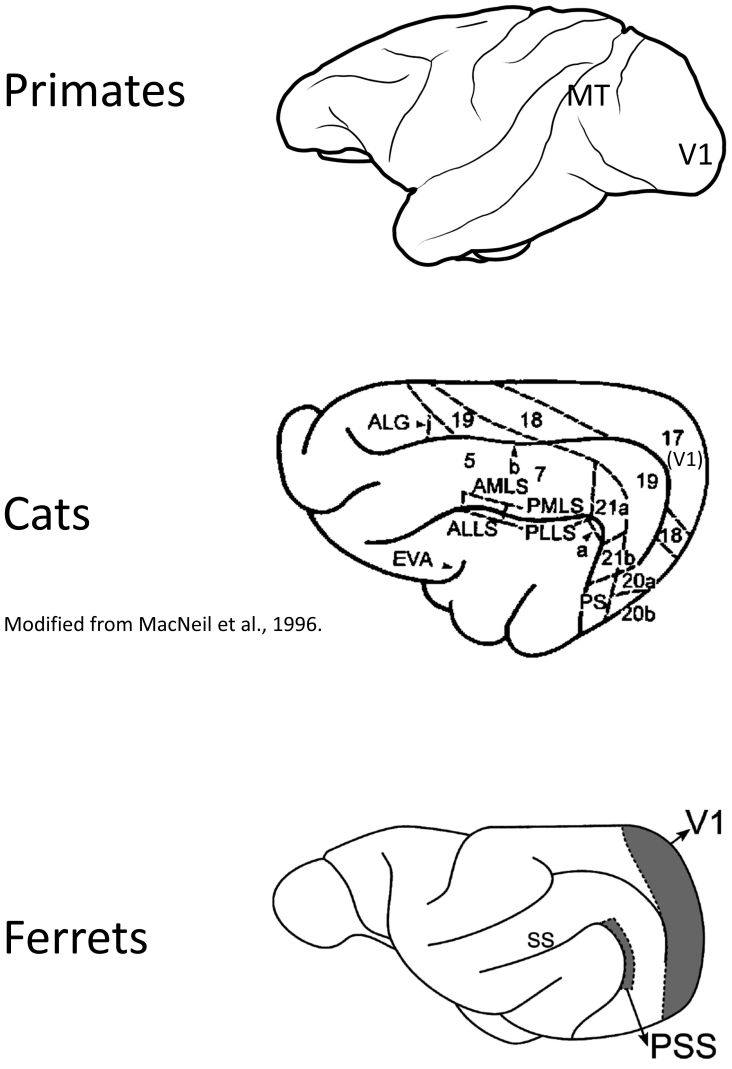

Figure 1.1: Anatomical location of higher-order motion areas.
Schematic representation of anatomical location of V1 and higher-order motion areas MT in primates (top), PMLS in cats (center, modified from MacNeil et al., 1996) and PSS in ferrets (bottom).

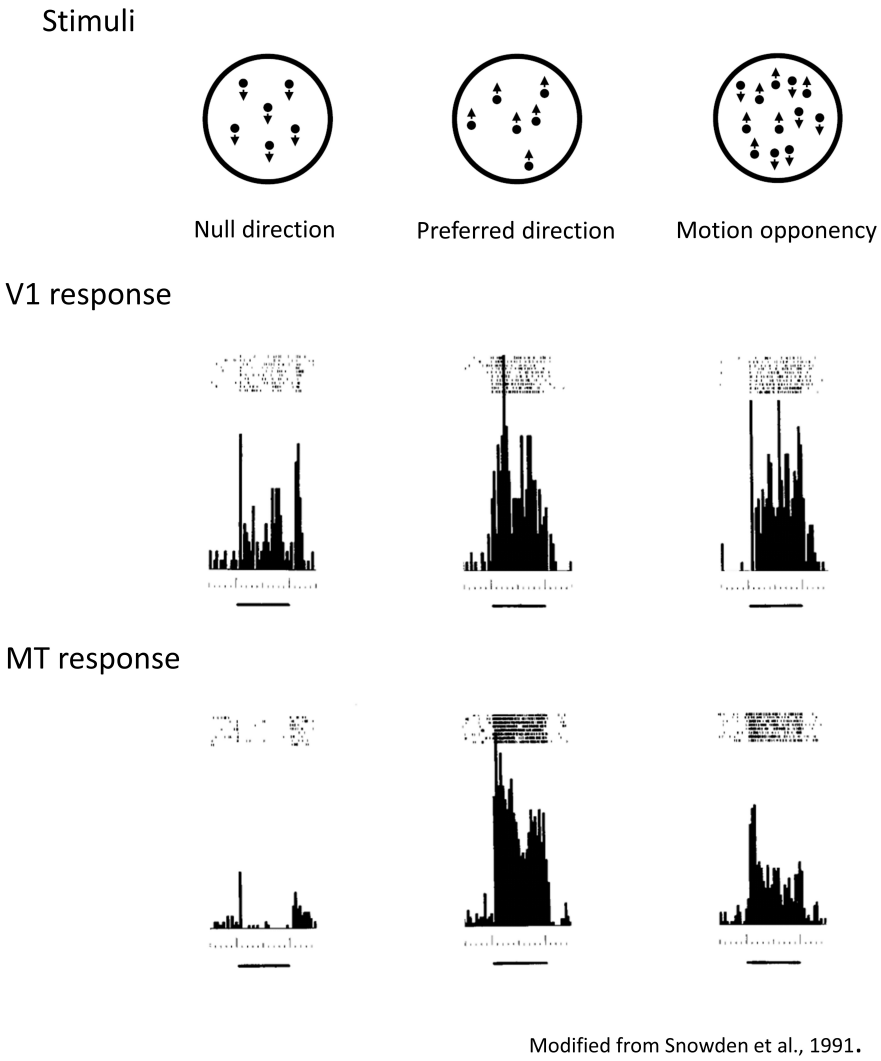

Figure 1.2: Motion opponency in MT.
Schematic representation of stimuli used to study motion opponency (top) and corresponding responses, shown as raster plots and peristimulus time histograms, of a representative V1 (center) and MT neuron (bottom). Dark bar corresponds to the stimulus presentation (1 second). Modified from (Snowden et al., 1991).

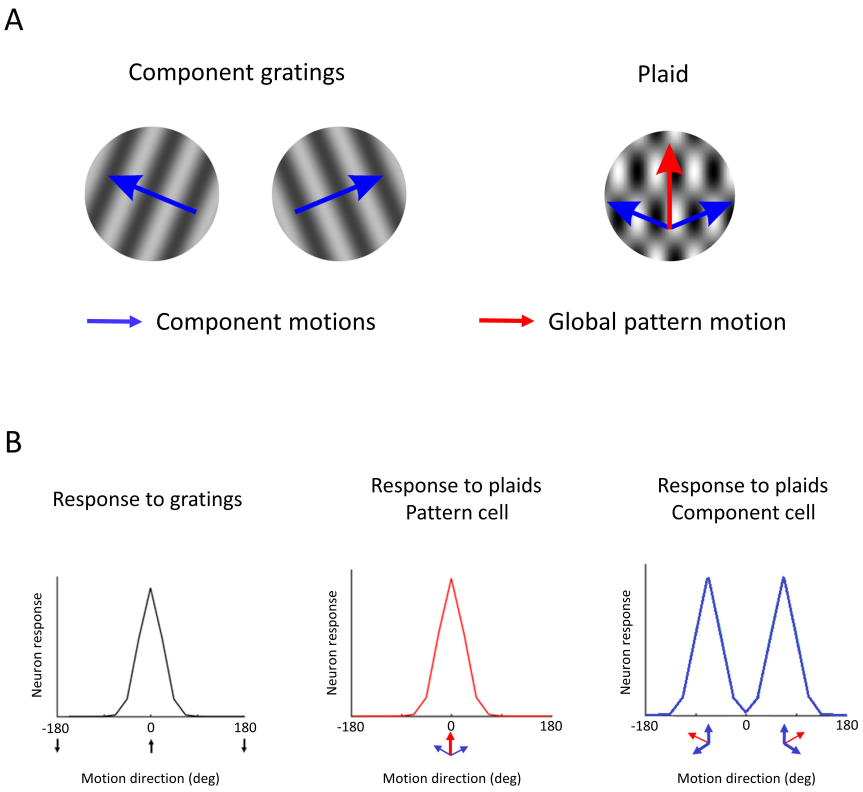

Figure 1.3: Study of pattern and component responses using plaid stimuli.
(A) Left: Pair of 50% contrast grating stimuli moving in two different directions. Right: Plaid resulting from the combination of the two gratings. Blue arrows represent component motion directions. Red arrow represents the perceived pattern motion direction of the plaid.
(B) Responses of a direction-selective cell to grating stimuli (left) and expected plaid responses if the neuron is a pattern cell (center) or a component cell (right). Direction is relative to the cell's preferred grating direction, and indicates the perceived direction of the grating or plaid (i.e., the pattern direction).

1.2 - Computational models of motion processing.

The processing of motion information by the visual system can be conceptualized using relatively simple computational models. These models are useful for making predictions about the interdependence of different neuronal signals, and for proposing potential mechanisms for how different response properties are computed. What is the nature of the input-output transformation that takes place in the circuits in higher-order cortex? What kind of information does higher-order visual cortex require from its input to produce complex motion signals? By combining experimental results with computational models, previous studies have established different hypotheses for these crucial questions.

In this section, I will review the most prominent models that have been used to explain the computation of motion signals both in V1 and higher-order motion area MT in the primate. I also discuss the experimental results that have validated or refuted the underlying neuronal mechanisms suggested by these models.

1.2.1 - Models of simple motion processing in lower-order visual areas.

Direction selectivity, a basic motion signal present in V1, was first modeled by Reichardt while attempting to describe the optomotor response to moving stimuli (Hassenstein and Reichardt, 1956). In essence, Reichardt's model achieves motion detection by combining the responses from two receptors separated in space and delayed temporally relative to each other. In order to generate direction-selective rather than simply motion-selective responses, a non-linearity (such as multiplication) must also be applied to the two receptor signals. Mechanisms similar to those proposed by Reichardt's model have been observed in both the fly optic lobe (Borst et al., 2010) and in the rodent retina (Borst and Euler, 2011;

Chiao and Masland, 2002). This model has been further elaborated and used to successfully model aspects of human motion perception (van Santen and Sperling, 1985). As discussed below, its principles form the basis for models of motion processing in the primate visual system. The apparent validity of Reichardt's model in such diverse organisms suggests that it represents a convergent strategy to solve the computation of motion direction.

One implementation of the Reichardt model was proposed by Adelson and Bergen to explain direction selectivity of V1 neurons (Adelson and Bergen, 1985, Figure 1.4). In this implementation, neuronal responses are computed using spatiotemporally oriented filters (Figure 1.4A) that can be modeled as Gabor functions given by the equations:

$$f(x,y,t) = cos\left(\frac{x' + \tau t}{\phi}\right) e^{-\left(\frac{x\prime^2 + \gamma y\prime^2 + \delta t}{\sigma}\right)}$$

$$x' = x\cos(\theta) + y\,sin(\theta)$$

$$y' = y\cos(\theta) - x\,sin(\theta)$$

where Θ is the spatial orientation of the filter, ϕ sets the spatial frequency, τ sets the temporal frequency (and therefore orientation in time), and σ, γ and δ describe the size and geometry of the filter in space and time.

In these filters, the phase of the spatial profile is displaced over time to create an orientation when the filter is seen in the space-time plane (De Valois et al., 2000. Figure 1.4A). This mechanism has been shown to be implemented by a subset of V1 neurons which display spatiotemporally oriented receptive fields (De Valois et al., 2000). This kind of receptive field can be made by combining a set of spatial filters at different phases, delayed relative

to each other by different time intervals. This could be implemented in direction-selective neurons by integrating the input from non-directional neurons with spatial receptive fields that have similar orientation but different phase tuning and adding a temporal delay between them. Alternatively, spatiotemporally oriented receptive fields can be created by integrating over two non-directional inputs with different temporal profiles (De Valois et al., 2000).

This implementation of the Reichardt model can successfully explain V1 direction selectivity. Yet, the responses it generates are dependent on the stimulus phase relative to the filters (Figure 1.4B). This phase dependence is characteristic of responses from simple cells in V1, but is absent in complex cells (Hubel and Wiesel, 1962). To provide a phase-independent direction-selective signal like that of complex V1 neurons, Adelson and Bergen expanded the Reichardt model by introducing a motion energy mechanism (Adelson and Bergen, 1985. Figure 1.4C). This mechanism combines the responses of two direction-selective simple cells with receptive fields in quadrature (phase difference of 90 degrees) using the following formula:

$$C(r) = S_1(r)^2 + S_2(r)^2$$

were C(r) is the resulting response of a complex direction-selective cell to a certain stimulus, and $S_1(r)$ and $S_2(r)$ are the responses of the two direction-selective cells with receptive fields in quadrature to that stimulus (Figure 1.4C). The phase independent direction-selective signals that result from the Adelson and Bergen model (Figure 1.4D) have been used to model direction-selective V1 input in a number of models of higher-

level motion processing (Baker and Bair, 2016; Rust et al., 2006; Simoncelli and Heeger, 1998. Figure 1.5).

1.2.2 - Models of complex motion processing in higher-order visual areas.

As described in the previous sections, the complex motion signal computed in higher-order visual cortex that has been most studied is the representation of pattern motion in MT. Several authors have developed computational models for describing possible mechanisms behind the transformation from V1 direction-selective component cells to MT pattern cells. One group of models use an 'integrationist' strategy (Zarei Eskikand et al., 2016), in which a pattern cell combines many local motion responses to compute pattern motion (Baker and Bair, 2016; Rust et al., 2006; Simoncelli and Heeger, 1998). An alternative class of models uses a "selectionist" strategy, which involves the selection of motion signals generated by object features such as corners, which can be provided by hypercomplex V1 cells (Zarei Eskikand et al., 2016). Lastly, a third group of models implements a combination of integration and selection to explain MT motion responses (Beck and Neumann, 2011). A detailed description of "selectionist" models is beyond the scope of this introduction. Instead, the next paragraphs will focus on describing one particular integration model developed by Rust et al. (Rust et al., 2006), since the computational models implemented in this thesis are based on it.

In short, the Rust model is a feed-forward cascade model in which the responses of a population of direction-selective V1 neurons are combined in a linear fashion by a downstream MT cell. After this linear combination, the MT responses are passed through a spiking threshold non-linearity, resulting in the final MT responses (Figure 1.5A). By

controlling normalization mechanisms in the V1 population, the weight function used for integration by the MT cell, and the non-linearity that follows, this model can explain the observed range of component, unclassified, and pattern cells in MT. In the following paragraphs, I will describe in greater detail each stage of this model and the different parameters that can be tuned to explain different response profiles.

The first stage of the Rust model consists of a group of complex direction-selective cells, each tuned for a different motion direction, whose responses are analogous to those resulting from the motion energy model described above. The responses of these cells are then normalized by both the population response (sum of all V1 cell responses, hereafter referred to as untuned normalization) and by the response of the neuron itself (hereafter referred to as tuned normalization). This latter normalization is equivalent to a response saturation or compressive non-linearity (Rust et al., 2006).

The untuned normalization is implemented by the formula:

$$\hat{R}_N(r) = \frac{R_N(r)}{\sum_K R_K(r) + \sigma_1}$$

were $\hat{R}_N(r)$ is the normalized V1 response of a neuron N to a stimulus, $R_N(r)$ is the V1 response of the same neuron to the stimulus before normalization, and σ_1 is a model variable that controls the strength of the untuned normalization.

Similarly, the tuned normalization is implemented by the formula:

$$\hat{\hat{R}}_N(r) = \frac{\hat{R}_N(r)}{\hat{R}_N(r) + \sigma_2}$$

where $R^{\wedge\wedge}_N(r)$ is the final response of the neuron after both normalizations, and σ_2 is a model variable that controls the strength of the tuned normalization.

In the second stage of this model, a linear weighted sum of all V1 responses is computed:

$$M(r) = \sum_N R^{\wedge\wedge}_N(r) * W_N$$

where M(r) is the resulting response of the MT cell to the stimulus, and W_N is the weight assigned to the V1 neuron N. Each weight in the linear sum is a variable of the model and can be tuned to best explain the responses of a given MT cell.

Finally, the spiking threshold non-linearity applied to the resulting MT responses is implemented using the formula:

$$M^{\wedge}(r) = Ae^{B*M(r)}$$

were $M^{\wedge}(r)$ is the MT response after threshold and A and B are parameters that can be fit to best explain MT responses.

Rust et al. applied this model to fit a variety of recorded MT responses. They then analyzed how the model parameters differed between pattern and component cells. They found that to explain pattern cells, the V1 population needed little untuned normalization and strong tuned normalization. This increased their responsiveness to plaid stimuli, which was required to explain experimentally observed levels of plaid responses in pattern cells. The responses of V1 neurons were then integrated by the MT pattern cell using a weight function with a large number of strong excitatory weights. Therefore, the MT cell integrated over responses from V1 cells with a wide range of direction preferences around

the MT neuron's preferred direction. This integration resulted in strong responses to plaids moving in the preferred direction, even when the component motions are far from this direction (Figure 1.5B). Moreover, pattern cells required a large number of strong inhibitory weights for directions around the null (or opposing) direction. This inhibition prevented the cell from responding to plaid stimuli moving in a direction far from the preferred, as these stimuli will contain a component motion that is closer to the null direction. It also served to suppress component responses (Figure 1.5B). In contrast, to explain component cells in MT, the model integrated over fewer V1 cells by using a weight function with a small number of strong excitatory weights. This led to a lack of responsiveness to plaids with pattern motion matching the preferred direction when the component responses are far from this direction (Figure 1.5C). In addition, component cells in the model were not inhibited by directions around the null direction, allowing for responses to plaid stimuli for which one component moves in the preferred direction, even if the second component moves in a direction close to the null direction (Figure 1.5C).

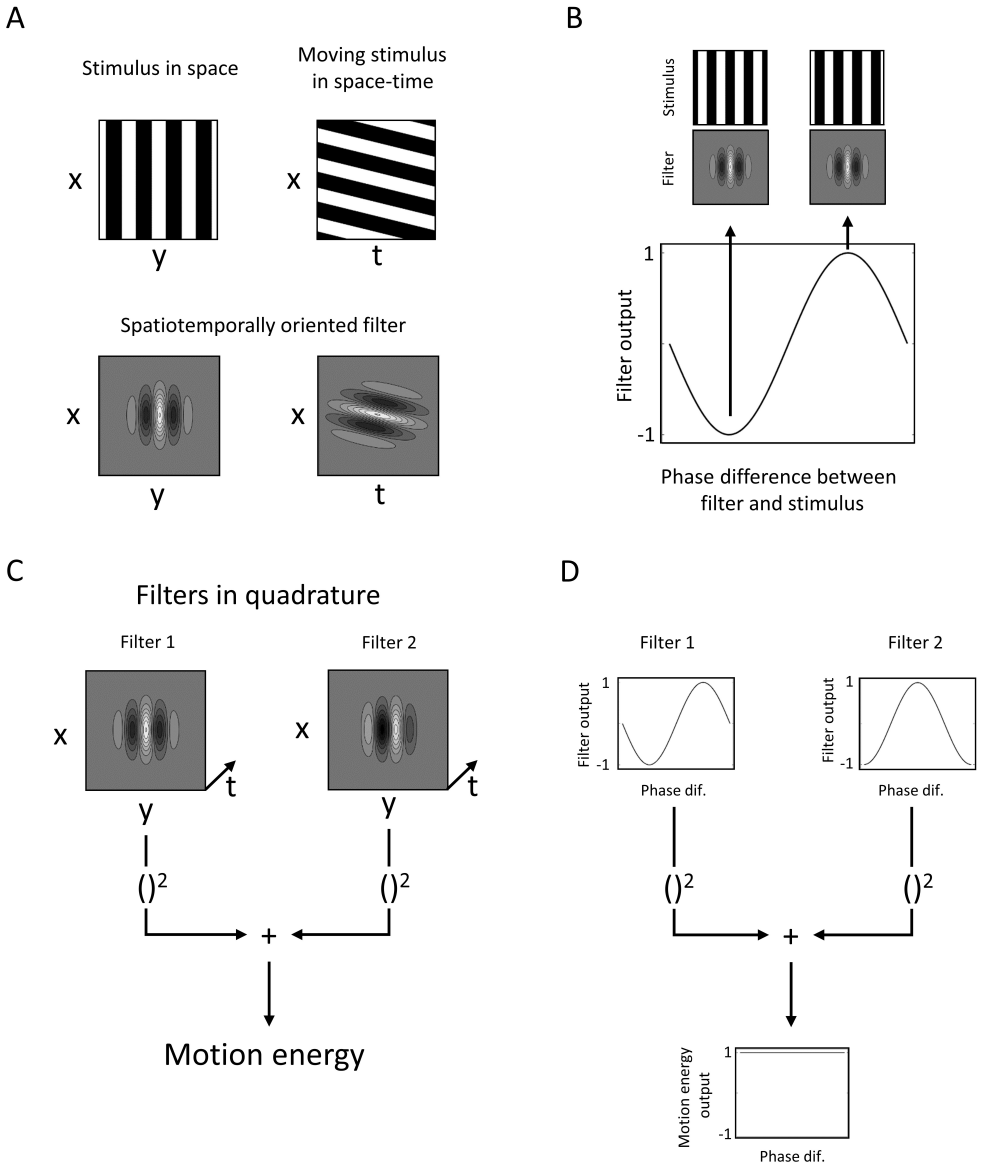

Figure 1.4: Adelson and Bergen motion energy model explains direction-selective responses of complex V1 cells.

(A) Schematic representation of a drifting square-wave grating (top) and a spatiotemporally oriented Gabor filter (bottom) as seen in the 2D spatial plane (left) and the space-time plane (right).

(B) Output of a Gabor filter as shown in (A) to square-wave gratings as a function of the phase difference between stimulus and filer. Filter output is maximized when stimulus and filter phases are aligned (right) and minimized for the opposite case (left). This output profile corresponds to the response of V1 simple cells.

(C) Schematic representation of the motion energy mechanism, which involves squaring the output of two spatiotemporally oriented filters (see A), and adding them. The two filters must be in quadrature relative to each other. This implies a phase difference of 90 deg between the filters.

(D) Filter output as a function of the phase difference between stimulus and filter for two filters in quadrature, like those shown in (C), and the resulting output of the motion energy mechanism.

A

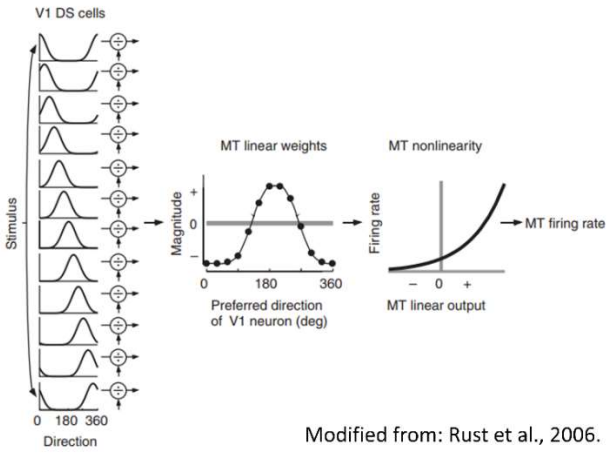

Modified from: Rust et al., 2006.

B

Pattern cell

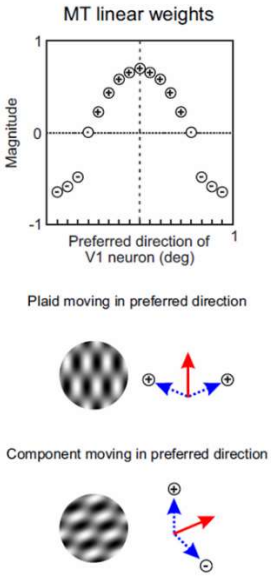

C

Component cell

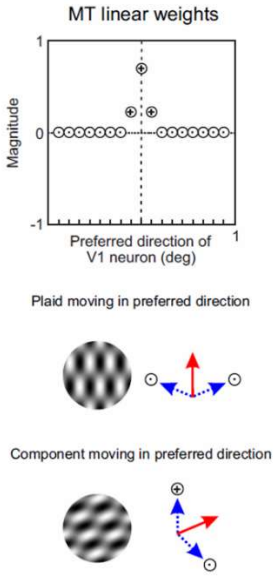

Figure 1.5: Feed-forward model proposed by Rust et al. for explaining pattern and component cell responses in MT.
(A) Diagram of the Rust model used to explain MT component and pattern responses (Rust et al., 2006). Stimuli first pass through direction selective filters in V1, followed by a normalization stage implementing tuned and un-tuned mechanisms. V1 responses are then integrated in MT using excitatory (positive) and an inhibitory (negative) linear weights. Finally, a threshold non-linearity is applied to yield final MT responses.
(B) Typical values of linear weights for the MT integration function of a pattern cell (top), as well as their effect on responses to plaids with pattern motion in the preferred direction (center) or component motion in the preferred direction (bottom). Pattern cells have an integration function with a broad excitatory peak centered on the preferred direction (vertical dashed line), and a broad inhibitory region surrounding the null direction. For a plaid moving in the preferred direction (center), the V1 responses to both plaid components fall into the excitatory integration region for a pattern cell, resulting in a strong response. To the contrary, for a plaid with one component moving in the preferred direction (bottom), only this component motion will fall into the excitatory region. The motion of the other component in the plaid moves closer to the null direction, and causes inhibition, thereby resulting in a reduced response.
(C) Typical values of linear weights for the MT integration function of a component cell (top), as well as their effect on responses to plaids with pattern motion in the preferred direction (center) or component motion in the preferred direction (bottom). Component cells have an integration function composed of a narrow range of excitatory weight surrounding its preferred direction (vertical dashed line), and weak or absent inhibitory weights surrounding the null direction. For a plaid moving in the preferred direction (center), the V1 responses to the components are far from the preferred direction, outside the excitatory region of the neuron. The component neuron therefore does not respond to this stimulus. If one of the components moves in the preferred direction (bottom), this component will fall into the excitatory region and drive a response. The motion of the other component in the plaid is closer to the null direction, and therefore does not contribute to the response, but also does not cause inhibition. This results in a positive response to the stimulus.

1.3 - Development of the motion pathway.

The great body of knowledge collected on the physiology of the visual system, along with the computational models that have been used to conceptualize the underlying mechanisms, make vision a great model system for investigating how neuronal circuits develop in both health and disease. For the visual system to function properly, our brains need to perform a series of complex computations on the information first gathered by the photoreceptors in the retina. Implementing these processes requires the many neuronal circuits in the visual system (retinal, thalamic and cortical) to be wired in a very specific way. This connectivity arises during development by means of genetic determination as well as intrinsic and stimulus-driven patterns of neuronal activity. In the following paragraphs, I will review some of our current knowledge of these developmental processes in both carnivores and primates, with a focus on the cortical visual circuits for motion processing. In addition, I will briefly discuss psychophysical and physiological experiments investigating the developmental timelines for motion processing in humans.

1.3.1 - Development of ferret V1.

In the ferret, V1 shows responsiveness to visual stimuli around postnatal day (P) 21 (Chapman and Stryker, 1993). Since eye opening does not occur until about P30 in ferrets, animals at P21 are naïve in terms of patterned visual experience. Yet, orientation selectivity and retinotopic organization are already present in V1 at this age (Chapman and Stryker, 1993). In contrast, direction selectivity is absent in ferret V1 before eye opening, but develops during the first week of visual experience (P30-36; Clemens et al., 2012; Li et al., 2006).

The developmental timeline of orientation selectivity and retinotopic organization suggests that they can develop in the absence of patterned visual experience. The mechanisms behind the functional development of the visual system pre-eye-opening have been studied in both ferrets (Chapman and Gödecke, 2000; Davis et al., 2015; Huberman et al., 2006; Penn et al., 1998; Stellwagen and Shatz, 2002) and rodents (Burbridge et al., 2014; Xu et al., 2011) and seem to be common across these species. These mechanisms include both genetically encoded molecular cues and intrinsic patterns of spontaneous neuronal activity, which are generated in the retina and spread throughout the visual system. The details of these mechanisms are outside the scope of this thesis, which focuses on the functional development after eye opening, but they can for example be found in a 2014 review article by Ackman and Crair (Ackman and Crair, 2014).

Unlike for orientation selectivity and retinotopic organization, the developmental timeline for direction selectivity suggests that visual experience plays a role in its development. The impact of visual experience on the development of direction selectivity was tested directly in a study by Li and collaborators. Ferrets were raised in the dark starting at P17, before the onset of cortical responsiveness (P21). Recordings were later performed at P30-77 to analyze direction selectivity in V1. In dark-reared animals, direction selectivity did not develop even at the oldest age sampled (Li et al., 2006). In these experiments, the developing ferret was deprived of all light stimulation. The study therefore could not resolve whether patterned visual experience, or simply unpatterned light stimulation of the retina, is needed for the emergence of direction selectivity. To answer this question, the animal must be provided with unpatterned light stimulation. When eye opening is prevented by suturing the eyelids, photostimulation of the retina is not completely

prevented, but the visual experience becomes devoid of most structure. So far, the impact of lid suture on the development of direction selectivity has not been investigated in the ferret. However, these experiments have been performed in the cat. When cats are raised with binocular lid sutures for extended periods of time (4 months to over a year), direction selectivity does not emerge, demonstrating that patterned visual experience is required for its development (Mower et al., 1981).

A second experiment by Li and collaborators further investigates the kind of visual experience required for the development of direction selectivity. In order to investigate in greater detail which aspects of visual experience are required for the development of direction selectivity, they provided ferrets with controlled, artificial visual stimulation before eye opening. When visually naïve kits were exposed to drifting gratings for a few hours, neurons in V1 developed direction selectivity (Li et al., 2008). If instead kits were exposed to static gratings, V1 neurons remained insensitive to motion direction (Li et al., 2008). These results indicate that the emergence of direction selectivity in V1 requires experience with moving visual patterns. One hypothesis for the mechanism behind this dependency is that the spatiotemporal patterns of moving stimuli could generate activity patterns in visual cortex that lead to the emergence of tuning by means of spike-timing-dependent plasticity. If this were the case, certain patterns of cortical activity should be required for direction selectivity to develop. In disagreement with this hypothesis, Roy and collaborators have reported that homogeneous optogenetic activation of neurons across V1 can induce the emergence of direction selectivity (Roy et al., 2016). It therefore appears that at least some mechanisms behind the development of direction selectivity do not depend on the precise structure of cortical activation.

Dark rearing and controlled visual stimulation experiments indicate that visual experience plays a key role in the development of direction selectivity. But is visual experience required at a particular developmental stage for the emergence of direction tuning? Li and collaborators investigated this question by exposing animals to normal visual experience after dark rearing them for different time periods. When ferrets were provided with visual experience for 2 to 3 weeks starting at P35 (just a few days after natural eye opening), direction selectivity emerged. In contrast, when ferrets were provided with visual experience for the same amount of time, but starting 10 days later (P45), direction selectivity did not develop (Li et al., 2006). These experiments demonstrate that direction selectivity fails to develop beyond a certain temporal window, even if visual experience is provided. We refer to the developmental period during which a tuning property can emerge, given the necessary visual experience, as the critical period.

The experiments discussed above indicate that visual experience is required for the emergence of direction selectivity. Yet, they do not address whether visual experience has an impact on the direction preference of V1 neurons. In general, it has been suggested that visual experience could play a permissive or an instructive role in development (Roy et al., 2018). In the first case, experience is required for the emergence of tuning, but does not impact the distribution of tuning preferences of the neurons. In the second case, visual experience shapes the stimulus preferences of neurons as they develop tuning. For direction selectivity, a permissive role would imply that experience with stimuli moving in a single direction should induce the emergence of direction selectivity exclusively in neurons that already showed preference for this direction. The overall distribution of direction preferences should not be impacted in this case. In contrast, an instructive role would imply

that experience with a single motion direction should train neurons with a pre-existing preference for other motion directions to prefer the trained direction. This would result in an increased proportion of neurons with preference for that direction. When visually naïve ferrets were exposed to drifting gratings moving in a single direction, direction selectivity emerged in neurons that showed a pre-existing preference for either the trained or opposite direction. Yet, the effect of training was strongest for the cells that preferred the trained direction before stimulation (Van Hooser et al., 2012), suggesting that the instructive role of visual experience is limited. Other experiments by Ritter et al. have shown that the temporal frequency of the stimulation does not affect the temporal frequency preference of neurons (Ritter et al., 2017), also supporting a less instructive and more permissive role of visual experience. These studies are confounded by the fact that the stimulation provided did not exceed 16 h and was mostly restricted to 8 h or fewer. It remains possible that longer stimulus exposure would overcome the initial tuning biases, and demonstrate a more instructive role of visual experience. For a more extensive review of this subject see Roy et al., 2018.

1.3.2 - Development of V1 in primates.

Developmental studies using primates are rare due to the difficulties of performing experiments in very young animals. Despite this, there are a few studies that have established baseline developmental timelines against which findings in other species can be compared. Electrophysiological recording of V1 responses in visually deprived infant monkeys revealed that orientation columns are present before visual experience (Wiesel and Hubel, 1974). Further experiments showed that single neuron orientation selectivity

increases during the first weeks of life (Chino et al., 1997). Given that visual experience in primates begins immediately after birth, these results suggest a parallel to carnivore development, where orientation selectivity emerges before eye opening and is later increased by visual experience. While some degree of direction selectivity appears to be present in primate V1 already at birth, it is clearly still immature. Full maturation of V1 direction selectivity does not occur until 4 weeks of age (Chino et al., 1997; Hatta et al., 1998). This timeline is roughly comparable to that of carnivores, for which - as described above - direction selectivity emerges shortly after eye opening. Whether the maturation of direction selectivity in primates requires visual experience, as in carnivores, remains to be determined, as the impact of dark rearing on the development of direction selectivity has not yet been investigated in the primate.

1.3.3 - Development of higher-order visual cortex in carnivores and primates.

In the previous section, I discussed our current knowledge on the functional development of V1. These studies have provided us with key insights into how visual properties develop both before and during the onset of visual experience. Yet, the principles that govern functional development in V1 cannot be directly translated to downstream visual areas. V1 implements a first, basic step of processing of visual information. Since V1 projects to many different higher areas with diverse functions, this initial processing is by necessity relatively general. In contrast, the role of higher-order areas is to represent different aspects of the visual stimuli in a compressed, stable, and explicit way, to help visual input drive actions and become stored in memory. In addition to this difference in function, the nature of the neuronal circuits in higher-order areas differs from that of V1. The most prominent

feed-forward input to extra-striate areas comes from other cortical areas, while in V1 it comes from subcortical structures. Considering these differences, it is relevant to extend the study of cortical development beyond V1.

Very few studies have looked into the emergence of response properties in a higher-order visual area. One example is an early electrophysiology study by Price and collaborators, who recorded from single neurons in motion area PMLS of young anesthetized cats (Price et al., 1988). Data from this study indicate that the developmental timeline of PMLS is similar, if not faster, than that of V1. Visual responsiveness and direction selectivity reach full maturity in both areas at the same time at about 10 days after eye opening. Interestingly, these findings indicate that development of the motion pathway may not follow a strictly hierarchical sequence.

In addition to describing the normal developmental timeline of PMLS functions, some studies have looked at the impact of visual experience on the functional development of this area. An early study by Spear and Tong analyzed PMLS response properties in cats raised under monocular deprivation (Spear and Tong, 1980). They observed that PMLS neurons that were driven by input to the deprived eye lacked direction selectivity (Spear and Tong, 1980), suggesting that the emergence of PMLS direction selectivity requires visual experience. In a later study, Spear and collaborators analyzed PMLS direction selectivity in cats raised in an environment illuminated by stroboscopic light, which disrupts motion perception (Spear et al., 1985). Again, they found severely disrupted PMLS direction selectivity. This result indicates that the emergence of direction selectivity in PMLS requires not just general visual experience, but exposure to motion, similar to the

findings for direction selectivity in ferret V1. We can therefore conclude from these early studies that simple motion responses in both PMLS and V1 develop during a similar temporal window and are equally dependent on visual experience.

Research on the development of higher-order cortex in primates is even more limited than that in carnivores. The only electrophysiological study to describe the developmental timeline of responses in area MT was conducted by Kiorpes and Movshon. In this pioneering study, the authors measured responses of MT neurons in infant macaque monkeys (Kiorpes and Movshon, 2014). Data indicate that pattern motion responses develop progressively for several months following birth (Kiorpes and Movshon, 2014).

1.3.4 - Development of motion processing and perception in humans.

As illustrated in the previous sections, most of our knowledge on the mechanisms governing the functional development of the visual system comes from controlled experiments in a variety of animal species. In humans, studies of brain development are restricted to non-invasive measurements, such as psychophysics, functional magnetic resonance imaging, and scalp recordings of visually evoked potentials (VEP). By applying these techniques, a number of studies have characterized the developmental timeline of behaviors and neural signals that relate to functions of the dorsal visual pathway, which is the primary pathway for processing of motion information in the primate brain. These studies suggest that the dorsal pathway develops ahead of the ventral pathway, which is concerned with form processing. In the following paragraphs, I will briefly review some of the most relevant conclusions that emerge from these studies. Much of this bibliography

has been reviewed in several articles by Atkinson, Braddick and Wattam-Bell (Atkinson, 2017; Braddick and Atkinson, 2011; Braddick et al., 2003).

When the development of direction and orientation tuning is analyzed in humans, results resemble the timeline described for the other species discussed above. VEP studies have shown that the infant cortex can discriminate orientations before motion directions (Braddick, 1993; Braddick et al., 2005). Behavioral signatures of motion discrimination can be found earlier than these cortical direction signals (Wattam-Bell, 1992, 1996). This behavioral result would be inconsistent with a comparable developmental timeline in humans and other species. However, the behavior may reflect early, immature motion processing, which has also been reported in infant primates (Kiorpes and Movshon, 2004). In addition, the behavioral studies rely on eye movement behavior, which may be governed more strongly by subcortical regions, and therefore follow a different developmental trajectory (Dobkins et al., 2004).

To investigate the development of higher-order cortex, studies have made use of complex stimuli that require integration of either global motion or form. When tuning for global motion and form is tested using both behavioral and electrophysiological techniques, motion integration seems to emerge before form integration (Braddick and Atkinson, 2007; Wattam-Bell et al., 2010). By using RDKs, VEP studies have shown that at least some cortical signatures of motion integration emerge at an age of about 12 weeks (Braddick and Atkinson, 2007). This is shortly after the emergence of local motion signals, which develop between week 10 and 12 when analyzed using VEPs (Braddick, 1993; Braddick et al., 2005). Some behavioral studies that analyzed eye movements in response to complex

stimuli, such as plaids and RDKs, disagree with this proposed timeline and suggest an even earlier development of motion integration (Banton et al., 2001; Dobkins et al., 2004; Manny and Fern, 1990; Mason et al., 2003). Despite this controversy, motion integration, presumably implemented by the dorsal pathway, consistently appears to mature before form integration, presumably implemented by the ventral pathway (Braddick and Atkinson, 2007). This conclusion is consistent with post-mortem histological studies of brain development in monkeys, which suggest an earlier maturation of area MT of the dorsal pathway than area V4 of the ventral pathway (Bourne and Rosa, 2006; Condé et al., 1996).

1.4 - Motivation and summary of chapters.

The goal of the work presented in this thesis is to establish the ferret as a model for studying the development of higher-order visual cortex. We decided to focus on the motion pathway – rather than other higher-order visual functions – for a number of reasons: As discussed in previous sections, the motion pathway is one of the best characterized visual processing pathways. This provides a solid framework for guiding the interpretation of any data collected in the ferret during development. In addition, relatively simple computational models have been proposed that can successfully explain many of the neuronal processes behind motion computations.

The ferret provides many advantages as a model organism for expanding studies of visual system development into higher-order motion processing. Ferrets have been used extensively in developmental studies due to their early parturition (Chapman and Stryker, 1993; Chapman et al., 1996; Sharma and Sur, 2014; White and Fitzpatrick, 2007), which has produced considerable background knowledge on developmental timelines for lower-order visual areas (see Section 1.3.1). In contrast, other prominent models of vision present a variety of limitations. Primates have the advantage of extensive previous research on complex motion properties in higher-order area MT (see Section 1.1.1), which the ferret lacks. Unfortunately, visual experience in primates starts shortly after birth, making the study of early functional development challenging. In addition, the costs and workload associated with the husbandry of very young primates make it extremely challenging to conduct these studies, in particular when trying to sample different developmental stages. The mouse, which has been used in many studies of visual system physiology and

development, lacks a clear transition from component to pattern motion signals between V1 and higher-order areas (Juavinett and Callaway, 2015; Muir et al., 2015; Palagina et al., 2017). In addition, no visual area with strong pattern motion signals was observed when measuring plaid responses (Juavinett and Callaway, 2015). The cat, another carnivore species, has been successfully used to study visual development. Several studies have investigated the physiology and development of simple tuning properties in higher-order area PMLS (See Sections 1.1.3 and 1.3.3). However, when plaid responses were analyzed in this area, no signatures of pattern motion computations were found (Gizzi et al., 1990; Movshon et al., 1985), preventing the study of complex motion processing.

As discussed above, ferrets appear to be the most promising candidate to study the development of complex motion processing in higher-order areas. In particular, studies in area PSS of ferret visual cortex showed signatures of motion processing, such as increased direction selectivity. Unfortunately, complex pattern motion tuning in this area has not yet been investigated. Taking all of this into consideration, the next chapters cover the following issues:

Chapter 2: In this chapter, I characterize complex motion processing in PSS of adult ferrets using plaids and RDKs, and compare PSS responses with those in V1. I then analyze PSS plaid responses using a feed-forward model similar to that proposed for MT. The goal of this chapter is to establish PSS as a model for studying the development of higher-order motion processing.

Chapter 3: In this chapter, I characterize the development of both direction selectivity and pattern responses in PSS using gratings and plaids. I also use a feed-forward model to

analyze PSS responses across development, and propose potential mechanisms for the emergence of pattern cells. I then investigate the possible contributions that maturing V1 motion signals make to this process. Finally, I perform PSS inactivation experiments to test the contribution of PSS feedback to V1 changes that occur as PSS pattern cells develop. The goal of this chapter is to establish a developmental timeline for basic and complex tuning properties in PSS, and to investigate possible neuronal mechanisms behind the emergence of complex motion representations.

Chapter 4: In the last chapter, I discuss the impact of my work on our current understanding of higher-order motion processing across species and the development of the visual cortex. I also discuss future directions suggested by the results presented in this thesis.

Chapter 2. Ferrets as a model for higher-level visual motion processing

This chapter has been published previously:

Lempel, A.A., and Nielsen, K.J. (2019). Ferrets as a Model for Higher-Level Visual Motion Processing. Curr. Biol. *29*, 179-191.

2.1 - Introduction.

Ferrets are paradigmatic for studying visual development because they are born at an early stage of brain development, and eye opening does not occur until about postnatal day 30 (Sharma and Sur, 2014). This provides a long window for investigation and manipulation of neural development, including developmental stages that occur *in utero* in other higher mammals. The late date of eye opening additionally enables experimental access to changes in emerging brain functions due to the onset of visual experience. So far, research in the ferret has focused on the development of early visual stages, but not the higher-level visual functions commonly investigated in non-human primates. Here, we show that ferrets share important principles of complex visual motion processing with primates. This opens a new opportunity to examine the development of higher-level vision.

Motion perception is an extensively studied aspect of higher-level visual processing. In order to analyze the complex moving patterns present in nature, the visual system needs to integrate over local motion signals in a meaningful way. In primates, area MT implements a major integration stage of motion signals from V1 (Born and Bradley, 2005; Orban, 2008). Because of their small receptive fields, direction-selective V1 neurons largely represent local motion signals. MT neurons then integrate these local motion signals into global signals. This change in motion processing is usually demonstrated using coherent plaids, which are generated by superimposing two gratings moving in different directions. Perceptually, plaids appear to move in a third, intermediate direction (Adelson and Movshon, 1982; Stoner et al., 1990) computed by integrating the two component grating

directions. Consistent with a transition from local to global motion processing, MT – but not V1 – contains a population of neurons sensitive to the integrated pattern direction (Born and Bradley, 2005; Orban, 2008).

In general, little is known about the functions of potential higher-level visual areas in the ferret. Yet, previous studies identified a visual area likely involved in motion processing, located in the posterior bank of the suprasylvian sulcus and referred to as PSS or PMLS (Figure 2.1A). PSS neurons are highly direction selective (Philipp et al., 2006), receive input from V1 neurons that is biased towards motion processing (Jarosiewicz et al., 2012), and PSS lesions impair motion perception (Hupfeld et al., 2007). Here, we use PSS responses to complex motion stimuli (including coherent plaids) to systematically assess the transformations in motion processing occurring between V1 and PSS, and to provide a detailed comparison with MT. Our data reveal signatures of motion integration in PSS that are not found in ferret V1. Changes in motion processing between V1 and PSS could be well explained by a computational model similar to those used to fit MT responses (Baker and Bair, 2016; Rust et al., 2006). Our study therefore demonstrates a clear transformation in motion processing between V1 and higher-level visual cortex in the ferret, in a manner that is consistent with changes occurring in the primate motion pathway.

2.2 - Results: Basic tuning properties indicate role in motion processing.

To provide the foundation for assessing responses to more complex motion stimuli, we first measured a number of basic tuning properties in PSS – direction selectivity, responses to static versus moving stimuli, and speed tuning. In addition, we directly compared these tuning properties between PSS and V1. In all experiments, recordings in PSS and V1 were performed in anesthetized animals using single tetrodes and multi-channel silicon probes (Figure 2.1B).

Direction selectivity was assessed by measuring responses to sine-wave gratings drifting in 12 or 16 different directions (see Figure 2.1C for an example PSS direction tuning curve). We then quantified direction tuning strength by computing a direction selectivity index (DSI), which compares responses to the preferred and the null direction. DSI values close to 1 indicate strong direction selectivity, while values near 0 show lack of direction tuning. In general, PSS neurons were highly direction selective with a median DSI of .93 (Figure 2.1D). This is consistent with the results of a previous PSS study, which used stochastic random dot stimuli to determine direction responses (Philipp et al., 2006). The degree of direction selectivity observed in PSS differed significantly from that in V1 (Figure 2.1C and 2.1D), in which neurons generally were less direction selective (median DSI: V1 = .43. Kolmogorov-Smirnov test: V1 vs PSS $p<.001$).

To further assess the processing of motion information in PSS and V1, we compared responses to static and moving stimuli. For this purpose, we systematically varied the temporal frequency of the drifting gratings. In both V1 and PSS, static gratings generally elicited weaker responses than moving gratings (Figure 2.1E and 2.1F). However, relative

to responses to the optimal temporal frequency, static gratings evoked firing rates that were significantly lower in PSS than V1 (Median static/moving: PSS = .06, V1 = .14. Rank-sum test: $p = .03$).

Lastly, we measured the speed tuning of PSS neurons using a drifting bar (Figure 2.2A). Bars could drift in 8 different directions at 5 different speeds, or remain static. PSS speed preferences were broadly distributed (Figure 2.2B): The median speed preference in PSS was 40 deg/s, but we encountered neurons with speed preference as high as 160 deg/s, the fastest speed sampled. Speed tuning of neurons was further assessed by computing a low-pass index as the ratio of responses to the fastest speed (160 deg/s) and the preferred speed. This analysis confirmed the broad tuning distribution (Figure 2.2C). Our PSS sample included both neurons that responded strongly to the fastest speed (low-pass index < .15, 9/27 cells), and neurons that did not respond to it (low-pass index > .85, 10/27 cells). Note that these conclusions are limited by the fact that speeds faster than 160 deg/s could not be sampled. None of the recorded neurons preferred static over moving stimuli (Figure 2.2D and 2.2E). Yet, on average responses to a static bar were greater than responses to motion in the null direction (median normalized response to static = .23. median response to null direction at 40 deg/s = 0. Signed-rank test: $p = .001$), suggesting that direction selectivity in PSS is partially driven by suppression of responses to the null direction. This is consistent with recent findings linking direction selectivity in layer 2/3 of ferret V1 to null-direction inhibition (Wilson et al., 2018).

In summary, the basic tuning properties of PSS neurons suggest a specialization for motion processing exceeding that of V1 (see Discussion for a comparison to the primate motion pathway).

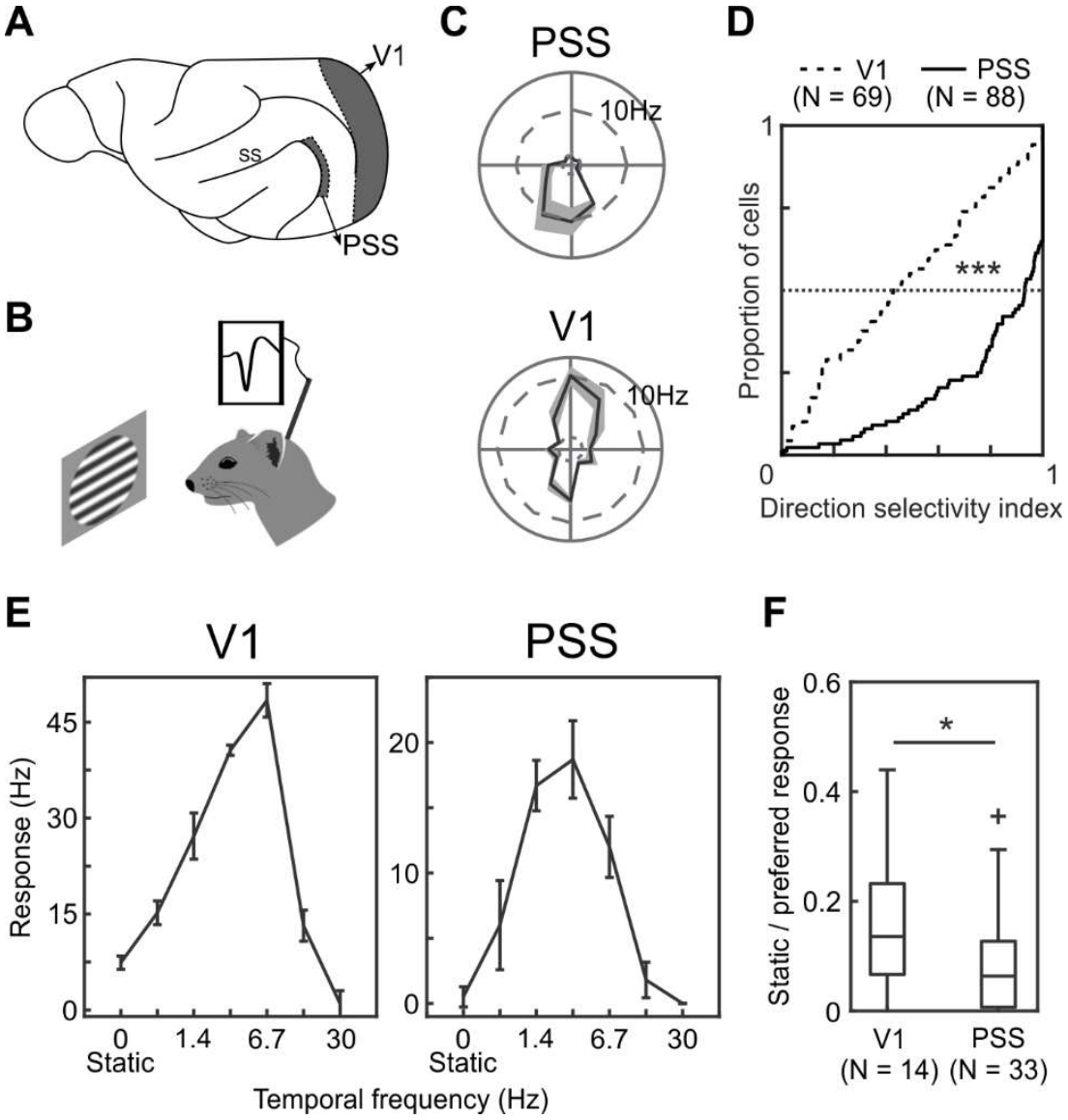

Figure 2.1: Basic PSS tuning properties indicate a role in motion processing.
(A) Sagittal view of the ferret brain indicating the location of PSS and V1 (ss: suprasylvian sulcus).
(B) Schematic of experimental setup. Neural responses to visual stimuli were recorded in anesthetized ferrets using tetrodes or multi-channel silicon probes.
(C) Direction tuning of an example PSS (top) and V1 neuron (bottom). The polar plot indicates mean firing rates to different directions (gray area: ± SEM).
(D) Cumulative DSI distributions for V1 and PSS.
(E) Example temporal frequency tuning for a V1 neuron (left) and PSS neuron (right), measured using sinusoidal gratings drifting at different temporal frequencies (0 Hz indicates a static grating). Error bars represent ± SEM.
(F) Responses to static gratings relative to responses to preferred temporal frequencies. Boxplots indicate the spread of the observed response ratios in V1 and PSS. In this and all subsequent figures, the box indicates 25th, 50th and 75th percentiles. Whiskers indicate range, and crosses indicate outliers.
* = $p < .05$; *** = $p < .001$.

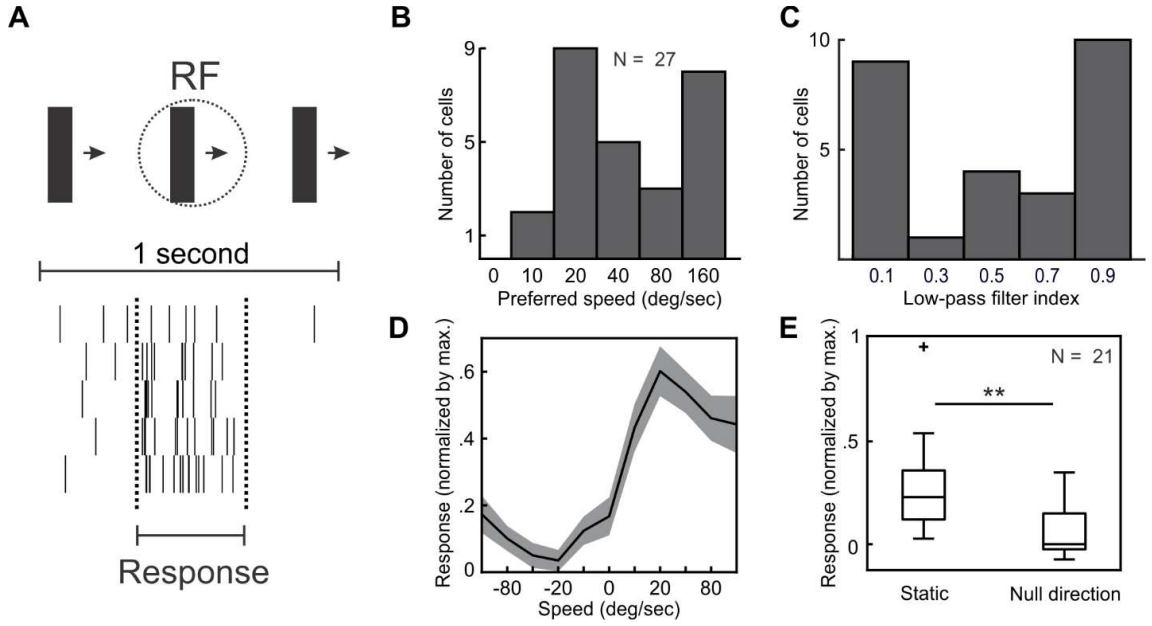

Figure 2.2: Speed tuning in PSS.
(A) Responses of an example PSS neuron to the drifting bar stimulus (illustrated on the top of the figure). Each row of the raster plot corresponds to one cycle of the bar drifting across the screen. The period during which the bar traverses the central 40 deg of the estimated receptive field is indicated by dashed lines. This time window was used to compute stimulus-evoked responses (see Methods).
(B) Distribution of preferred speeds.
(C) Distribution of low-pass indices for the same neurons as in (B).
(D) Average PSS speed tuning curve. To compute this curve, the response of each neuron was normalized by its maximum before averaging (same neurons as in (B)). Positive speeds indicate movement in the preferred direction, negative speeds movement in the null direction. 0 corresponds to a static bar. Note the decreased response to motion in the null direction relative to the static stimulus. Gray area: ± SEM.
(E) Comparison of responses to static bars and motion in the null direction at 40 deg/s. All responses were normalized by the maximum response per neuron.
** = $p < .01$.

2.3 - Results: PSS neurons show motion opponency.

In MT, responses to a stimulus drifting in the preferred direction can be strongly suppressed by superimposing a second stimulus drifting in the opposite direction (Qian and Andersen, 1994; Snowden et al., 1991). This phenomenon is termed motion opponency. Inhibition by opposing direction signals is believed to be a crucial aspect of how MT neurons combine local direction signals (Adelson and Bergen, 1985; Simoncelli and Heeger, 1998). As a first assessment of PSS responses to more complex motion stimuli, we tested whether PSS neurons similarly exhibit motion opponency. To this end, we used a stimulus set previously used to measure MT motion opponency (Snowden et al., 1991). The main stimulus set (Figure 2.3A) consisted of three different random dot kinematograms (RDKs). For two of these stimuli, all dots in the RDK moved in one direction, which was chosen to be either the preferred direction of the neuron under study (preferred stimulus) or the null direction (null stimulus). In the third stimulus, the preferred and null stimulus were superimposed to generate a RDK with opposing motion signals in the same region of space (motion-opponency stimulus). Note that the motion-opponency stimulus contained twice the number of dots in the other two RDKs, but maintained the same number of dots per direction. Perceptually, the motion-opponency stimulus appears as two surfaces sliding across each other (Qian et al., 1994; Snowden et al., 1991).

In general, PSS neurons responded vigorously to the preferred stimulus. Addition of the opposing direction signal in the motion-opponency stimulus reduced responses, demonstrating the presence of motion opponency. We quantified the strength of this effect by computing a motion opponency index (MOI) for each neuron. MOI values near 0 indicate equal responses to the preferred and motion-opponency stimulus, or a lack of

motion opponency. MOI values near 1, on the other hand, indicate suppression of firing rates to baseline levels for the motion-opponency stimulus. The population data (Figure 2.3B) confirm strong motion opponency in PSS (median MOI = .62). In contrast, V1 neurons displayed a significantly lower degree of motion opponency (median MOI = .36. Rank-sum test: V1 vs PSS $p = .002$).

To test whether this difference in motion opponency could be explained by the differences in direction selectivity in the two areas, we separately computed the MOI for direction-selective V1 cells only (DSI > .75). Indeed, the mean MOI for direction-selective V1 neurons was not significantly different from PSS cells (median MOI = .53. Rank-sum test: direction-selective V1 vs PSS $p = .53$). In general, plotting motion opponency against direction selectivity (Figure 2.3C) revealed that motion opponency and direction selectivity were positively correlated in both areas, and that V1 and PSS data formed a continuum (correlation for the combined data set: $r = .44$. $p < .001$). These results suggest that suppression of null direction responses may play a role in shaping direction selectivity across the ferret's motion pathway. Furthermore, the observed levels of motion opponency, as well as the relationship to direction selectivity, replicate findings for the primate motion pathway (see Discussion).

One possible confound in this experiment is the increased dot density in the motion-opponency stimulus. To rule out effects of dot density, we generated a second motion-opponency stimulus that maintained the same dot density as the preferred stimulus by halving the number of dots per direction (Figure 2.3A, 'constant density' stimulus). We then compared responses between the constant density and the preferred stimulus for an

additional group of PSS and V1 neurons (Figure 2.3B). For V1, using the constant density stimulus increased MOI levels (median MOI = .52. Rank-sum test between the two motion opponency stimuli: $p = .02$). This change is likely due to the fact that the constant density stimulus contained fewer dots moving in the preferred direction than the original motion opponency stimulus, which would result in lower responses for the constant density stimulus and therefore stronger motion opponency (the preferred stimulus has the same number of dots in both experiments). At the same time, motion opponency remained stronger in PSS than V1 despite the changes in dot density (median MOI PSS = .65, Rank-sum test: V1 vs PSS. $p = .01$).

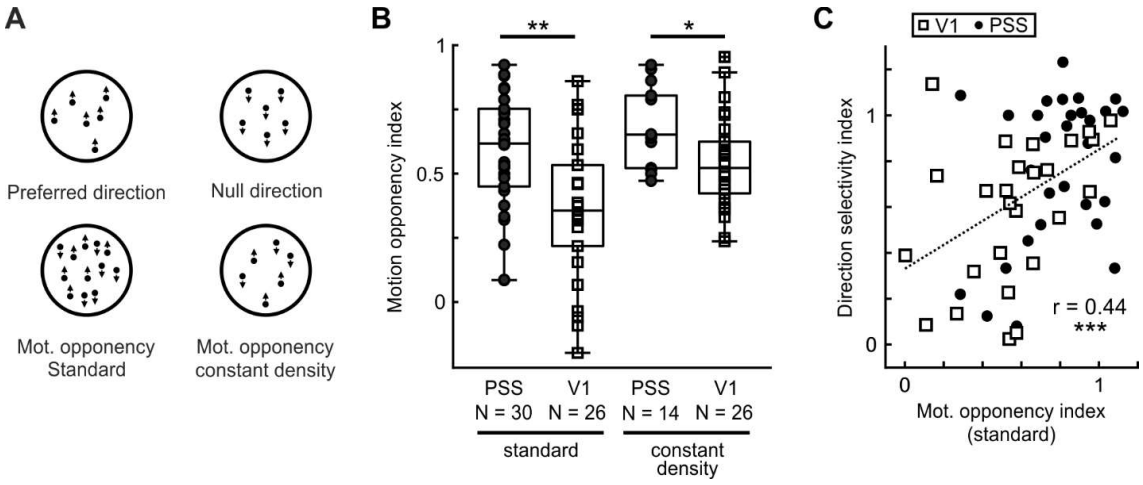

Figure 2.3: PSS neurons show motion opponency.
(A) Illustration of RDKs used to investigate motion opponency in PSS and V1.
(B) MOI distributions for PSS and V1, using either the standard motion opponency stimulus (lower left in (A)) or the constant density version (lower right in (A)).
(C) DSI versus MOI for V1 and PSS neurons, calculated based on the standard motion opponency stimulus. Dotted line represents fit for both data sets combined.
* = $p < .05$; ** = $p < .01$; *** = $p < .001$.

2.4 - Results: A subset of PSS neurons encodes pattern motion.

One of the hallmarks of information processing in primate higher-order motion cortex is the computation of plaid pattern motion, which requires integration of local motion signals (Adelson and Movshon, 1982; Movshon et al., 1985). We therefore investigated whether PSS neurons similarly encode pattern motion. As in the initial MT experiments (Movshon et al., 1985), we addressed this question by measuring neuronal responses to 50% contrast sine-wave gratings and coherent plaids. Plaids were generated by superimposing two 50% contrast sine-wave gratings with directions that were 135 deg apart (Figure 2.4A). Perceptually, plaids appear to move in a direction bisecting the angle between the component directions (Adelson and Movshon, 1982; Stoner et al., 1990). For both gratings and plaids, 16 motion directions were sampled. The degree of motion integration exhibited by a neuron was then determined from the tuning curves for plaids and gratings, using the same analysis commonly employed for MT (Movshon et al., 1985; Smith et al., 2005). It rests on the following assumptions: Neurons that are only sensitive to the integrated pattern motion (so called pattern neurons) should have plaid tuning curves with a single peak, corresponding to the plaid moving in their preferred direction (Figure 2.4B). On the other hand, neurons sensitive to the individual components (so called component neurons) should have a bi-lobed plaid tuning curve, with maximal responses when either one of the components moves in the preferred direction (Figure 2.4C). The degree of motion integration by a neuron can then be quantified by comparing its actual plaid tuning curve to these predictions.

More precisely, we used each neuron's grating tuning curve to generate two predictions for its plaid tuning curve. One prediction assumed pattern cell-like responses, and was identical to the grating tuning curve. The other prediction assumed component cell-like responses. It was computed as the sum of two copies of the grating tuning curve, shifted relative to each other to account for the direction difference between the two components. We then computed Z-corrected partial correlations between the measured plaid tuning curve and the two predictions. Z_P indicates the strength of pattern responses, and Z_C the strength of component responses. Cells were classified as pattern or component through comparisons of their Z_P and Z_C values. Neurons with significantly higher Z_P than Z_C (using $p < .1$ as in the primate studies; Smith et al., 2005) were classified as pattern cells, while neurons that met the opposite criterion were classified as component cells (see Figure 2.4E and 2.4F for a depiction of the category boundaries; also see Methods). Using this analysis, 17% of PSS neurons (13/77) were classified as pattern cells, while 27% (21/77) were classified as component cells (Figure 2.4E). The rest of the cells remained unclassified. This result indicates that a substantial proportion of PSS neurons exhibits signatures of motion integration.

Given the existence of pattern cells in PSS, an important question is how much of this tuning is inherited from V1, i.e. whether V1 neurons can similarly extract pattern motion. To investigate this issue, we recorded responses to grating and plaid stimuli in V1. None of the recorded V1 neurons (0/22) was classified as a pattern cell, while 77% of V1 neurons (17/22) were classified as component cells (Figure 2.4F). Since comparisons based on the number of pattern and component cells depend on the criteria used to classify cells, we further compared PSS and V1 by computing a criterion-independent pattern index as Z_P-

Z_C (Figure 2.4D). Across the population, pattern indices were significantly higher in PSS than in V1 (median pattern index: PSS = -0.41, V1 = -2.62. Kolmogorov-Smirnov test: $p < .001$). These data strongly suggest that pattern motion selectivity in PSS is not inherited from V1, just as pattern responses in primate MT are not inherited from V1.

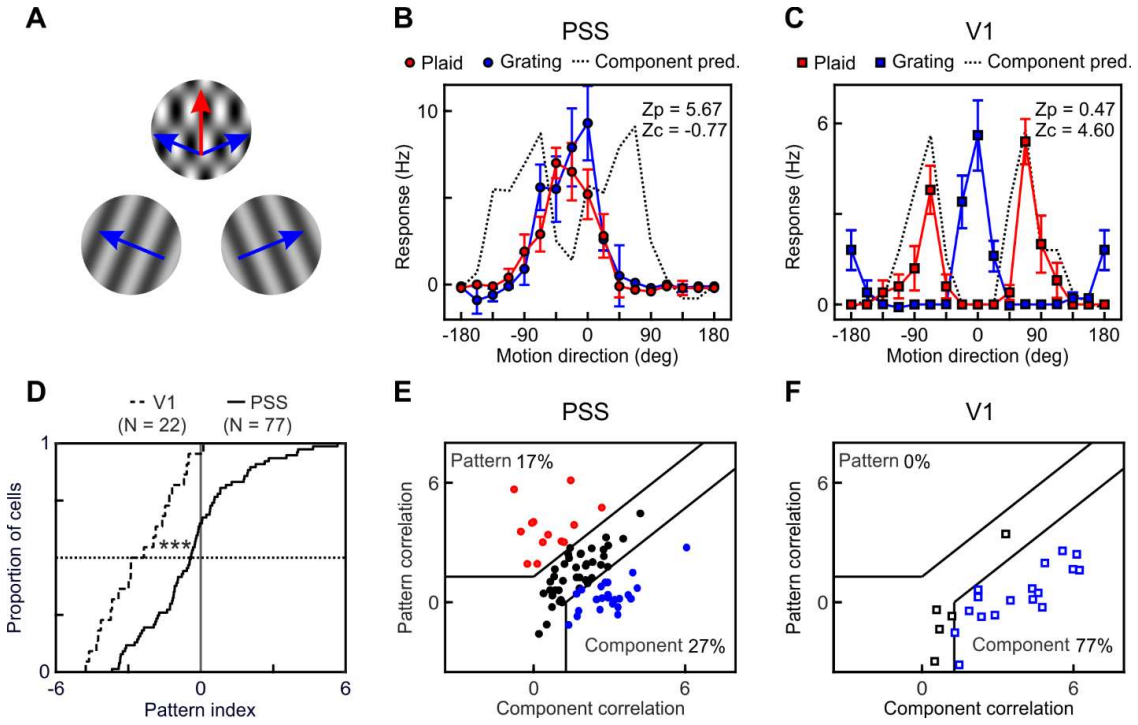

Figure 2.4: A subset of PSS neurons encodes pattern motion.
(A) Schematic representation of gratings and plaids used to investigate pattern motion responses in PSS and V1. Blue arrows indicate the directions of the component gratings, the red arrow the perceived plaid direction.
(B) Direction tuning curve of an example PSS pattern cell measured using plaids (red) and gratings (blue). Direction is relative to the neuron's preferred direction for the grating. For plaids, direction indicates the perceived pattern direction (the components move at ±67.5 deg relative to this direction). For each neuron, the measured plaid tuning curve is compared to two predictions, one for idealized pattern responses (tuning curve identical to the grating tuning curve), one for idealized component responses (prediction indicated by dashed line). Z-transformed partial correlation indices Z_P and Z_C indicate how closely the measured plaid tuning curve resembles these predictions. Error bars: ± SEM.
(C) Plaid and grating direction tuning curves of an example V1 component cell. Same format as in (B).
(D) Pattern index distributions for V1 (dashed line) and PSS (solid line).
(E) Pattern versus component selectivity for PSS neurons. For each neuron, Z_P is plotted against Z_C. Black lines indicate the category boundaries used to classify cells into pattern, unclassified and component cells. Percentages indicate the portion of neurons falling into the different categories.
(F) Pattern versus component selectivity for V1, using the same format.
*** = $p < .001$.

2.5 - Results: Detailed characterization of PSS pattern selectivity.

The above experiment assessed motion integration using plaids with one particular angle between the component directions (dOri). Yet, plaids can be constructed with a range of dOri values (as long as the extreme values of 0 and 180 deg are excluded). Importantly, while changing dOri impacts the overall appearance of the resulting plaid (Figure 2.5A), the perception of coherent pattern motion is maintained (Adelson and Movshon, 1982). We therefore expanded our stimulus set by including more dOri values to probe PSS motion integration more finely. The expanded stimulus set consisted of 7 dOri values combined with 16 plaid directions. We also measured responses to individual gratings drifting in 16 directions, as well as a blank stimulus. To efficiently sample this large stimulus set, we modified the stimulus presentation paradigm. Instead of surrounding each stimulus presentation by blank periods as before, we adopted a streaming stimulus paradigm previously used for MT (Rust et al., 2006; Smith et al., 2005). In this paradigm, each trial contained a 1 minute-long sequence of short stimulus presentations, with 3 to 6 stimuli presented per second (Figure 2.5B). Stimulus sequences were determined randomly from all conditions. The responses to individual stimuli embedded in these sequences were determined by computing firing rates during 150 ms-long windows time-locked to stimulus onset. To account for response latency, the temporal window used for firing rate calculations was shifted relative to stimulus onset by a delay optimized for each neuron individually (see Methods).

We first validated the effectiveness of this paradigm by analyzing only responses to plaids with a dOri value of 135 deg, the angle used in the first experiment. As before, we used

each neuron's plaid and grating tuning curves to compute Z_P and Z_C. Based on this analysis, 23% of PSS cells (9/40) were classified as pattern cells, and 38% (15/40) as component cells, in agreement with the first experiment. The pattern index distribution also did not differ significantly between experiments (Kolmogorov-Smirnov test: $p = .4$). We therefore concluded that the rapid succession of stimuli in the streaming paradigm did not interfere with the detectability of PSS pattern responses.

We then used the full stimulus set to provide a more general analysis of PSS motion integration. Each plaid in the stimulus set could be described by two parameters, pattern direction and dOri. dOri influences the plaid's spatial parameters (such as spatial frequency) and apparent speed (Adelson and Movshon, 1982; Ferrera and Wilson, 1991). Since both parameters could be expected to impact neuronal responses, we chose to summarize the stimulus space as the 2D space spanned by them (see Figure 2.5C and 2.5D). We also assumed that direction and dOri tuning were separable, so that tuning curve predictions for the entire stimulus ensemble could be generated as the product of direction and dOri tuning curves.

Similar to the standard analysis, we quantified the amount of motion integration exhibited by a neuron by comparing its actual tuning curve to pattern and component predictions. Both predictions were generated by estimating a direction tuning curve and a dOri tuning curve and computing their product (see Figure 2.S1 for examples). All tuning curves were estimated based on the entire data set (i.e., gratings and plaids) to increase their robustness. More precisely, the direction tuning curve for the pattern prediction was computed by averaging across all plaids moving in the same direction (independent of dOri) as well as

the matching gratings. The dOri tuning curve was similarly computed by collapsing across all stimuli with the same dOri. For the component prediction, we first computed direction tuning as a function of component direction. This was achieved by averaging across all plaids based on component direction (i.e. each plaid contributed twice), again including the matching gratings. Since we chose to represent tuning curves in a 2D space spanned by plaid direction and dOri, we then transformed the direction tuning curve from a function of component direction to a function of plaid direction. For this transformation, we summed two copies of the component direction tuning curve at each dOri, shifted relative to each other according to the dOri value. The dOri tuning curve for the component prediction was identical to that of the pattern prediction. After generating both predictions, they were compared to the actual responses of each neuron by computing Z-corrected partial correlations.

In agreement with our previous results, we observed a range of motion integration behavior in PSS, including both pattern and component cells. 45% of cells (29/65) were classified as pattern cells, 35% (23/65) as component cells, and the rest remained unclassified (Figure 2.5E). In contrast, using the same stimulus set and analysis in V1 resulted in 100% component cells (26/26) and no pattern or unclassified cells (Figure 2.5F). The pattern index distributions were also significantly different between PSS and V1 (Figure 2.5G), with generally higher pattern indices in PSS than V1 (median pattern index: PSS = .45, V1 = -9.27. Kolmogorov-Smirnov test: $p < .001$).

In conclusion, the streaming stimulus experiment further confirms that signatures of motion integration can be found in PSS but not V1. It extends our other findings by

demonstrating that PSS pattern cells extract pattern motion despite changes in dOri, in agreement with the perception of these stimuli. This is consistent with the behavior of pattern cells in MT (Rust et al., 2006). In comparison with the previous data set, the analysis based on the larger stimulus set enhanced the differences between V1 and PSS. The large number of component cells detected in V1 rules out that the increased number of pattern cells in PSS is simply a product of the chosen analysis method. Rather, we suggest that the increased number of stimuli used for tuning curve computations, as well as the increased number of data points used for computing partial correlations, enhance the ability to differentiate the two cases.

This data set allowed a further comparison between PSS and MT: MT pattern cells tend to respond more strongly to plaids than gratings, reflected in a significant correlation between the pattern index and the ratio of firing rates for plaids versus gratings (Wang and Movshon, 2016). We similarly observed a significant correlation between pattern index and plaid/grating response ratio (expressed in logarithmic scale) in PSS ($r = .5$. $p < .001$; Figure 2.5H).

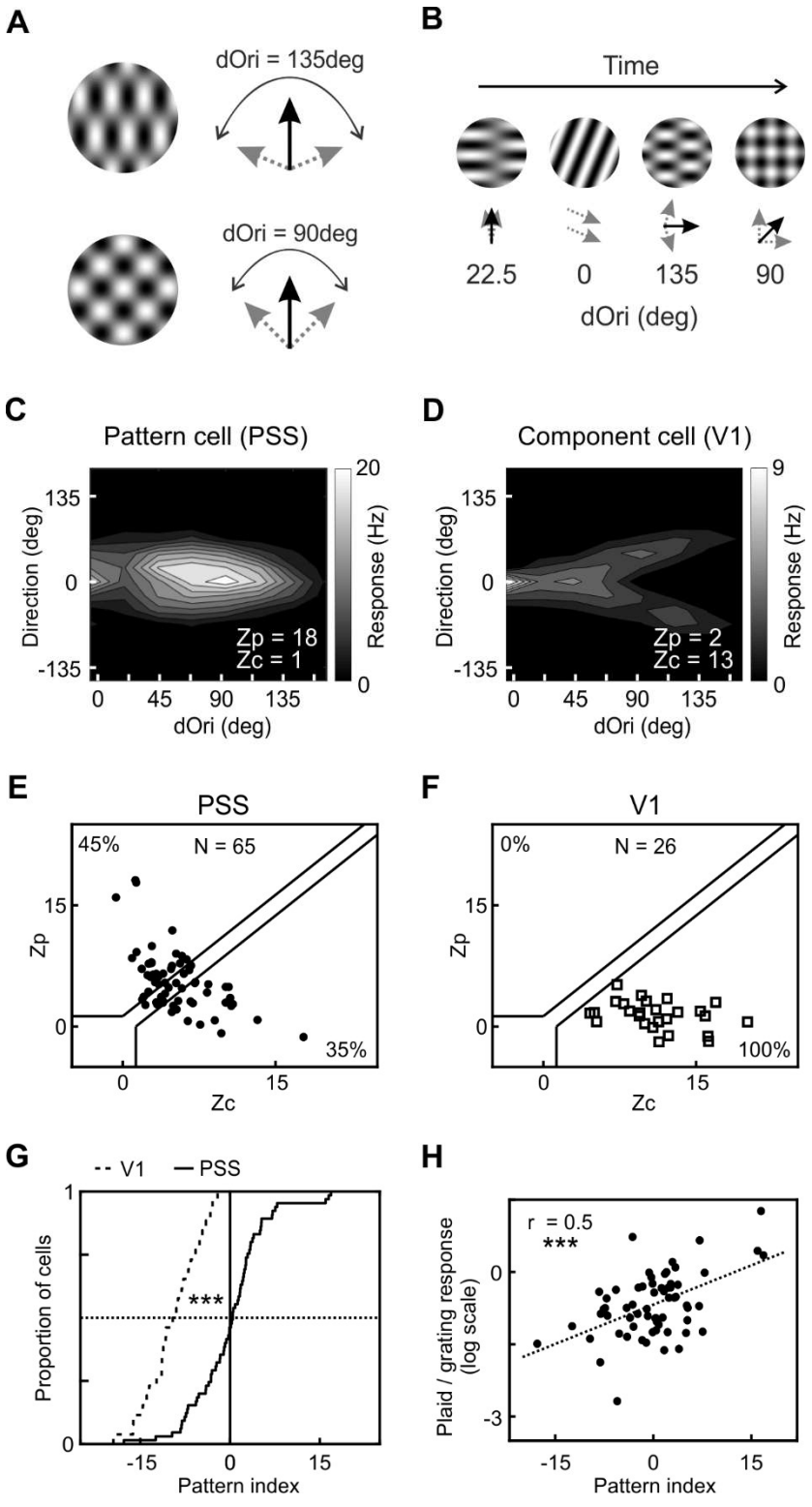
A
dOri = 135deg
dOri = 90deg
B
Time
22.5
0
135
90
dOri (deg)
C
Pattern cell (PSS)
Direction (deg)
135
0
-135
Zp = 18
Zc = 1
0 45 90 135
dOri (deg)
Response (Hz)
20
0
D
Component cell (V1)
Zp = 2
Zc = 13
9
E
PSS
45%
N = 65
35%
Zp
Zc
15
F
V1
0%
N = 26
100%
G
-- V1 — PSS
Proportion of cells
1
***
-15 0 15
Pattern index
H
r = 0.5
***
Plaid / grating response (log scale)
-3

Figure 2.5: Detailed characterization of PSS pattern selectivity.
(A) Illustration of the stimulus set containing plaids generated from component gratings with different dOri values (left).
(B) Schematic representation of the streaming stimulus paradigm used to measure responses to the larger stimulus set.
(C) 2D contour plot showing responses of a PSS pattern cell as a function of dOri and direction (dOri = 0 deg corresponds to 100% contrast gratings). Direction is relative to the cell's preferred grating direction, and indicates the perceived direction of the grating or plaid (i.e., the pattern direction). The response profile shows consistent responses to gratings and plaids moving in the preferred direction, independent of dOri, as would be expected for a pattern cell. The plot indicates Z_P and Z_C for the neuron, computed using the entire 2D response profile as described in the Methods.
(D) 2D contour plot for a V1 component cell (same format as (C)). The response profile shows the regular direction tuning curve for gratings at dOri = 0 deg. For plaids (dOri > 0 deg), direction tuning curves show two peaks with increasing distance for larger dOri values, which correspond to one of the two components moving in the neuron's preferred direction.
(E) Pattern versus component selectivity for PSS neurons based on the large stimulus set. Plot format as in Figure 2.4E. See Figure 2.S1 for examples of the predicted tuning curves underlying the computation of pattern and component selectivity.
(F) Pattern versus component selectivity for V1 neurons for the same stimulus set.
(G) Distribution of pattern indices for V1 and PSS based on the same data.
(H) Relationship between pattern index and the relative response to plaids versus gratings. Only responses to plaids with dOri = 90 deg were considered in this analysis. The response ratio compares the maximum response measured for all plaids with dOri = 90 deg to the maximum response measured for all 100% contrast gratings. The dotted line represents the linear fit for these data.
*** = $p < .001$. See also Figure 2.S1.

2.6 - Results: Motion representation in PSS can be explained by a cascade model.

The results presented so far suggest strong similarities between PSS and MT. To further test this idea, we asked whether computational models developed for the primate motion pathway could be adapted to the ferret. To this end, we developed a multistage model of the ferret's motion pathway based on recent V1-MT pathway models (Baker and Bair, 2016; Rust et al., 2006). The model consisted of the following stages (Figure 2.6A):

(1) Contrast scaling: The first model stage implements the scaling of visual inputs resulting from contrast response functions in processing stages preceding V1. Contrast response functions were modeled using the Naka-Rushton equation (Albrecht and Hamilton, 1982), with the shape of the functions controlled by the parameters C_{50} and N. We included this stage to allow future developmental studies to model the impact of maturing contrast response functions (Boothe et al., 1988; Popović et al., 2018; Zheng et al., 2007) on overall motion pathway behavior. Additionally, contrast scaling provides a mechanism for controlling the relative V1 response to gratings and plaids. This is necessary for generating pattern cells that respond more strongly to plaids than gratings, as observed in the data. For the same reason, recent V1-MT models included a so-called 'tuned' normalization stage in V1, which served to scale the responses of individual V1 direction channels. Here, contrast scaling was implemented as the first model stage to maintain contrast-invariant orientation tuning in V1 (Alitto and Usrey, 2004; Sclar and Freeman, 1982).

(2) Direction filters: The second stage represents a bank of 16 V1 direction filters. Direction selectivity was implemented using motion energy detectors (Adelson and Bergen, 1985) as in previous models (Baker and Bair, 2016; Simoncelli and Heeger, 1998; Tsui et al., 2010). All parameters determining the direction filters were set to published values for the ferret (see Methods). Note that we chose not to include a divisive normalization stage in V1 as often found in V1-MT models (Baker and Bair, 2016; Rust et al., 2006; Simoncelli and Heeger, 1998; Tsui et al., 2010). The divisive normalization serves to scale overall responses across all direction channels. In V1-MT models using both this 'untuned' and the previously mentioned 'tuned' V1 normalization, the weight of the untuned normalization was generally low (Baker and Bair, 2016; Rust et al., 2006). We therefore omitted the divisive normalization stage to reduce the number of model parameters.

(3) PSS integration: In the third stage, integration of V1 responses was modeled as a linear combination of the V1 direction channels. To account for motion opponency, we chose to include two weight functions in this stage, one for excitation and one for inhibition. The excitatory weight function was modeled as a von Mises function of concentration k_E, centered on the preferred direction. The amplitude of the excitatory weight function was fixed at 1. Inhibition was similarly modeled as a von Mises function of concentration k_I and amplitude I, centered on the null direction. The complete weight function was then computed by subtracting the inhibitory weights from the excitatory weights.

(4) *PSS non-linearity:* In the last model stage, a threshold non-linearity with threshold T was applied to the PSS responses.

To test whether this model was capable of reproducing the range of plaid responses observed in PSS, we used it to fit a set of strongly direction-selective (DSI > .75) PSS neurons for which we had collected responses to the large plaid set. For each neuron, the fit procedure determined the best values for the six parameters listed above (C_{50}, N, k_E, k_I, I, T). The model was able to explain not only PSS component and pattern responses, but also the responses of unclassified, intermediate cells (Figure 2.6B). Generally, tuning profiles generated from the model fit agreed well with the actual data. Across neurons, the median correlation between model fit and actual data was .81, which is remarkable given that only six variables were used to fit 128 data points per tuning profile. As a control, we also fit the model to a shuffled data set, in which each neuron's responses were shuffled across stimuli to destroy the tuning profile while preserving overall response rates. The model poorly explained the random structure of the shuffled data set (Figure 2.6C), resulting in significantly lower correlation values for the shuffled than the actual data (median correlation coefficient shuffle data = .46. Kolmogorov-Smirnov test: data vs shuffle $p < .001$).

In an effort to identify potential mechanisms responsible for generating pattern cells, we investigated how different model parameters contributed to the emergence of pattern responses. To this end, we tested how well individual parameters correlated with the pattern index. Amongst the six parameters, the concentration k_E of the excitatory PSS weight function (Figure 2.6D) correlated most strongly with the pattern index ($r = -0.52$. $p < .001$).

In addition, the strength of inhibitory weights I (Figure 2.6E) was also significantly correlated with the pattern index ($r = .38$. $p = .005$). Together, these findings imply that pattern cells have an overall weight function with a broad excitatory peak and a strong inhibitory component (Figure 2.6F). Component cells, on the other hand, have a narrow excitatory peak with little inhibition (Figure 2.6F). Similar observations were made for MT (Rust et al., 2006). The C_{50} component of the contrast response function (Figure 2.6G) was also strongly correlated with pattern index ($r = -0.39$. $p = .003$) while the PSS threshold parameter T (Figure 2.6H) showed a weaker, but still significant correlation ($r = .35$. $p = .01$). The remaining parameters of the model (N and k_I) were not correlated with the pattern index (data not shown).

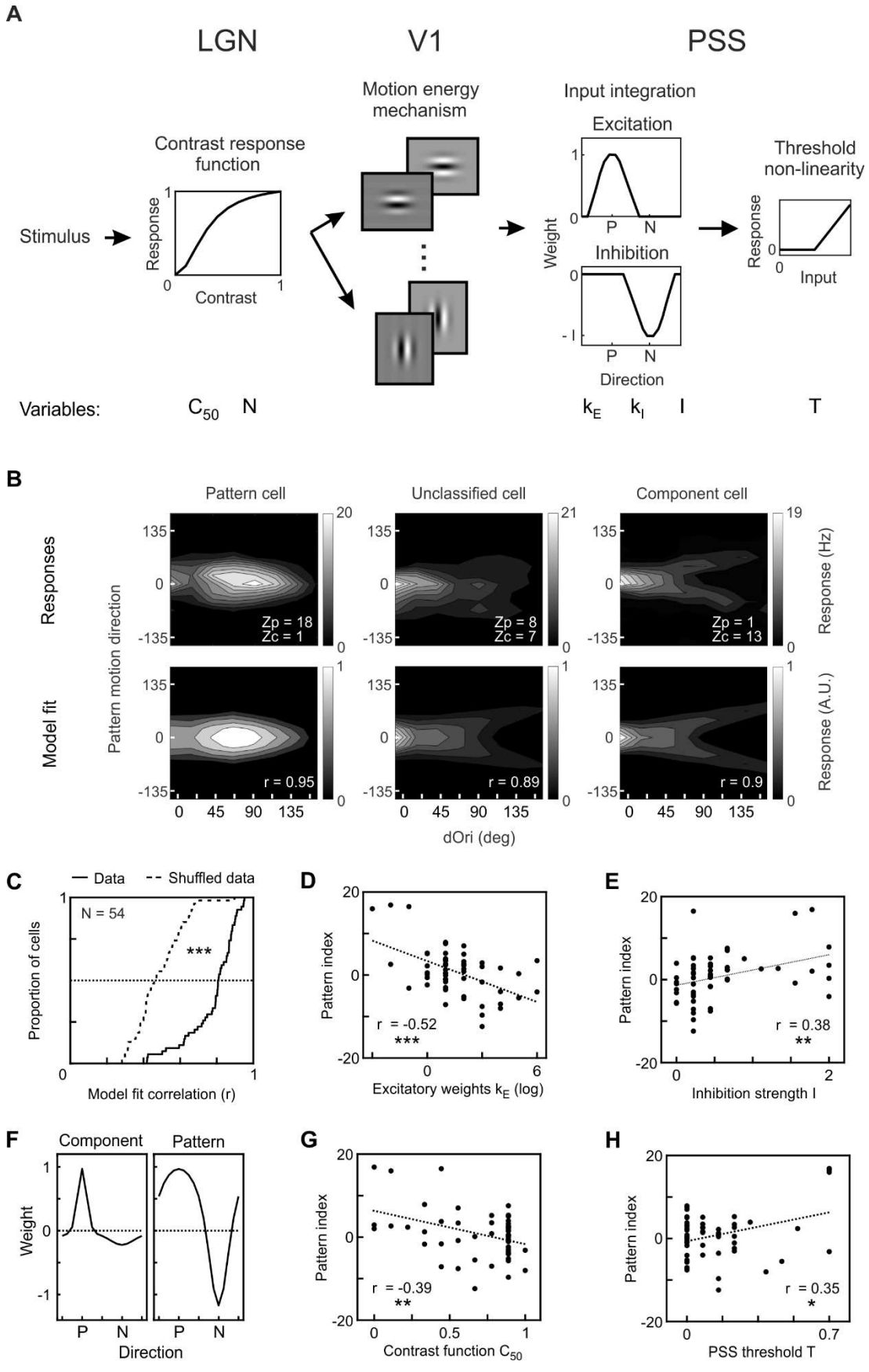
A
LGN
V1
PSS
Motion energy mechanism
Input integration
Excitation
Inhibition
Contrast response function
Threshold non-linearity
Stimulus
Response
Contrast
Weight
Input
Direction
Variables:
C_{50} N
k_E k_I I
T
B
Pattern cell
Unclassified cell
Component cell
Responses
Model fit
Pattern motion direction
Zp = 18
Zc = 1
Zp = 8
Zc = 7
Zp = 1
Zc = 13
r = 0.95
r = 0.89
r = 0.9
Response (Hz)
Response (A.U.)
dOri (deg)
C
Data
Shuffled data
N = 54
***
Proportion of cells
Model fit correlation (r)
D
Pattern index
r = -0.52
***
Excitatory weights k_E (log)
E
Pattern index
r = 0.38
**
Inhibition strength I
F
Component
Pattern
Weight
P N P N
Direction
G
Pattern index
r = -0.39
**
Contrast function C_{50}
H
Pattern index
r = 0.35
*
PSS threshold T

Figure 2.6: Motion representation in PSS can be explained by a cascade model.
(A) Diagram of model used to explain PSS plaid responses (see Methods for details). Stimuli first passed through LGN spatial filters, which also served to scale responses according to contrast. The next stage was composed of 16 V1 motion-energy filters. Responses from the V1 stage were integrated in PSS using a combination of an excitatory and an inhibitory weight function (P – preferred direction; N – null direction). Finally, an output non-linearity was applied to the PSS responses. The model had 6 variables, which are listed below the stage to which they belong. All other parameters were fixed based on published values for the ferret.
(B) Top: Responses of 3 example PSS neurons to the large plaid set (format as in Figure 2.5C). Bottom: Model fits, chosen to minimize the mean square error for each of the 3 cells. For each cell, r denotes the correlation coefficient between modeled and measured responses.
(C) Cumulative distribution of the correlation coefficient between modeled and measured PSS responses (solid line) or between modeled and shuffled responses from the same neurons (dashed line).
(D, E, G, H) Relationship between different model parameters and the pattern index. Correlation coefficients and their significance are indicated for each parameter.
(F) PSS weight function for the component cell (left) and pattern cell (right) shown in (B). The weight functions show the shape and relative contribution of the excitatory and inhibitory components determined for these cells by the model. Component cells have a sharp excitatory weight function with little inhibition, while pattern cells have a broad excitatory function combined with strong inhibition. P – preferred direction; N – null direction. Note that the amplitude of the excitatory weight function was fixed at 1.
* = $p < .05$; ** = $p < .01$; *** = $p < .001$.

2.7 Tables.

Table 2.1: Number of animals and neurons for all experiments.

Figure	Experiment / Analysis	Experimental group	Animals	Neurons
2.1D	Direction selectivity index	PSS	10	88
2.1D	Direction selectivity index	V1	9	69
2.1F	Static vs moving stimulus response	PSS	5	33
2.1F	Static vs moving stimulus response	V1	5	14
2.2B-D	Speed tuning	PSS	4	27
2.2E	Static vs null motion response	PSS	4	21
2.3B,C	Motion opponency	PSS standard	7	30
2.3B,C	Motion opponency	V1 standard	5	26
2.3B	Motion opponency	PSS constant density	4	14
2.3B	Motion opponency	V1 constant density	3	26
2.4D,E	Pattern motion, single plaid stimuli set	PSS	8	77
2.4D,F	Pattern motion, single plaid stimuli set	V1	4	22
2.5E,G,H	Pattern motion, streaming stimulus	PSS	12	65
2.5F,G	Pattern motion, streaming stimulus	V1	7	26
2.6C-G	Cascade model	PSS	12	54

2.8 Discussion.

In this study, we investigated the properties of visual area PSS in ferrets. While previous studies pointed towards a general involvement in motion processing, our findings now identify PSS as a higher-level motion area. This conclusion is based on striking similarities between PSS and primate MT. Anatomically, PSS – like MT – is more heavily myelinated than the surrounding areas (Philipp et al., 2006; Van Essen et al., 1981), and also receives direct input from V1 (Born and Bradley, 2005; Cantone et al., 2006; Jarosiewicz et al., 2012). In terms of basic responses properties, PSS and MT exhibit a similarly high degree of direction selectivity. In our data, the mean DSI in PSS was .84; previous MT studies report a mean DSI of .8 – 1.05 depending on primate species and stimuli used (Albright, 1984; Baker et al., 1981; Chaplin et al., 2017; Maunsell and Van Essen, 1983). For both PSS and MT, the degree of direction selectivity is significantly higher than that found in V1 (ferret mean V1 DSI = .48. Macaque mean = .56; Albright, 1984; Maunsell and Van Essen, 1983), consistent with an increased specialization for motion processing in PSS/MT.

Similarities extend to more complex motion processing. PSS shows strong motion opponency, at comparable levels to MT (ferret median MOI = .62. Ferret mean = .59. Primate median = .54; Snowden et al., 1991. Primate mean = .36; Qian and Andersen, 1994). In both species, these levels are higher than those observed in V1 (ferret median and mean = .36. Primate median = .04; Snowden et al., 1991. Primate mean = .2; Qian and Andersen, 1994). In addition, in ferrets and primates motion opponency correlates well with direction selectivity in V1 and PSS/MT (Qian and Andersen, 1994; Snowden et al., 1991), and the overall differences in motion opponency between areas can largely be

explained by their different degrees of direction selectivity (Qian and Andersen, 1994). Thus, suppression of opposing direction signals may play an important role in generating direction selectivity across areas and species.

The most important similarity, however, is the existence of pattern cells in PSS, combined with the absence of these cells in V1. As for the primate, this allows us to conclude that lower visual stages like V1 are largely concerned with the extraction of local motion signals, while higher stages like PSS handle local motion integration. We observed 17% pattern cells in PSS for the most commonly used MT stimulus set. Enlarging the stimulus set so that more conditions could be included in the analysis increased this fraction to 45%, with the changes most likely due to an increase in discriminability of pattern and component predictions. In macaque MT, data pooled over many studies resulted in 23% pattern cells (Wang and Movshon, 2016), while 19% pattern cells have been observed in the marmoset (Solomon et al., 2011). Note, however, that these studies usually only include highly direction-selective neurons in their analyses. If we similarly restrict our data set for the 'classic' stimulus set (criterion: DSI > .75), the proportion of pattern cells increases to 27% (13/49). Thus, the proportion of pattern cells in the ferret is comparable to that in the primate. This also holds for the fraction of component cells, which is 27% in PSS using the classic stimulus set, and 37% in the macaque (Wang and Movshon, 2016).

Finally, PSS responses could be fit well with a computational model recapitulating main features of recent MT models, suggestive of similarities between areas on a more fundamental level. This is further supported by the observation that both PSS and MT modeling efforts point to the shape of the direction integration function in PSS/MT as an

important determinant of pattern index. For both models, broader excitatory integration with stronger inhibition is linked with higher pattern indices (Rust et al., 2006). Whether these predictions – which are based on the implementation of a particular motion pathway model – indeed accurately capture the mechanisms underlying motion integration in PSS and MT remains to be verified experimentally.

It should be noted that there are differences between PSS and MT, which so far largely seem to be related to the ferret's overall lower visual acuity (Baker et al., 1998; Price and Morgan, 1987). This includes the observation that PSS receptive fields are significantly larger than those in MT (Figure 2.S2), and that preferred spatial frequencies are lower in PSS (PSS = .06 – .12 cycles/deg. MT = .1 – 4 cycles/deg; Priebe et al., 2003). For other processing aspects it is currently unknown how PSS compares with MT. For example, it remains to be determined whether PSS shares MT's columnar organization for direction (Albright et al., 1984) and whether disparity is represented as strongly as in MT (DeAngelis et al., 1998).

The evolution of motion processing from V1 to higher visual areas is well established in primates (Born and Bradley, 2005; Orban, 2008). The findings presented here are the first demonstration of a very similar cortical motion processing cascade in the ferret, and more generally in a non-primate species. Complex motion processing in carnivores has previously been investigated in the cat. As in the ferret and primate, processing in cat V1 is restricted to local motion signals (Gizzi et al., 1990; Movshon et al., 1985). A number of higher-level visual areas were found to have strong direction tuning in the cat (Spear, 1991). Motion integration was tested explicitly in one of these areas, PMLS, but failed to

reveal pattern cells (Gizzi et al., 1990; Movshon et al., 1985). So far, pattern cells were only found in cat frontal cortex and pulvinar (Merabet et al., 1998; Scannell et al., 1995). Our results strongly suggest the existence of a higher-level visual area with pattern cells in the cat, most likely one of the motion areas not tested so far. Motion processing has also been investigated in the mouse, in which local motion directions are already robustly represented at the level of retina and LGN (Huberman and Niell, 2011; Vaney et al., 2012). Motion integration similarly appears to occur earlier. When probed with coherent plaids, the largest fraction of mouse V1 neurons consistently falls into the 'unclassified' category, in which neurons have intermediate levels of motion integration (Juavinett and Callaway, 2015; Muir et al., 2015; Palagina et al., 2017), unlike the strong predominance of component cells in primate and carnivore V1. Thus, motion processing in the mouse differs notably from that in ferrets and primates. It is possible that motion processing in other rodents proceeds differently: Visual areas ML and L of the squirrel have been shown to contain a large number of direction-selective neurons (Paolini and Sereno, 1998), but motion integration has not yet been studied in this species.

In summary, our data show striking similarities in complex motion processing in ferrets and primates. This presents opportunities for the investigation of higher-level visual processing: A transgenic ferret model of microcephaly was recently established (Johnson et al., 2018), raising the prospect that transgenic ferrets might become increasingly more available. More important, however, are the advantages of ferrets as a developmental animal model. Previous research has already established the developmental timeline of direction selectivity in V1, as well as the impact of visual experience (Clemens et al., 2012; Li et al., 2006, 2008). Our results in adult ferrets lay the foundation to expand this research

into development of complex motion processing in higher-level visual cortex, both under normal and abnormal conditions.

2.9 Methods.

2.9.1 Experimental model and subject details.

All procedures were approved by the Johns Hopkins Animal Care and Use Committee and adhered to the guidelines of the National Institute of Health. Experiments were performed in female sable ferrets (*Mustela putoris furo,* Marshall Farms) with normal immune status, with ages between 1.5 months and 1.8 years. Animals were housed in a 16h light/8h dark or a 12h light/12h dark cycle. Ferrets were not involved in previous studies.

2.9.2 Animal preparation and surgery.

Ferrets were pretreated with atropine (.05 mg/kg, IM) and anesthesia was induced with ketamine (40 mg/kg, IM). After induction, anesthesia was maintained with isoflurane (during surgery: 1.5 – 3%, during recording: .5 – 2%). A tracheostomy was performed and an IV catheter was inserted into the external jugular vein for delivery of 2.5% dextrose in lactated Ringer's solution (4 mL/kg/hr). Body temperature was maintained at 37 – 39 deg C using a heat pad. A small metal plate was attached to the skull with dental acrylic (Dentsply or Lang Dental), which was then connected to a custom stereotaxic apparatus to rigidly hold the head. Two screws were implanted over frontal cortex to record the EEG. Throughout the procedure, heart rate, SpO2, EKG, EtCO2 and EEG were monitored continuously to maintain the animal in an adequate plane of anesthesia. Before the start of recording, animals were paralyzed with pancuronium bromide (.15 mg/kg/hr). Respiration was maintained with a ventilator (Ugo Basile), adjusting breathing rate and volume to maintain the EtCO2 between 3.3 and 4.8%. Neosynephrine and atropine were applied to the eyes to retract the nictitating membrane and dilate the pupil, and animals were fitted

with contact lenses. Before recordings, craniotomies were made above either V1 or the posterior bank of the suprasylvian sulcus to reach PSS. We targeted central visual field regions in V1, and central and more peripheral visual field regions in PSS. Small durotomies were made inside the craniotomies to allow recording probes to penetrate the brain. The brain was covered with 1.5 – 5% agarose (type III-A, Sigma-Aldrich) in artificial cerebrospinal fluid during recordings.

2.9.3 Electrophysiology.

Neural signals were recorded using either custom-made tetrodes made from 12µm nichrome wire (California Fine Wire Company) or 64-channel silicon microprobes (Masmanides lab, UCLA). Tetrodes were plated using a gold solution (Sifco ASC) to reach final impedances of 150-500 kΩ; silicon probes were gold-plated to reach final impedances of 150-300 kΩ. Signals were amplified and recorded using a CerePlex Direct amplifier (Blackrock Microsystems) or a RHD2000 amplifier (intan Technologies). Raw data was acquired at 30 kHz and filtered between 250 Hz and 5 kHz. Spike detection threshold was set manually for each recording based on noise levels. Single unit isolation was performed off-line using MATLAB (MathWorks) custom-made software. Isolation was based on multiple waveform characteristics (e.g., spike amplitude peak, area under the waveform, repolarization phase slope) recorded on the four tetrode channels or on neighboring channels of the silicon probe. Quality of isolation was confirmed by inter-spike interval (ISI) analysis. Units that displayed ISIs below 1.2ms were not included in further analyses.

2.9.4 Visual stimuli and experiment design.

Visual stimuli were generated using the Psychophysics Toolbox extensions for MATLAB (Brainard, 1997; Pelli, 1997) and displayed on a 24-inch LCD monitor with refresh rate of

120 Hz, placed 25 - 35 cm in front of the ferret. The monitor was gamma corrected using a SpectraScan 655 (PhotoResearch). For a subset of experiments, a 43-inch LCD monitor with a refresh rate of 60 Hz was used instead.

Classic stimulus presentations: Experiments consisted of 5 repetitions of each stimulus condition (including a blank condition), presented in a pseudo-random sequence. This presentation mode was used with gratings, plaids, bars, and random dots. Stimulus parameters that varied across conditions are described for each experiment in the results section. Other stimulus parameters for the different experiments are listed below.

Gratings and plaids: Stimulus sizes were optimized for each neuron. In most experiments, stimuli were shown in circular aperture with radius 8 – 30 deg (see Figure 2.S2 for example receptive field sizes); in a few experiments, we instead used rectangular stimuli of 65 x 50 deg.

All experiments used sine-wave gratings. Grating spatial frequency was set to the optimal value for each neuron (range .05 - .1 cycles/deg), as was temporal frequency (range 2 - 6 Hz) outside of the temporal frequency experiment. In plaid experiments, gratings were shown at 50% contrast; otherwise they were shown at 100% contrast. Plaids shown using the classic presentation mode were generated by superimposing two 50% contrast sine-wave gratings of optimal spatial and temporal frequency at an intersection angle of 135 deg. Plaids were always shown at full contrast. Stimuli were presented interspersed with presentation of a gray screen of equal mean luminance. Stimuli were presented for 1 s with inter-stimulus intervals of 2 – 5 s.

Drifting bar stimulus: We presented either a white bar on a black background or a black bar on a white background, depending on the preferences of the neuron under study. Bar size was set to 10 x 5 deg. Bars moved perpendicular to their orientation, and their starting point was adjusted such that the bar reached the center of the neuron's receptive field at half the stimulus presentation time. Static bars were positioned in the center of the neuron's receptive field. Bar presentations were interspersed with presentation of a blank stimulus of background color. Stimuli were shown for 1 s, and inter-stimulus intervals ranged from 2 to 5 s.

Random dot kinematograms: Random dot stimuli consisted of white dots on a black background. Dot size, density and speed were set manually to elicit the strongest neuronal responses. Dot radius ranged from 1 – 2 degrees, speed from 15 - 60 degrees/s, and dot density from .8 – 3.5 dots per 100 degree^2. This resulted in inter-dot distances of 3 - 7.5 deg, similar to a previous PSS study using random dot stimuli (Philipp et al., 2006). The overall size of the stimulus was also optimized for each neuron (either circular with radius of 15 – 30 deg, or 65 x 50 deg). To avoid contamination of responses by luminance changes, the presentation of dot motion was preceded by a static presentation of the first frame of the random dot stimulus, displayed for 2 – 3 s. The dots were then moved for 1 s. Any dot that left the stimulus aperture during this time period was replotted in a random position on the opposite side of the stimulus to preserve dot density. At the end of the stimulus, the last frame was shown static for another 1 – 2 s. Different random dot stimuli were separated by brief presentations of a black screen. In some of the motion opponency experiments (mostly using tetrodes), we first determined the preferred direction of each neuron manually, and then only presented the preferred, null and motion opponency stimuli. In the

rest of the experiments, we instead sampled 8 or 12 directions for the single direction stimuli. We also generated motion opponency stimuli for each of these directions by superimposing the opposing direction.

Streaming stimulus presentation: Each trial consisted of a 60 s long sequence of short stimulus presentations (3 - 6 stimuli/s). Each sequence was preceded and followed by a 2 s presentation of a gray screen of equal mean luminance. Stimulus sequence was determined randomly by picking from all stimulus conditions with replacement. The following stimulus conditions were used: blank (uniform gray screen), 100% contrast sine-wave gratings moving in 16 directions, and plaids with 7 different component intersection angles (dOri; 22.5, 45, 67.4, 90, 112.5, 135 and 157.5 deg) moving in 16 directions. In a subset of experiments, we also included 50% contrast gratings moving in 16 directions. Spatial frequency (.05 - .15 cycles/deg), temporal frequency (2 – 5 Hz) and stimulus size (circular aperture of radius 10 – 35 deg) were optimized per neuron. For each stimulus, the initial phase of each grating was chosen randomly from 4 possible values (0, 90, 180 and 270 deg). 30 or 45 trials were run for each experiment, which ensured that each stimulus was presented at least 10 times.

2.9.5 Data analysis and inclusion criteria.

Classic stimulus presentations: For gratings, plaids and random dots, neuronal responses were calculated as the firing rate during stimulus presentation minus the firing rate during the last second of the pre-stimulus period. For bar stimuli, firing rates were measured during the time period in which the stimulus was within 20 deg of the center of the receptive field, corrected assuming a fixed response latency of 50 ms. All neurons were then screened

for general stimulus responsiveness. For gratings, plaids and bars, we performed this test by using a one-way ANOVA to compare responses across all stimulus conditions (including the blank). Only cells that passed $p < .01$ for the ANOVA were included in further analyses. For random dot stimuli, we tested for responsiveness using a t-test between the best single direction stimulus and the blank, using a Bonferroni correction to adjust for multiple comparisons (either 2, 8 or 12, depending on how many directions were shown in an experiment). Cells that passed $p < .05$ were included in further analyses. In addition to these tests, neurons with a mean response lower than 2 Hz for the best stimulus condition were excluded. For all remaining neurons, tuning properties were then calculated from mean responses across stimulus repetitions.

Streaming stimulus presentation: Computing stimulus-evoked responses from the streaming stimulus requires shifting spike times relative to stimulus onset to account for response latency. The analysis used to determine the optimal delay was based on the assumption that stimulus differences would be most pronounced for the real response latency, while other delay values would dilute these differences because of incorrect stimulus-response assignments (Smith et al., 2005). First, we computed mean responses for all stimuli in stimulus-locked, 150 ms-long windows, offset from stimulus onset by 20 different delays ranging from 0 to 475 ms. When computing the mean, the initial phase of the gratings was ignored. For each delay, we then subtracted the mean blank response from all stimulus conditions (including the blank), and compared all conditions using a one-way ANOVA. The resulting p-values were Bonferroni corrected to account for the 20 comparisons. The delay resulting in the smallest p-value was then used in all further analyses for the neuron. At this point, neurons for which the smallest p-value was larger

than .01 (after correction) were excluded. Two additional criteria were used to remove cells with limited responsiveness to gratings and/or plaids: For one, cells had to pass an ANOVA across all plaids with dOri = 90 deg and the blank with $p < .01$, using the optimal delay to compute responses. For the other, the responses to the best grating and the best plaid with dOri = 90 deg had to be larger than 2 Hz.

2.9.6 Tuning curve analyses.

Direction selectivity was quantified using a direction index comparing responses between preferred and null direction, which was computed as

$$DSI = 1 - \frac{R(N)}{R(P)}$$

where R(P) is the response to the preferred direction, and R(N) is the response to the null direction. For drifting bar experiments we computed a low-pass index as

$$Low - pass\ index = 1 - \frac{R(S_{max})}{R(S_{pref})}$$

where S_{max} indicates the fasted speed sampled (160 deg/sec), and S_{pref} indicates the neuron's preferred speed. The strength of motion opponency was determined by computing the following index:

$$MOI = 1 - \frac{R(MO)}{R(P)}$$

Here, R(MO) indicates the response to the motion opponency RDK and R(P) the response to the preferred RDK.

2.9.7 Analysis of plaid responses:

Classic stimulus presentations: We used standard methods to compute partial correlations between the measured responses to plaids and predictions for pattern and component responses (Movshon et al., 1985). Partial correlations were then Z-transformed to stabilize the variance and allow comparisons across conditions. The Z-transform was computed as (Smith et al., 2005):

$$Z = \sqrt{N-3}\frac{1}{2}\ln\left(\frac{1+r}{1-r}\right)$$

where r is the partial correlation (either pattern or component), and N refers to the number of points in the correlation (here, 16). Cells were classified as pattern cells if they met $Z_P - Z_c > 1.28$ for $Z_C \geq 0$, and $Z_P > 1.28$ otherwise. Component cells had to meet the opposite criterion. We also computed a pattern index as Z_P-Z_C. As in the cell classification, any negative values (Z_P or Z_C) were set to 0 when computing the index.

Streaming stimulus presentation: Each neuron's pattern and component predictions were computed for the larger plaid stimulus set in the following way: For the pattern prediction, we computed a direction tuning curve by averaging responses across all plaids with a shared pattern direction, as well as the gratings moving in the same direction. We also computed a dOri tuning curve, which was estimated by averaging across all stimuli with the same dOri. The complete pattern prediction was then computed as the product of the direction and dOri tuning curves.

For the component prediction, we first estimated a direction tuning curve as a function of component direction by averaging across all plaid stimuli with a shared component direction (i.e. each plaid contributed twice), as well as the gratings moving in the same

direction. This tuning curve was then transformed into a function of plaid direction by summing two copies of the component direction curve at each dOri, shifted relative to each other according to the dOri value. The resulting direction tuning curve was multiplied with the dOri tuning curve (identical to the one used for the pattern prediction) to generate a complete component prediction. We then computed partial correlations of each neuron's actual responses with the two predictions, and converted these values to Z-scores as before (with N set to 112 to account for the 7 plaid sets and 16 directions involved in the computation).

2.9.8 Image-computable cascade model.

Stimulus: We presented 1 s of each stimulus, divided into 50 frames, to the model. Stimuli were modeled to span 50 by 50 degrees of visual space, with a spatial resolution of .25 degree/pixel. Thus, each stimulus could be summarized by a 200 x 200 x 50 matrix. Stimuli consisted of gratings and plaids. Spatial frequency was fixed at .1 cycles/deg and temporal frequency at 1 cycles/s. Gratings and plaids could move in 16 different directions. Gratings were shown at 50% and 100% contrast, and plaids were constructed from 50% gratings using 7 different values of dOri. This stimulus set replicates the entire set of conditions used in the streaming stimulus experiments.

Thalamic layer: LGN responses were calculated for each pixel in each frame of the stimulus matrix using a 2D LGN receptive field centered on each pixel. Receptive fields consisted of center and surround components modeled as 2D Gaussian functions with σ = 2 deg and 6 deg, respectively. Values were set to reflect the size of ferret LGN receptive field centers (Tavazoie and Reid, 2000; Zahs and Stryker, 1985) and center-surround size

ratios of cat LGN (Cai et al., 1997), similar to a previous image-computable LGN model (Koch et al., 2016). Gaussian amplitudes were set so that the response to a homogeneous field with no contrast was 0 and the maximum response to a 100% contrast grating was 1.

Following the spatial filtering induced by the receptive field structure, we scaled responses at each pixel according to a contrast response function. This function was implemented as a hyperbolic function of the form

$$R = \frac{r^N}{r^N + C_{50}^N}$$

with r representing the value at each pixel derived after applying the spatial filters. C_{50} and N are free model parameters. This kind of function has been widely used to model contrast-response functions, and fits well to experimental data (Albrecht and Hamilton, 1982; Alitto and Usrey, 2004; Koch et al., 2016; Rathbun et al., 2016).

V1 simple cell layer: Responses of V1 simple cells were computed by applying space-time oriented Gabor filters to the output of the LGN layer, and then summing the output of each filter across all pixels and time. Following the standard motion energy model (Adelson and Bergen, 1985), we used two Gabor filters with a quadrature relationship per direction channel. In total, we used 16 direction channels, set to be 22.5 deg apart. We set the width of the V1 receptive fields (σ) to 5 deg, the spatial frequency to .1 cycles/deg, and the temporal frequency to 1 cycle/s. Receptive field size was chosen based on experimental estimations of LGN to V1 receptive field ratios in carnivores (Alonso et al., 2001; Jin et al., 2011). The ratio between V1 receptive field size and spatial frequency determines the orientation tuning of modeled V1 neurons. It was set so that V1 orientation tuning

(quantified as the circular variance (Batschelet, 1981; Mazurek et al., 2014; Ringach et al., 2002) of the model's complex cells) was consistent with the high end of circular variance encountered in our own recordings from ferret V1 (circular variance of .81). All of our model V1 neurons were direction selective by design. This is consistent with MT motion pathway models, which usually assume a purely direction-selective V1 stage (Baker and Bair, 2016; Rust et al., 2006; Simoncelli and Heeger, 1998; Tsui et al., 2010).

V1 complex cell layer: Responses in the complex cell layer were computed by combining the output of the even and odd Gabor filter for each direction channel, following the standard motion energy model (Adelson and Bergen, 1985; Baker and Bair, 2016):

$$c = \sqrt{s_{even}^2 + s_{odd}^2}$$

where s represents the output of the V1 simple cell stage for one direction channel. We compute the square root of the simple cell responses to maintain the shape of the contrast response functions set in the LGN stage. For plaids, the phase difference between the two component gratings impacts the model's response at the complex cell stage. To eliminate response contaminations caused by phase differences, responses to four plaids with different phase differences were computed, and the responses were averaged in the complex cell layer before being passed to the PSS layer.

PSS layer: In the last stage of the model, the responses of the 16 V1 complex cells were combined linearly. We used two weight functions for this purpose, one representing excitatory interactions and one inhibitory. Weight functions were modeled as

$$W_E(\theta) = \frac{1}{\sqrt{2\pi B_0(k_E)}} \exp(-k_E \cos(\theta - \theta_P))$$

and

$$W_I(\theta) = \frac{1}{\sqrt{2\pi B_0(k_I)}} \exp(-k_I \cos(\theta - \theta_N))$$

Here, $B_0(k)$ is a modified Bessel function of order 0, θ is one of the 16 directions represented in V1, θ_P is the direction preference of the PSS neuron, and θ_N is its null direction (i.e., $\theta_N = \theta_P + 180$ deg). k_E and k_I define the width of the weight functions and are free model parameters. The two weight functions are then combined into one final weight functions by computing

$$W(\theta) = W_E(\theta) - I * W_I(\theta)$$

I, which determines the relative amplitude of the inhibitory weights, is another free model parameter. The final stage of the model represented an output nonlinearity in PSS. We implemented this nonlinearity as a half-wave rectification by setting all responses below a threshold T to 0. T was the final free model parameter, and was expressed as a fraction of the maximum response of the modeled PSS neuron.

Model fitting: One million instances of the model were computed using 10 possible values for each of the 6 variables described above. For each direction-selective PSS cell (DSI > .75), we then picked the model instance with the lowest mean square error. To test for model over-fitting, a control data set was generated by shuffling the responses of each neuron across all conditions. We then fit the model to this control data set as described above for the real data.

2.9.9 Quantification and statistical analysis.

We used a one-way ANOVA or two-sided t-test to decide whether to include neurons in the data sets used for more detailed analysis (described in the previous section). Results of any test were Bonferroni-corrected where necessary. For statistical comparisons of two data sets, we used Wilcoxon rank-sum or Wilcoxon signed-rank tests as well as Kolmogorov-Smirnov tests. Center and spread values are reported as median or mean ± SEM, unless noted otherwise. Correlations were calculated as Pearson's. Statistical tests and significance levels are reported in the Results section and Figure legends, and exact n values in Table 2.1. No tests were conducted to check for normality or homogeneity of variance. All statistical analyses were performed using MATLAB software.

2.10 Supplementary figures.

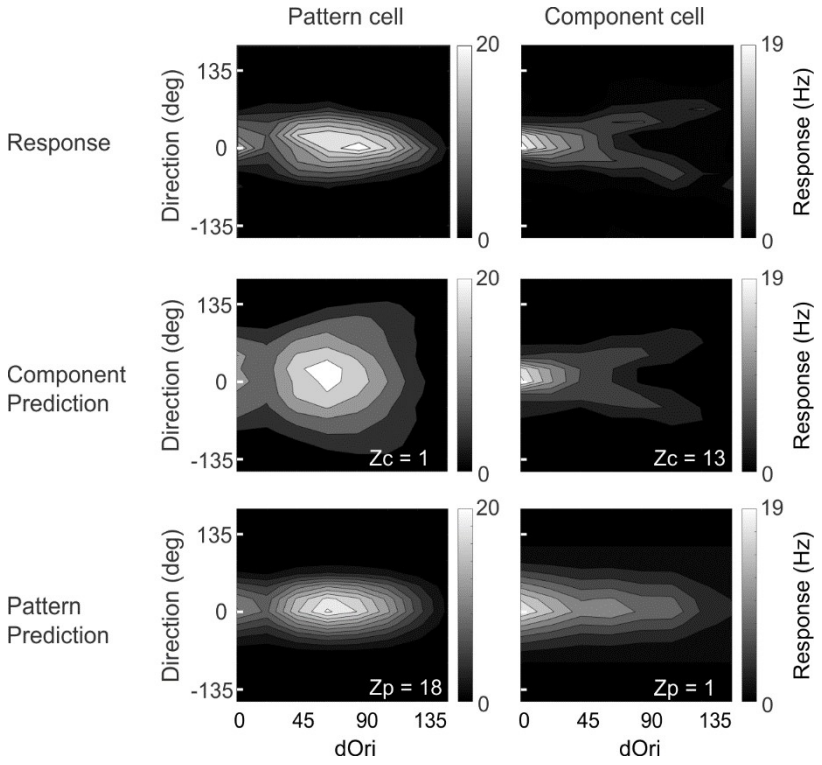

Figure 2.S1: Example pattern and component predictions based on streaming stimulus set.
Pattern and component predictions for two PSS neurons, computed based on responses to the large plaid stimulus set. The figure shows responses (upper row), component predictions (middle row) and pattern predictions (bottom row) for a pattern (left column; same neuron as in Figures 2.5C and 2.6B) and component cell (right column; same neuron as in Figure 2.6B). Z_C and Z_P for both neurons are indicated in the plots.

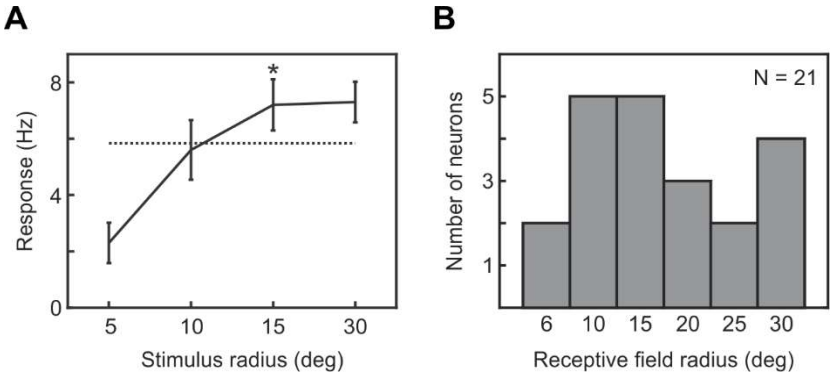

Figure 2.S2: PSS receptive field estimation using gratings.
(A) Example response of a PSS neuron to gratings of different sizes drifting in the neuron's preferred direction (error bars: ± SEM). The receptive field size of the neuron (indicated by *) was estimated as the smallest stimulus size that elicited a response of at least 80% of the maximum response (dotted line).
(B) Estimated receptive field radius across all recorded PSS neurons. The median receptive field radius for our population of PSS neurons was 15 degrees.

Chapter 3. Development of multi-stage processing in the ferret motion pathway

3.1 - Introduction.

Information processing in cortical pathways involves multiple, increasingly complex transformations, which are commonly implemented by different brain areas. To understand how cortical pathways develop, we must investigate how their different stages interact as they mature. The visual system is one of the best understood sensory processing pathways. So far, the study of visual cortex development has, with few exceptions, been limited to primary visual cortex (V1). Therefore, knowledge of possible mechanisms behind the emergence of multi-stage cortical processes is limited.

The processing of complex motion signals by the visual system provides a unique opportunity to investigate multi-stage information processing. The transformation of motion signals across the visual hierarchy has been studied most extensively in the primate. In this species, local direction-selective signals are first computed in V1 (Hubel and Wiesel, 1968; Orban et al., 1986), and then further processed in area MT. In particular, MT integrates the local motion signals extracted in V1 to compute global pattern motion (Movshon et al., 1985). This transformation can be studied using plaid stimuli, which are constructed from two component gratings moving in different directions, but are perceived to move in a third, intermediate global direction (Adelson and Movshon, 1982). In addition to a set of established stimuli commonly used to study motion integration, relatively simple

feed-forward models have also been developed to explain the motion integration observed in MT (Baker and Bair, 2016; Rust et al., 2006; Simoncelli and Heeger, 1998; Zarei Eskikand et al., 2016). These models can serve as key tools for probing possible mechanisms underlying the processing of complex motion signals. The framework provided by these previous experimental and computational studies make the motion pathway a particularly useful system for studying the development of multi-stage processes.

Currently, very limited data on the development of higher-level motion areas has been collected in cats (Price et al., 1988; Spear and Tong, 1980; Spear et al., 1985) and primates (Kiorpes and Movshon, 2014). The ferret offers a unique opportunity to study visual development due to its immature state at birth. Previous studies have taken advantage of the ferret to study development in lower-order visual structures (Sharma and Sur, 2014). This research revealed that direction selectivity matures in V1 during the first week after eye opening and is dependent on visual experiences (Clemens et al., 2012; Li et al., 2006, 2008). Preceding this thesis, it was unknown whether ferret visual cortex contained dedicated higher-order motion areas. Therefore, developmental studies could not extend beyond early stages of motion processing. In Chapter 2, we used plaid stimuli to show that ferret V1 and PSS form a motion pathway comparable to that formed by V1 and MT in the primate. The ferret motion pathway therefore offers a unique model to study the development of multi-stage processing in the visual system.

In this chapter, we combine extracellular recordings in PSS and V1 across development with a computational model and inactivation experiments to study the development of

multi-stage processing in the ferret motion pathway. By analyzing responses to gratings and plaids, we establish a developmental timeline for the emergence of direction selectivity and pattern motion tuning in PSS. Our data show that PSS direction selectivity develops during the first week after eye opening, a similar timeline as that described for development of direction selectivity in V1 (Clemens et al., 2012; Li et al., 2006). In contrast, pattern motion tuning develops after direction selectivity during the second week after eye opening. Fitting a feed-forward computation model for the motion pathway to the PSS responses identified potential mechanisms behind the observed emergence of pattern responses. These mechanisms include changes in PSS inhibition and an increase in V1 response strength for plaids versus gratings. By comparing model predictions with actual V1 responses, we show that temporary changes in V1 relative plaid responses are consistent with the model predictions. In addition to this change, plaid responses in V1 were shifted to be less component-like and more pattern-like as pattern cells emerge in PSS. Finally, we show that PSS inactivation reverses the aforementioned temporary changes in V1. Our results show coordinated changes in V1 and PSS that, at least in part, depend on feedback. This conclusion is consistent with a role of the bi-directional interaction between V1 and PSS in the emergence of pattern responses. The mechanisms proposed here for the development of the ferret motion pathway may represent more general strategies driving the emergence of multi-stage processing in the visual system.

3.2 - Results: General description of experiments.

In order to investigate the development of motion responses in area PSS, single unit recordings were performed in anesthetized, paralyzed ferrets. Recordings were done using either custom-made tetrodes or multi-channel silicon probes (see methods). PSS responses were measured for a variety of visual stimuli in adult ferrets (3-13 months old) and kits aged postnatal day (P) 30 - 48. This age range spans a developmental period from just before eye opening (~P30) to about 18 days of visual experience.

3.3 - Results: Simple direction tuning properties develop in PSS during the first week of visual experience.

As a first step, we determined the development of direction selectivity in PSS, since it is fundamental to processing of motion information. To analyze simple direction tuning, responses of PSS neurons to gratings moving in 12 different directions were measured. Gratings were either sinusoidal or square-wave and were displayed at 100% contrast. For a subset of the adult data, 50% contrast sinusoidal gratings moving in 16 directions were used instead. From these responses, direction selectivity was computed using a direction selectivity index (DSI). Values close to 1 for this index indicate strong selectivity, while values close to 0 indicate a lack of selectivity. We also used the grating responses to quantify orientation tuning using the circular variance (OCV). Similar to the DSI, values close to 1 for this index indicate strong selectivity, while values close to 0 indicate a lack of selectivity.

Both of these tuning properties changed across development (Figure 3.1). Differences were significant when all ages are considered (one-way ANOVA with factor age: DSI $p = .001$, OCV $p = .003$). To further compare differences across age groups, post-hoc Rank-sum tests were computed. For this and all other statistical analyses in this chapter, only significant p values are mentioned in the text. A complete list of all tests can be found in Table 3.1. These post-hoc tests revealed that PSS direction selectivity was significantly lower around the time of eye opening than in adults (median DSI: P30-32: = .45, adult = .82; Rank-sum test: $p < .001$). After P35, the DSI distribution shifted towards higher values, indicating that direction selectivity emerges between P35 and P37 (median DSI: P35 = .59, P37 = .91. Rank-sum test: $p = .01$). Orientation selectivity similarly matured a few days after eye opening: While the OCV distribution was significantly shifted to lower values around eye opening (median OCV: P30-32 = .17, Adult = .40; Rank-sum test: P30-32 vs Adult $p < .001$), it reached the adult state around P35 (median OCV P35 = .41. Rank-sum test: P30-32 vs P35 $p < .001$.).

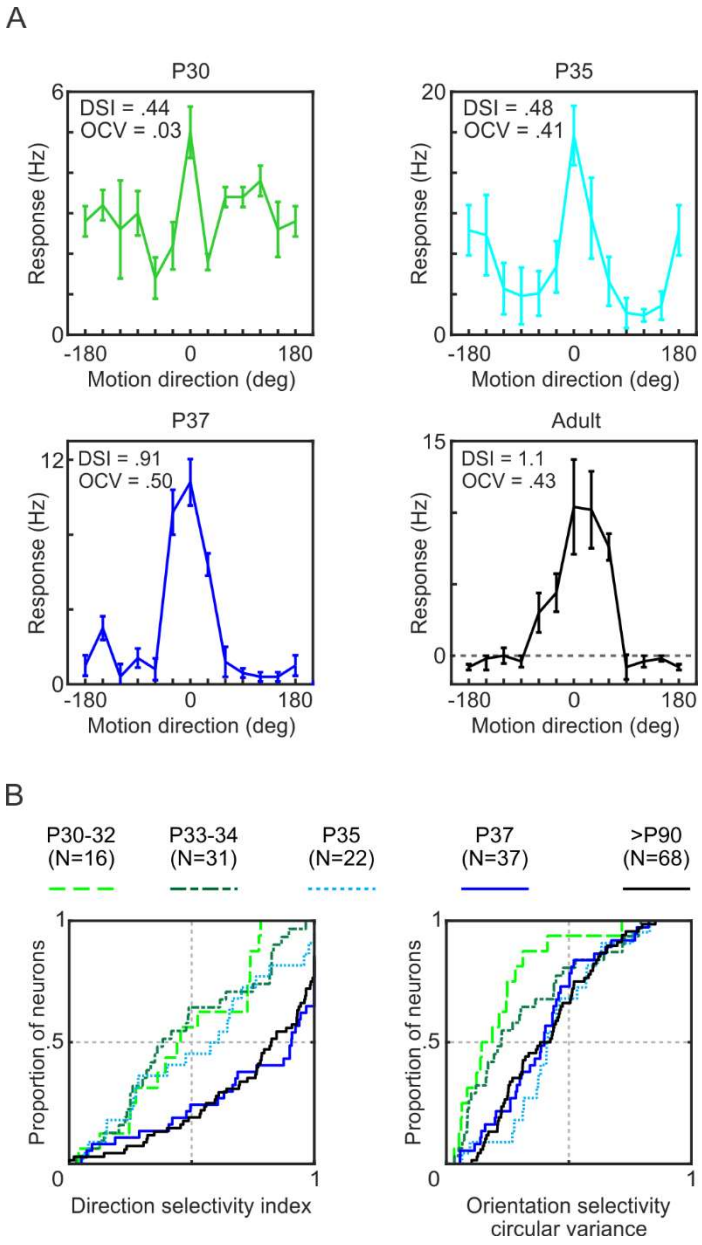

Figure 3.1: Direction selectivity develops in PSS during the first week after eye opening (P30-37).
(A) Direction tuning of example PSS cells at different developmental stages. Error bars represent ± SEM. (B) Cumulative distribution plots for the direction selectivity index (DSI, Left) and orientation selectivity circular variance (OCV, Right) in PSS at different ages. Significance tests between data from different age groups can be found in Table 3.1.

3.4 - Results: Pattern motion tuning develops in PSS during the second week of visual experience and continues to be refined until adulthood.

After characterizing the development of simple tuning properties, we then focused on the emergence of complex pattern responses in PSS. As a first approach to analyze pattern motion tuning across development, we used 50% contrast gratings, as well as plaid stimuli similar to those commonly used for MT (Movshon et al., 1985). Here, plaid stimuli were constructed from two sinusoidal gratings with an intersection angle (dOri) of 135 deg between their directions (Figure 3.2A). This large difference between the two component directions helps to differentiate pattern and component responses in cells with wide direction tuning curves. Gratings and plaids could move in 16 different directions. Stimuli lasted 1 s and were presented in a pseudo-random order (see methods). Responses to the gratings were used to compute direction tuning curves for each neuron. Based on the direction tuning curves, we then generated predictions for pattern and component responses to the plaids, and compared them to the experimentally measured plaid responses (Figure 3.2B). The similarity between the measured responses and each prediction was quantified by computing a Fisher z-corrected correlation (see methods). This computation yielded a pattern and component correlation for every cell that could be used to assess the degree to which it resembled a pattern or component neuron. To more directly quantify the amount of motion integration observed in a neuron, we also computed a pattern index by subtracting the pattern correlation from the component correlation. Positive numbers for this index represent stronger pattern motion responses, while negative numbers represent stronger component responses.

Considering that pattern cells in adult PSS are exclusively direction-selective (using a criterion of DSI > .7; Figure 3.2C), only direction-selective cells were considered for this analysis. In addition, the youngest age sampled by these experiments was after complete maturation of direction tuning (P37-41). At this age, the majority of PSS cells were classified as component cells (71%, N = 14. Figure 3.2D) and we found no pattern cells. In contrast, when the same analysis was applied to adult PSS cells, a sizable proportion of pattern cells were found (21%, N = 33. Figure 3.2D). Furthermore, the pattern index of PSS cells (Figure 3.2E) was significantly lower at P37-41 than in adults (median pattern index: P37-41 = -2.79, adults = -0.25. Rank-sum test: P37-41 vs Adult p = .005). These results indicate that pattern responses are still immature in PSS after the first week of visual experience.

In this first experiment, plaids were constructed using a single dOri. Yet, plaids can be constructed from a range of dOris. Even though plaids with different dOris differ in appearance (Figure 3.3A) and perceived speed, the perception of coherent pattern motion is maintained (Adelson and Movshon, 1982). In agreement with this perception, pattern cells in PSS have a consistent direction tuning for plaids of different dOri values, albeit with some modulations in response strength that depend on dOri (see Chapter 2). In addition, we have shown that including a wider diversity of plaid stimuli enhances the ability to differentiate between component and pattern responses (see Chapter 2). Using plaids with different dOri values therefore is a useful tool to test whether the lack of pattern cells at P37-41 could be due to a lack of responsiveness to the particular plaid stimuli used or a failure to differentiate between component and pattern responses at this age.

To resolve this question and to analyze motion processing across development in more detail, we tested plaid responses in PSS from P37 to adulthood using a larger set of plaids. A 'streaming stimulus' paradigm (Figure 3.3A. See methods) was used to measure responses to 7 sets of plaid stimuli with dOri values ranging from 22.5 to 157.5 deg. As before, gratings were also included in this stimulus set. Based on responses to this large stimulus set, we computed component and pattern predictions as previously described (see Chapter 2). In short, responses to the stimulus set can be summarized as two-dimensional tuning profiles across stimulus direction and dOri (Figure 3.3B). We therefore computed two tuning curves: one for either component or pattern motion direction and one for dOri. The component direction tuning curve was computed by averaging responses across plaids that share a motion direction for one component (each plaid stimulus contributed twice) as well as gratings moving in the same direction. Similarly, the pattern direction tuning was computed by averaging responses across plaids that share the same pattern motion direction, again including gratings with matching directions. The dOri tuning curve was calculated as the mean responses to plaids that share the same dOri. Finally, component and pattern predictions were generated by combining the dOri tuning curve with either the component direction or the pattern direction tuning curve, respectively. Predictions were then compared with measured responses by computing Z-corrected partial correlations.

Both pattern (Figure 3.3C) and component cells (Figure 3.3D) were found across all age groups in these experiments. Yet, when responses were analyzed at the population level, the distribution of both component and pattern correlations changed significantly between P37 and P48 (one-way ANOVA across all age groups: Z_C $p < .001$. Z_P $p < .001$). In the youngest age group (P37-41), this analysis revealed an undeveloped state of pattern

responses in PSS. At this age, we found a lower percentage of pattern cells than in the adult (12% vs 39% in adults. Figure 3.4A), as well as an overall lower pattern correlation (median pattern correlation: P37-41 = 2.57, adult = 5.23. Rank-sum test: P37-41 vs Adult $p < .001$. Figure 3.4B). Interestingly, this undeveloped stage of PSS motion responses was not characterized by a general lack of both pattern and component tuning. Instead, we observed a robust representation of component motion. This is illustrated both by a higher percentage of component cells (76% vs 42% in adults. Figure 3.4A) and a higher component correlation (Figure 3.4B) than observed in the adult (Median component correlation: P37-41 = 7.88, adult = 5.24. Rank-sum test: P37-41 vs Adult $p < .001$). The strong component responses at the population level could also be identified by computing a population plaid tuning curve, which was computed by averaging the responses of all cells after normalizing them by their maximum. Again, the population tuning function showed a strong component-like response at P37-41 (Figure 3.4C).

By applying the same analysis to plaid responses in animals only few days older (P42-43), significant changes in PSS motion processing were observed. At this age, pattern motion tuning became stronger, as illustrated both by an increase in the proportion of pattern cells (29%. Figure 3.4A) and the pattern correlation (Median pattern correlation: P42-43 = 4.07. Rank-sum test: P42-43 vs P37-41: $p = .02$. Figure 3.4B). In addition, the representation of component motion was weaker than in the younger age group (Component cell proportion 54%. Median component correlation: P37-41 = 7.88, P42-43 = 5.45. Rank-sum test: $p = .002$. Figure 3.4A and 3.4B). At the same time, plaid responses at this age appear immature when compared to the adult. The proportion of pattern cells was smaller than in the adult (P42-43 29%. Adult 39%, Figure 3.4A). In addition, there was a tendency to smaller pattern

correlation values at P42-43 than in the adult (median pattern correlation: P42-43 = 4.07, adult = 5.23. Rank-sum test: p = .07. Figure 3.4B). Finally, computing the population tuning profile resulted in a tuning shape that did not resemble either component or pattern responses (Figure 3.4C).

By age P44-48, a week after the maturation of direction selectivity, pattern motion tuning in PSS reached mature levels. At this age, both the proportion of pattern cells (44%. Figure 3.4A) and the degree of pattern correlation (Figure 3.4B) increased relative to that at P42-43 (Median pattern correlation: P42-43 = 4.07, P44-48 = 5.36. Rank-sum test: p = .01) and were comparable to that in the adult (Rank-sum test: P44-48 vs adult: p = .68). The population tuning at this age was similar to that in the adult and appeared more pattern like than that in younger animals (Figure 3.4C).

The fast developmental timeline of pattern motion processing can also be summarized by computing the pattern index for each recorded PSS neuron (Figure 3.4B). Consistent with the timeline outlined above, the pattern index increased during the second week after eye opening (one-way ANOVA across all age groups: Z_C $p < .001$. Z_P $p < .001$). The largest shift of this index occurred between P37-41 and P42-43 (Median pattern index: P37-41 = -5.55, P42-43 = -1.38. Rank-sum test: p = .002) and reached mature levels by P44-48 (Median pattern index: P44-48 = 0.18, adult = 0.14. Rank-sum test: p = .72).

The analysis discussed so far revealed that, while the proportion of pattern cells found in PSS increases across development, a population of pattern cells can be detected even at P37-41. As mentioned above, pattern cells can modulate their response to plaids as a function of dOri while still representing pattern motion. It remains untested whether pattern

cells differ across development in this or some other aspect that may not affect the representation of pattern motion itself. To investigate this, a plaid tuning curve was computed by averaging the responses of pattern cells after normalizing them by their maximum. The overall plaid tuning of pattern cells was similar for all age groups (Figure 3.4D). This result indicates that pattern cells represent plaid motion similarly across development.

Consistent with previous results (see Chapter 2), the pattern index was correlated with an increased response to plaids relative to gratings in adult animals (Figure 3.5A). This could be important for increasing the relative weight of pattern over component responses in PSS. We therefore analyzed potential developmental changes in the relative plaid responses of pattern cells. To this end, we focused on pattern cells exclusively, and normalized their responses to plaids moving in the preferred direction by the response to a grating moving in the same direction as a function of dOri. The resulting relative response curves were then averaged across all pattern cells within each age group (Figure 3.5B). The relative response to plaid stimuli increased significantly across development (two-way ANOVA across all age groups. Age and dOri as variables. Contribution of age $p < .001$). At P37-41 plaid responses were less than half of those for gratings even for dOri values below 90 deg. Relative plaid responses increased throughout development to reach final magnitudes of 60 to 100% of the grating response. The developmental increase in relative plaid responses was significant between P42 and adults (two-way ANOVA contribution of age: P42-43 vs P44-48: $p = .02$; P44-48 vs Adult: $p = .03$). No significant increase was found between P37-41 and P42-43 (two-way ANOVA P37-41 vs P42-43: contribution of age $p = .11$). Therefore, the maturation of these responses may occur later than the change in component

correlation between P37-41 and P42-43, and it may extend for a longer period between P42 to adulthood. In addition to the increase in the relative plaid responses of pattern cells, the overall correlation between relative plaid response and pattern index increased significantly from P37-41 to adults (Correlation coefficient: P37-41 = .23. Adult = .63. Z-scored difference in correlations p = .01. Figure 3.5A).

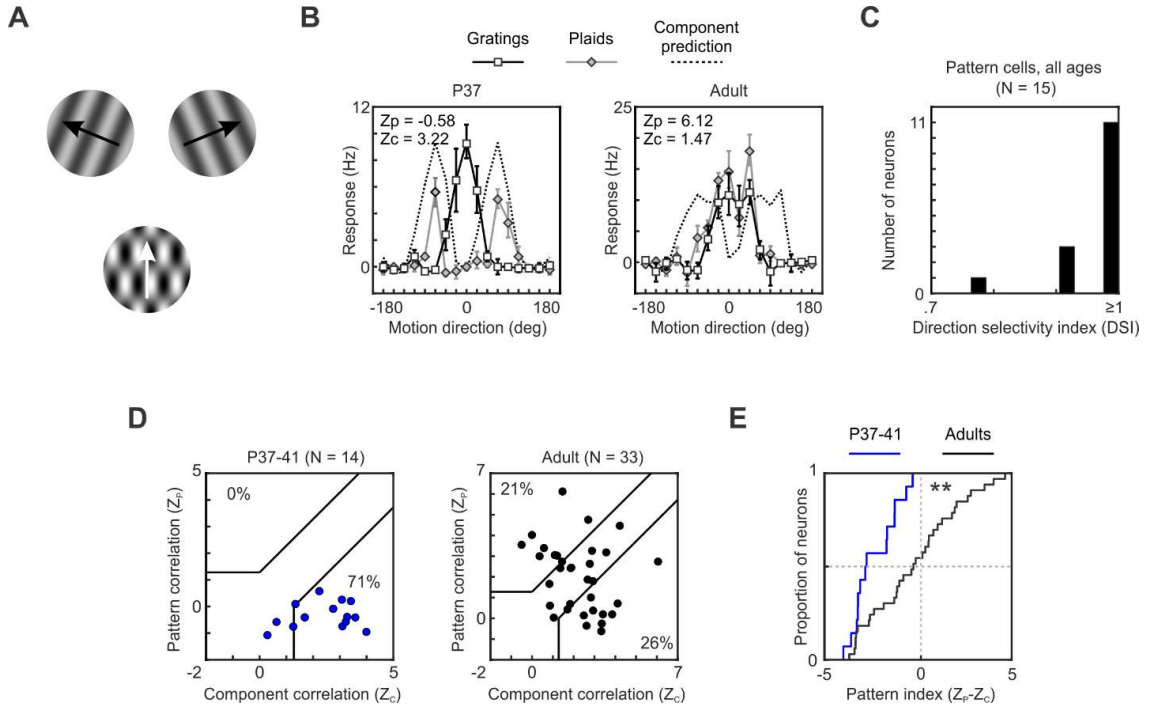

Figure 3.2: PSS pattern responses are immature at P37-41.
(A) Schematic representation of plaid construction for the 'classic' stimulus paradigm: Two component gratings and their directions are shown on the top. The direction difference angle for these components is 135 deg (top). The resulting plaid and its pattern direction is shown on the bottom.
(B) Direction tuning curves of an example PSS component cell at P37 (left) and a PSS pattern cell in an adult ferret (right). Direction tuning was measured using plaids (gray) and gratings (black). Direction is relative to the neuron's preferred direction for the grating. For the plaid responses, direction indicates the perceived pattern direction (the components move at ±67.5 deg relative to this direction). For each neuron, the measured plaid tuning curve is compared to two predictions, one for idealized pattern responses (tuning curve identical to the grating tuning curves), one for idealized component responses (prediction indicated by dashed lines). Z-transformed partial correlation indices Z_P and Z_C indicate how closely the measured plaid tuning curve resembles these predictions. Error bars: ± SEM.
(C) DSI distribution for all PSS pattern cells encountered in experiments using the 'classic' presentation mode (independent of age). A subset of this data was collected from animals aged P45-P88 and is not included in the following graphs.
(D) Pattern versus component selectivity for PSS neurons at P37-41 (left) and in adult animals (right). For each neuron, Z_P is plotted against Z_C. Black lines indicate the category boundaries used to classify cells into pattern, unclassified and component cells. Percentages indicate the portion of neurons falling into the different categories.
(E) Cumulative pattern index distribution for PSS neurons at P37-41 and in adults. Same data as (D). ** = $p < 0.01$ using rank-sum test (see Table 3.1).

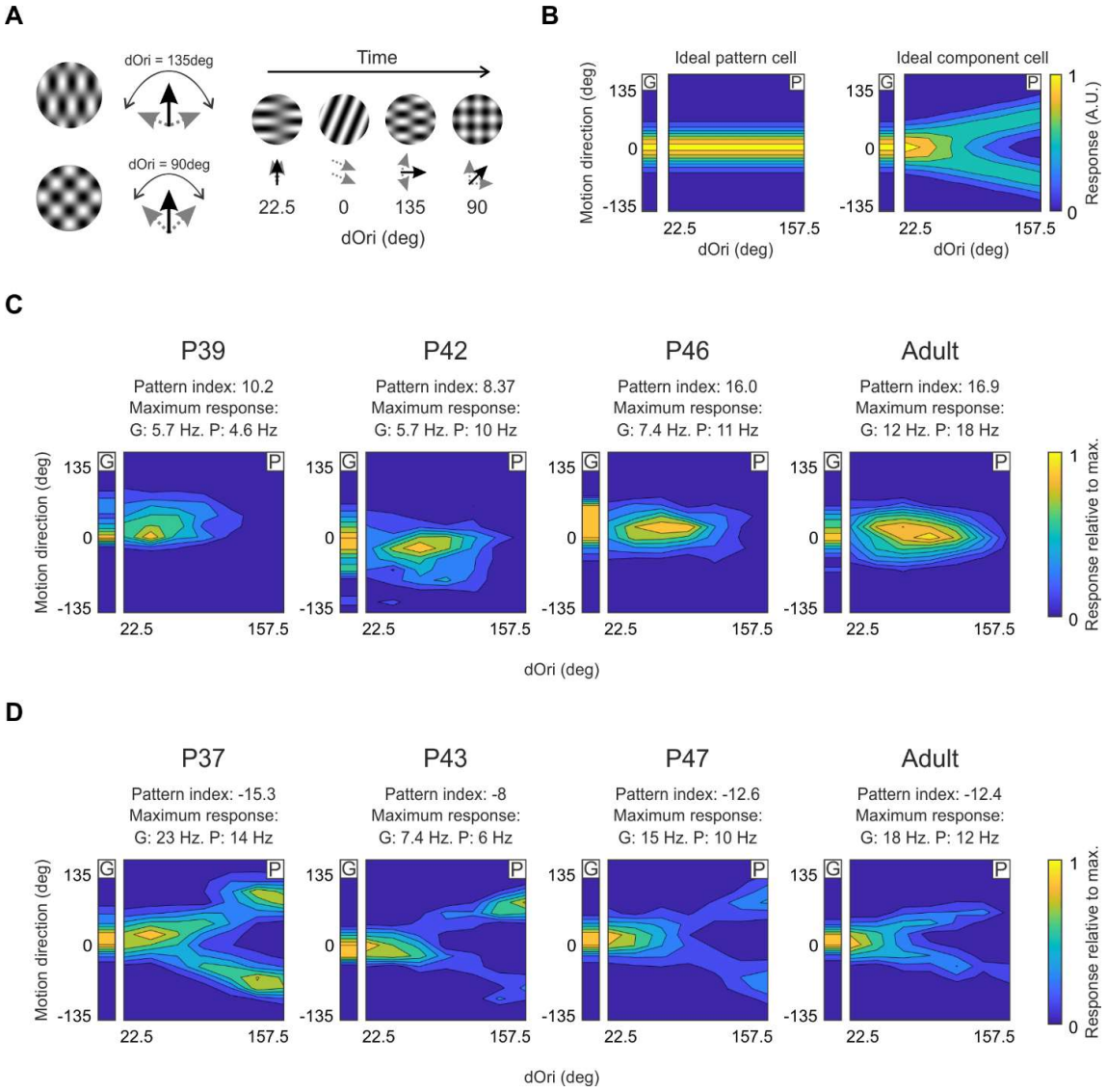
A
dOri = 135deg
dOri = 90deg
Time
22.5
0
135
90
dOri (deg)
B
Ideal pattern cell
Ideal component cell
Motion direction (deg)
135
0
-135
G
P
22.5
157.5
dOri (deg)
1
0
Response (A.U.)
C
P39
P42
P46
Adult
Pattern index: 10.2
Maximum response:
G: 5.7 Hz. P: 4.6 Hz
Pattern index: 8.37
Maximum response:
G: 5.7 Hz. P: 10 Hz
Pattern index: 16.0
Maximum response:
G: 7.4 Hz. P: 11 Hz
Pattern index: 16.9
Maximum response:
G: 12 Hz. P: 18 Hz
Motion direction (deg)
dOri (deg)
Response relative to max.
D
P37
P43
P47
Adult
Pattern index: -15.3
Maximum response:
G: 23 Hz. P: 14 Hz
Pattern index: -8
Maximum response:
G: 7.4 Hz. P: 6 Hz
Pattern index: -12.6
Maximum response:
G: 15 Hz. P: 10 Hz
Pattern index: -12.4
Maximum response:
G: 18 Hz. P: 12 Hz

Figure 3.3: PSS contains pattern and component cells from P37 on.
(A) Illustration of the streaming stimulus paradigm: A large stimulus set was used consisting of plaids generated from component gratings with different dOri values (left). Stimuli were shown in quick succession during the experiment for efficient sampling (right).
(B) Tuning profiles expected for an ideal pattern cell (left) and an ideal component cell (right) based on responses to the large stimulus set. The bar shown on the left for each neuron (labeled 'G') indicates responses to gratings moving in different directions, with directions shown relative to the preferred direction of the neuron. The 2D contour plot shown on the right (labeled 'P') summarizes the responses to plaids as a function of direction and dOri. Direction is relative to the cell's preferred grating direction, and indicates the perceived direction of the plaid (i.e., the pattern direction). The tuning profile of the ideal pattern cell shows consistent responses to gratings and plaids moving in the preferred direction, independent of dOri. The tuning profile of the ideal component cell shows two peaks for plaids, with increasing distance between the peaks for larger dOri values. These peaks occur for conditions in which one of the two components moves in the neuron's preferred direction.
(C) Example pattern cells at different ages (same format as (B)). Plots are color coded to indicate response strength for each condition relative to the cell's maximum response. The plots also indicate the pattern index and maximum response evoked by gratings and plaids for each cell.
(D) Example component cells at different ages (same format as (C)).

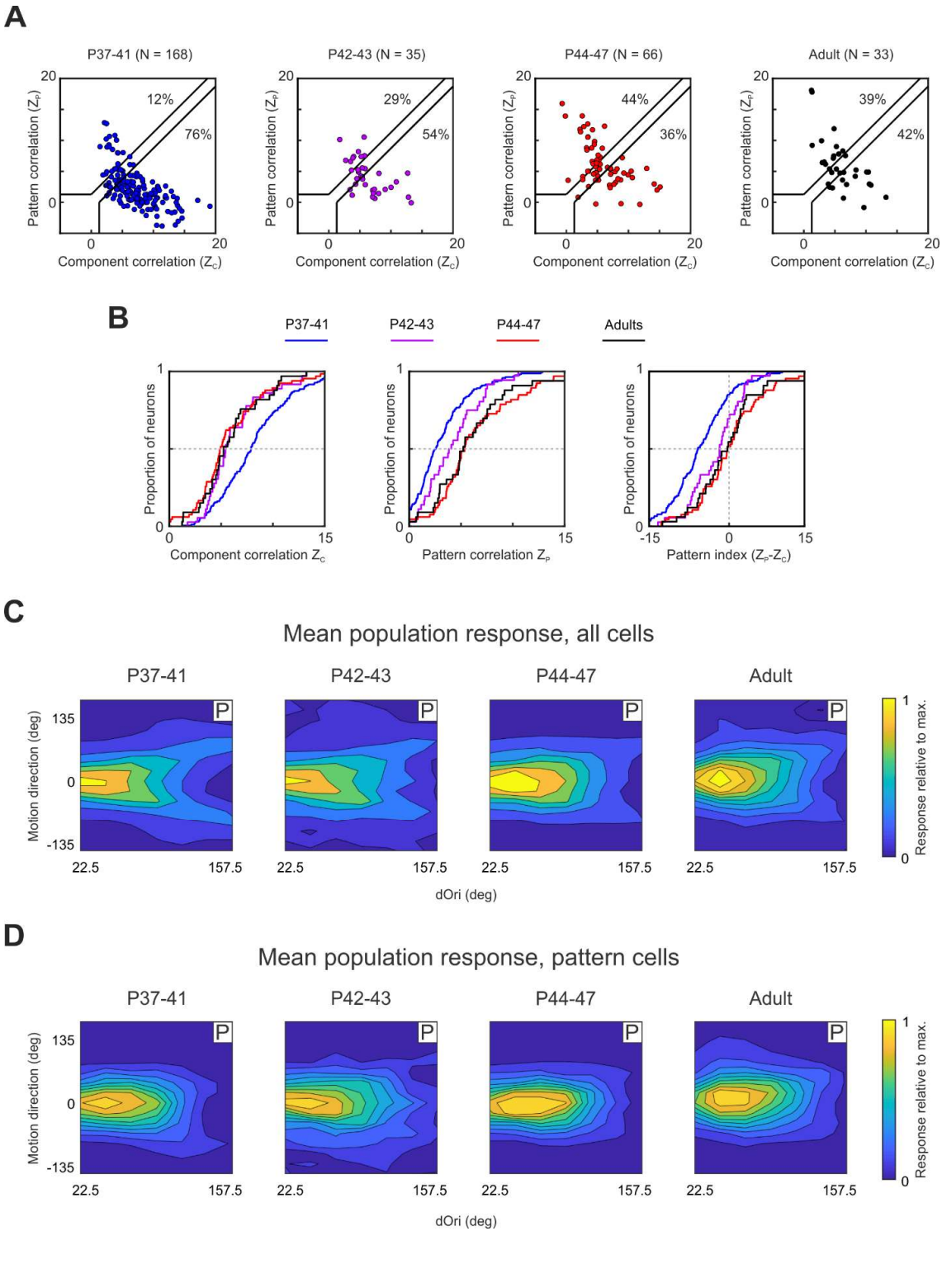
A
P37-41 (N = 168)
P42-43 (N = 35)
P44-47 (N = 66)
Adult (N = 33)
12%
76%
29%
54%
44%
36%
39%
42%
Pattern correlation (Z_P)
Component correlation (Z_C)
B
P37-41
P42-43
P44-47
Adults
Proportion of neurons
Component correlation Z_C
Pattern correlation Z_P
Pattern index (Z_P-Z_C)
C
Mean population response, all cells
P37-41
P42-43
P44-47
Adult
Motion direction (deg)
dOri (deg)
Response relative to max.
D
Mean population response, pattern cells

Figure 3.4: PSS pattern integration matures in the second week after eye opening.
(A) PSS pattern versus component selectivity in different age groups based on the streaming stimulus paradigm. Plot format as in Figure 3.2D.
(B) Cumulative distribution of component correlation (left), pattern correlation (center) and pattern index (right) across age groups for the same data as shown in (A). Significance tests between data from different age groups can be found in Table 3.1.
(C) 2D contour plots of mean population plaid responses at different ages. Population responses are computed by averaging the responses of all cells after normalizing them by their maximum. The direction axis uses the same format as in Figure 3.3B. The population response profile changes from a component-like response at P37-41 to a more pattern-like response in adults (see Figure 3.3B).
(D) 2D contour plots of mean population plaid responses for pattern cells only in the different age groups. These plots show that the average tuning profile for pattern cells remains similar across development.

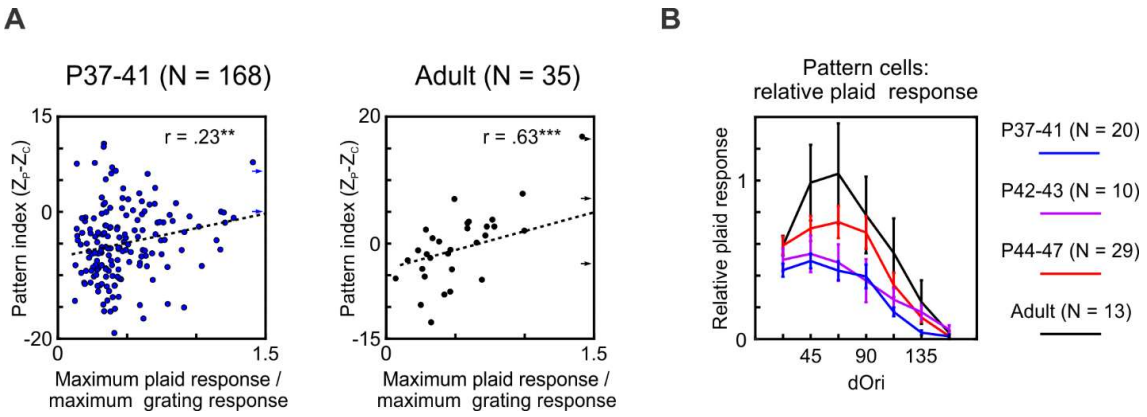

Figure 3.5: The relative response to plaids versus gratings increases in PSS with development.
(A) Relationship between the pattern index and the relative response to plaids versus gratings at P37-41 (left) and in adulthood (right). The relative plaid response was computed as the ratio of the maximum plaid response and the maximum grating response. Data points falling outside the limits of the x-axis are indicated by arrows. Black dashed lines indicate the linear fits to the data. ** = $p < .01$ and *** = $p < .001$ for Pearson correlation coefficients (r). Correlation coefficient is greater for the adult data, $p = .01$.
(B) Relative plaid responses of PSS pattern cells as a function of dOri. Here, the relative plaid response is computed as the ratio of the response to plaids moving in a neuron's preferred direction (which evokes maximal responses) and the response to a grating moving in the same direction. Relative plaid responses are shown for pattern cells at different ages. Error bars: ± SEM. Significance tests between data from different age groups can be found in Table 3.1.

3.5 - Results: The degree of PSS maturation differs between young kits of similar age but with different amounts of binocular visual experience.

In the previous section we analyzed the developmental time course of pattern responses purely as a function of age. Yet, the developmental state of visual processing could also be affected by other factors. Visual experience has been shown to impact the development of direction selectivity in V1, and the age at eye opening, which marks the start of patterned visual input, is variable across animals. The amount of visual experience of an animal is therefore an important factor that could affect the developmental state of pattern responses in PSS independent of age. To investigate this issue, we focused on animals in the youngest group, P37-41, as we expect them to be most sensitive to variations in the amount of visual experience.

To analyze the possible contribution of visual experience on the developmental state of PSS pattern responses, data from the age group P37-41 was divided according to the days of binocular vision (V) experienced by each animal. When data from animals with only 4 days of visual experience (V4) was compared to that from animals with 5 or more (≥V5), clear differences in the development of pattern responses emerged: Animals with more visual experience had more than double the proportion of pattern cells than those with less (V4: 5%. ≥V5: 11%. Figure 3.6A). In addition, the pattern index (Figure 3.6B) was significantly lower in animals with limited visual experience (Median pattern index: V4 = -8.44, ≥V5 = -4.28. Rank-sum test: $p = .001$).

Although the analysis was restricted to a very limited age range, a correlation between age and days of visual experience could confound these conclusions. Indeed, animals with less

visual experience tended to be younger (mean age: V4 = 37.7 days, ≥V5 = 38.8 days. Age range: V4: P37-40, ≥V5: P37-41). We therefore performed two control analyses. First, we divided the data set into two age groups: P37, the youngest age in the group, and P40-41, the oldest. The proportion of pattern cells (Figure 3.6C) was similar between these groups (10% in both groups). In addition, while a higher median pattern index (Figure 3.6D) was observed in the older kits, this difference did not reach significance (Median pattern index: P37 = -7.66, P40-41 = -4.78. Rank-sum test: $p = .28$). This analysis shows that age per se does not drive differences in pattern responses between P37 and 41. Second, we restricted the data set even further, and exclusively focused on animals age P38 - 40. Data was again grouped by days of visual experience. Similar to the findings in the larger group, animals with limited visual experience (V4) had a smaller pattern index (Figure 3.6F) than animals with more visual experience (Median pattern index: V4 = -9.30, ≥V5 = -3.91. Rank-sum test: $p < .001$). In addition, we found no pattern cells in the group with limited visual experience (V4: 0%. ≥V5: 12%. Figure 3.6E). These results strongly suggest a role of visual experience in the development of motion processing that goes beyond the development of direction selectivity in V1, and includes the emergence of pattern tuning in PSS.

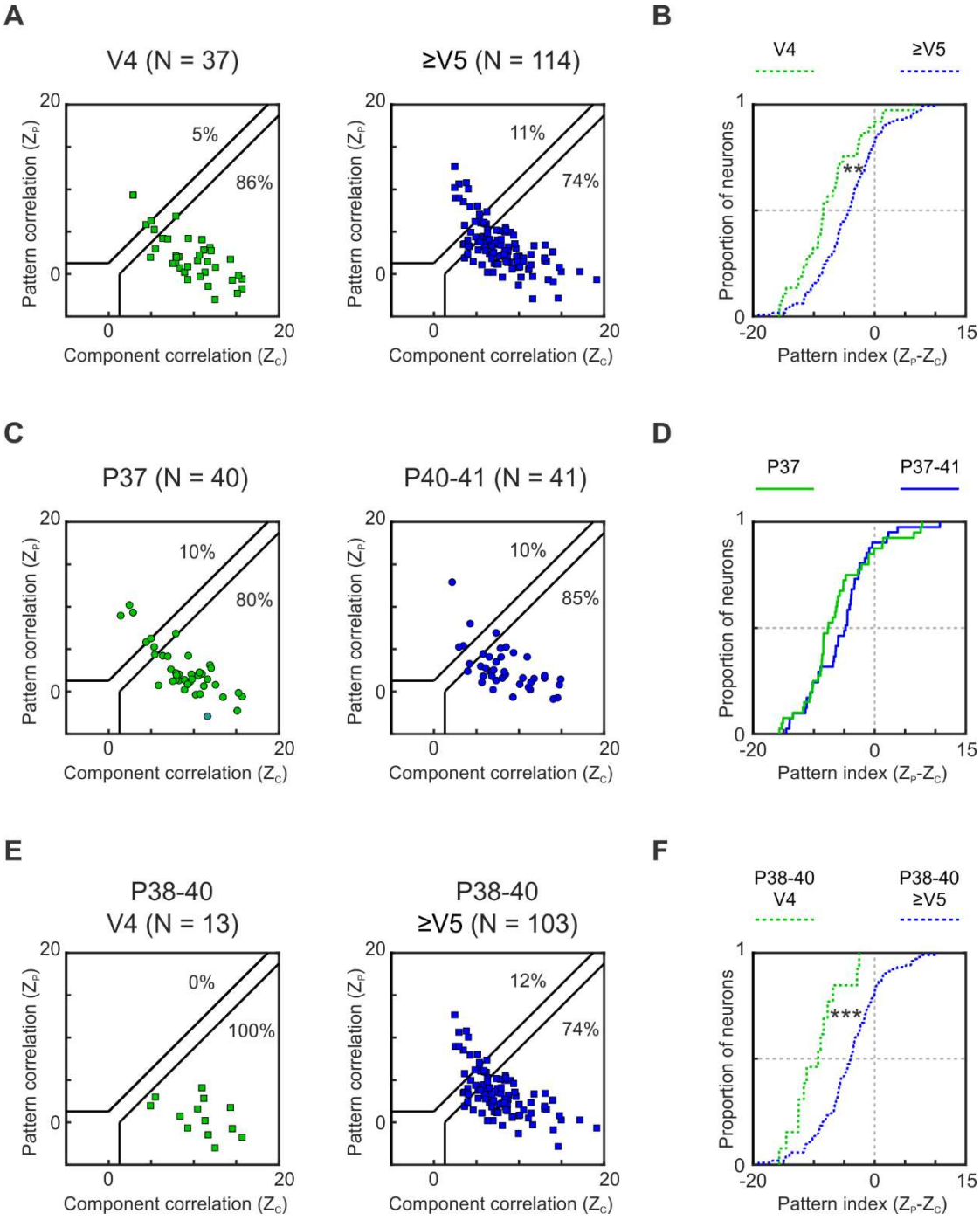
A
V4 (N = 37)
≥V5 (N = 114)
5%
86%
11%
74%
Pattern correlation (Z_P)
Component correlation (Z_C)
B
V4
≥V5
**
Proportion of neurons
Pattern index (Z_P-Z_C)
C
P37 (N = 40)
P40-41 (N = 41)
10%
80%
10%
85%
D
P37
P37-41
E
P38-40
V4 (N = 13)
P38-40
≥V5 (N = 103)
0%
100%
12%
74%
F
P38-40
V4
P38-40
≥V5
***

Figure 3.6: PSS pattern responses are less developed in animals with 4 days of visual experience than in animals of similar age but longer visual experience.
(A) Pattern versus component selectivity for PSS neurons in animals aged P37-41 with 4 days of binocular visual experience (V4, left) and longer visual experience (≥V5, right). Plot format as in Figure 3.2D.
(B) Cumulative PSS pattern index distribution for animals aged P37-41 with 4 (V4) or more (≥V5) days of visual experience. Same data as (A). ** = $p < .01$ using Rank-sum test.
(C) & (D) Comparison between animals at P37 (left) and at P40-41 (right), independent of duration of visual experience (same format as in (A & B))
(E) & (F) Comparison between animals at P38-40 with 4 days of visual experience (left) and longer visual experience (right). (same format as in (A & B)). *** = $p < .001$ using Rank-sum test.

3.6 - Results: A feed-forward model explains the development of PSS pattern responses through changes in inhibitory mechanisms and V1 input.

We have previously described a computational model for the ferret's motion pathway (see Chapter 2) that shares important similarities with comparable models developed for the primate (Rust et al., 2006). In short, the model explains PSS responses to visual stimuli through the following mechanisms: First, LGN responses are implemented using antagonistic center/surround mechanisms and a contrast response function (CRF). Next, responses of a population of V1 neurons with different direction preferences are modeled using Gabor filters and motion energy mechanisms. Then, PSS responses are calculated as a linear combination of the V1 responses, with weights applied to the V1 responses according to their direction preference. Weights include both excitation (positive values) and inhibition (negative values). Both the excitatory and inhibitory weight functions are modeled as von Mises functions, with the excitatory function centered at the preferred direction of the PSS cell, and the inhibitory function centered at the null direction. Finally, the resulting PSS response is passed through a threshold non-linearity. Overall, the model included 5 variables for controlling different computations: C_{50} and N controlled the CRF saturation and non-linearity respectively. K_E controlled the width of excitatory weights, with smaller values indicating wider excitation. Similarly, K_I controlled the width of the inhibitory function, and I controlled its strength. Finally, T_{PSS} (referred to as T in Chapter 2) controlled the threshold non-linearity applied to PSS responses. For an explanatory flow chart of the model see Chapter 2 Figure 2.6.

As a first step towards identifying potential mechanisms underlying the development of pattern responses, this model was fit to PSS responses from animals age P37-48. The model was able to fit data across all developmental stages with high correlation values (Median r values: P37-41 = .81, P42-43 = .71, P44-48 = .86, adult = .81.). Yet, model fits at P37-41, the youngest age group, often required the highest possible value for C_{50} (maximum C_{50} was reached in 63% of the neurons). By design, passing the stimulus through a first contrast-sensitive stage changes the strength of plaid responses relative to those for gratings in the model V1 stage. The observed high C_{50} values imply that to fit the data in young animals, the lowest possible V1 plaid responses were required. To avoid maximizing C_{50} and provide better fits, we therefore modified the model to include an additional mechanism for lowering V1 plaid responses. To this end, we included a threshold non-linearity in V1, placed after the computation of direction-selective responses (Figure 3.7A). The strength of the V1 threshold was controlled by the variable 'T_{V1}'. The addition of this mechanism increased the number of model parameters, which could cause the model to over-fit the data. To avoid this, the CRF variables were fixed to fit measured contrast responses in V1 (Fixed model values: C50 = .23, N = 3.1. Median of measured values: C50 = .32, N = 3.2). Note that very similar results can be obtained for a model in which T_{V1} is fixed and the CRF variables are allowed to change (Figure 3.S1).

The modified motion pathway model was successful at explaining data across all age groups with high correlation values (Median r values: P37-41 = .83, P42-43 = .73, P44-48 = .85, adult = .81. Figure 3.7B). Note that performance was significantly worse for neurons in P42-43 animals (see Table 3.1), hinting at potential additional mechanisms at this age that the model currently does not capture optimally. More data will be needed to further

resolve this issue. The following analyses therefore focus on the results from the remaining age groups (P37-41, P44-48 and adults), which are better fit by the model.

As a first analysis of the model results, the values of each model variable were compared across the different age groups. To simplify the analysis, the two variables controlling inhibition (K_I and I) were combined into a single metric by computing the area under the curve of the resulting inhibitory weight function (W_I, see methods). This analysis revealed no significant differences between P44-48 and adults. This is consistent with the analysis of plaid responses described above, which indicated that pattern responses reach maturity after the second week of eye opening (Figure 3.4B). Therefore, in all subsequent analyses we combined the two older groups (≥P44), and compared the combined data with that for animals aged P37-41.

In mature animals, the pattern index was correlated with higher plaid responses (lower T_{V1}), wider excitation (lower K_E) and stronger PSS thresholds (higher T_{PSS}. See Table 3.2 for correlation values and statistics). This observation is consistent with our previous reports (see chapter 2). We also observed a trend for higher pattern indices to coincide with stronger inhibition (higher W_I), but the correlation did not reach significance (see Table 3.2). All of the model parameters showed a significant change between P37-41 and ≥P44 (see Table 3.1 for statistics). Intriguingly, all of the parameters changed in the direction associated with stronger pattern indices in the adult: T_{V1} and K_E decreased, while W_I and T_{PSS} increased with development (Figure 3.7B). The developmental changes suggested by the model therefore could explain the emergence of pattern cells.

While developmental changes were significant across all model variables, the difference in mean excitation width (K_E) was marginal (mean K_E: P37-41 = 2.03, ≥P44 = 1.36), and the value of T_{PSS} was 0 for most cells across all age groups (Figure 3.7B). Therefore, we consider the decrease in T_{V1} (corresponding to an increase in V1 plaid responses) and the increase in W_I as the dominant mechanisms suggested by the model for explaining the development of PSS pattern cells. As discussed above, the emergence of pattern responses in PSS is characterized by two distinct changes. The first is a suppression of PSS component responses as measured by the component correlation of plaid responses (Figure 3.4B). The second is an increase in PSS pattern responses relative to gratings (Figure 3.5B). These developmental changes are entirely consistent with an increase in PSS inhibitory mechanisms and an increase in V1 plaid responses, respectively.

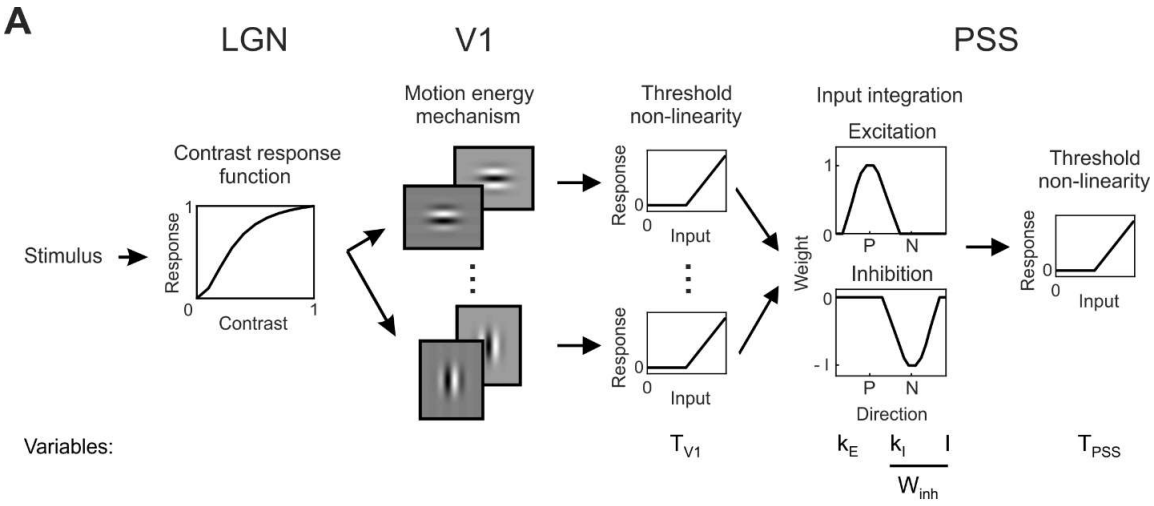
A
LGN
V1
PSS
Motion energy mechanism
Threshold non-linearity
Input integration
Contrast response function
Excitation
Threshold non-linearity
Stimulus
Response
Contrast
Input
Weight
Inhibition
P
N
Direction
Variables:
T_{V1}
k_E
k_I
I
W_{inh}
T_{PSS}

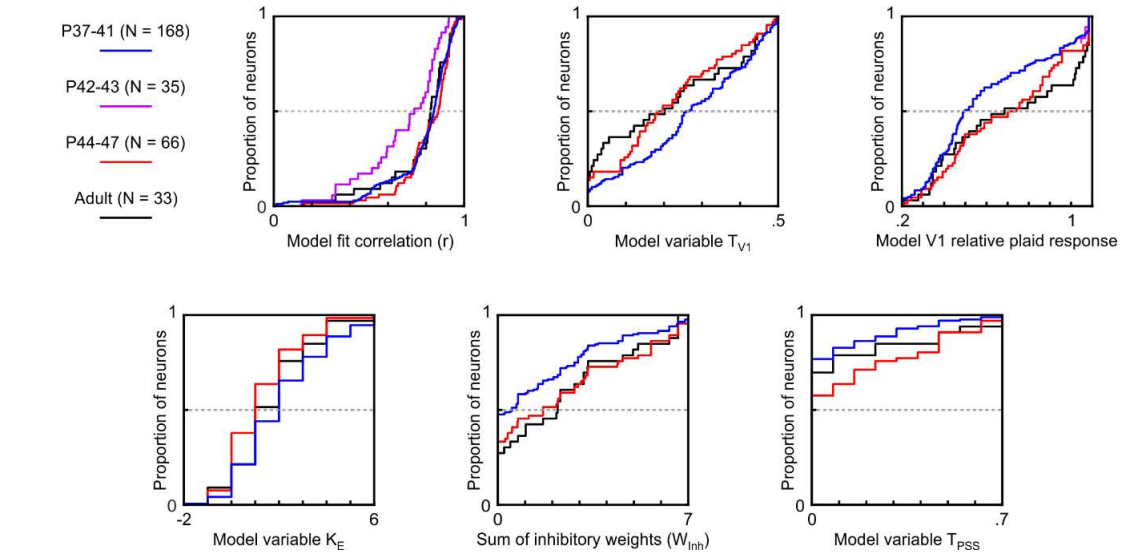
B
P37-41 (N = 168)
P42-43 (N = 35)
P44-47 (N = 66)
Adult (N = 33)
Proportion of neurons
Model fit correlation (r)
Model variable T_{V1}
Model V1 relative plaid response
Model variable K_E
Sum of inhibitory weights (W_{Inh})
Model variable T_{PSS}

Figure 3.7: Using a computational model to identify possible mechanisms driving the development of PSS pattern cells.
(A) Diagram of the computational model used to fit PSS plaid responses (see Methods for details). Stimuli first passed through LGN spatial filters, which also served to scale responses according to contrast. The next stage was composed of 16 V1 motion-energy filters. The response of each V1 filter was then passed through a threshold non-linearity. Responses from the V1 stage were integrated in PSS using a combination of an excitatory and an inhibitory weight function (P – preferred direction; N – null direction). Finally, another threshold non-linearity was applied to the PSS responses. The model used 5 variables, which are listed below the stage to which they belong. W_{inh} represents the sum of inhibitory weights, which is controlled by the two parameters K_E and I. This metric was computed to simplify further analysis. The parameters controlling the contrast response function in the LGN layer were fixed based on ferret V1 contrast responses (see methods). All other parameters were fixed based on published values for the ferret.
(B) Cumulative distributions of the model fit correlation and different model parameters at different ages. Since model fit correlation values were significantly lower for data at P42-43, these data were excluded from further analyses. Significance tests between data from different age groups can be found in Table 3.1.

3.7 - Results: Developmental changes in V1 responses agree with model predictions during the second week of visual experience but not in adult ferrets.

As discussed above, the modelling effort suggests that changes in V1 responses may be an important factor in the development of PSS motion integration. Specifically, we predict that the relative response to plaids versus gratings in the V1 input to PSS increases between P37-41 and P44-48, with no subsequent changes between P44-48 and adulthood (Figure 3.8B).

To test this model prediction, responses to drifting gratings and plaids were recorded from V1 at different ages, using the same streaming stimulus paradigm as previously described for PSS. In a first analysis of this data, we investigated the responses to plaids relative to gratings (Figure 3.8A) and compared them to the model predictions (Figure 3.8B-D). A dOri tuning curve was computed for each cell by averaging responses to plaids with the same dOri, independent of their direction. This dOri tuning curve was then normalized by each neuron's mean grating response. Finally, the normalized dOri curve was compared between age groups (Figure 3.8C). As predicted by the model, a significant increase in relative plaid responses was observed in V1 between the P37-41 and the P44-48 age groups (2-way ANOVA dOri versus age for groups P37-41 and P44-48. Contribution of age: $p < .001$). In addition, for both age groups the mean relative response to plaids closely matched the mean relative response predicted by the model (Figure 3.8D). This good agreement between measured data and predicted values is remarkable, as the model fits all parameters purely based on PSS responses, without access to any V1 data. Note that our data show a

decrease in V1 plaid responses with increasing dOri in the youngest kits (2-way ANOVA dOri versus age for groups P37-41 and P44-48. Contribution of dOri: $p = .005$. Figure 3.8C). While the overall level of the relative plaid response was predicted well by the model, the dependency of relative plaid response on dOri was not predicted (Figure 3.8B). The model fits therefore resulted in slightly lower responses at low dOri values and slightly higher responses at high dOri values than seen in the actual V1 data (Figure 3.8D). This discrepancy can be explained by the lack of motion opponency mechanisms in the model V1 stage, which are known to exist in ferret V1 (see Figure 2.3).

In contrast to the good agreement between predicted and measured V1 responses up to P48, the predicted responses deviated strongly from the actual measurements in adult ferrets (Figure 3.8D). While the model predicted the same relative plaid responses for P44-48 animals and adults (Figure 3.8B), the measured responses (Figure 3.8C) were significantly lower in adults (2-way ANOVA dOri versus age for groups P44-48 and adults. Contribution of age: $p < .001$). In interpreting this observation, it is important to reiterate that the model could fit PSS data from adults and younger animals equally well (Figure 3.7B). The failure to correctly account for the relative plaid responses in adult V1 only becomes apparent because of the good fit between the predicted and measured V1 responses in the two younger age groups. A likely reason for the deviation in predicted and measured V1 responses in adults is the observation that PSS responses to plaids (Figure 3.8E and 3.8F) rise between P44-48 and adulthood (2-way ANOVA dOri versus age for groups P44-48 and adults. Contribution of age: $p < .001$). Since the model predictions are based purely on a fit to the PSS data, this increase in PSS responses forces a deviation of the model predictions from the observed drop in V1 plaid responses in adult animals. In

short, the developmental drop in V1 plaid responses without a corresponding drop in PSS plaid responses cannot be explained using the mechanisms implemented in the model. Instead, this discrepancy between model predictions and measured data in the adult requires additional mechanisms, such as a selective V1 input or non-linear mechanisms in PSS (see discussion).

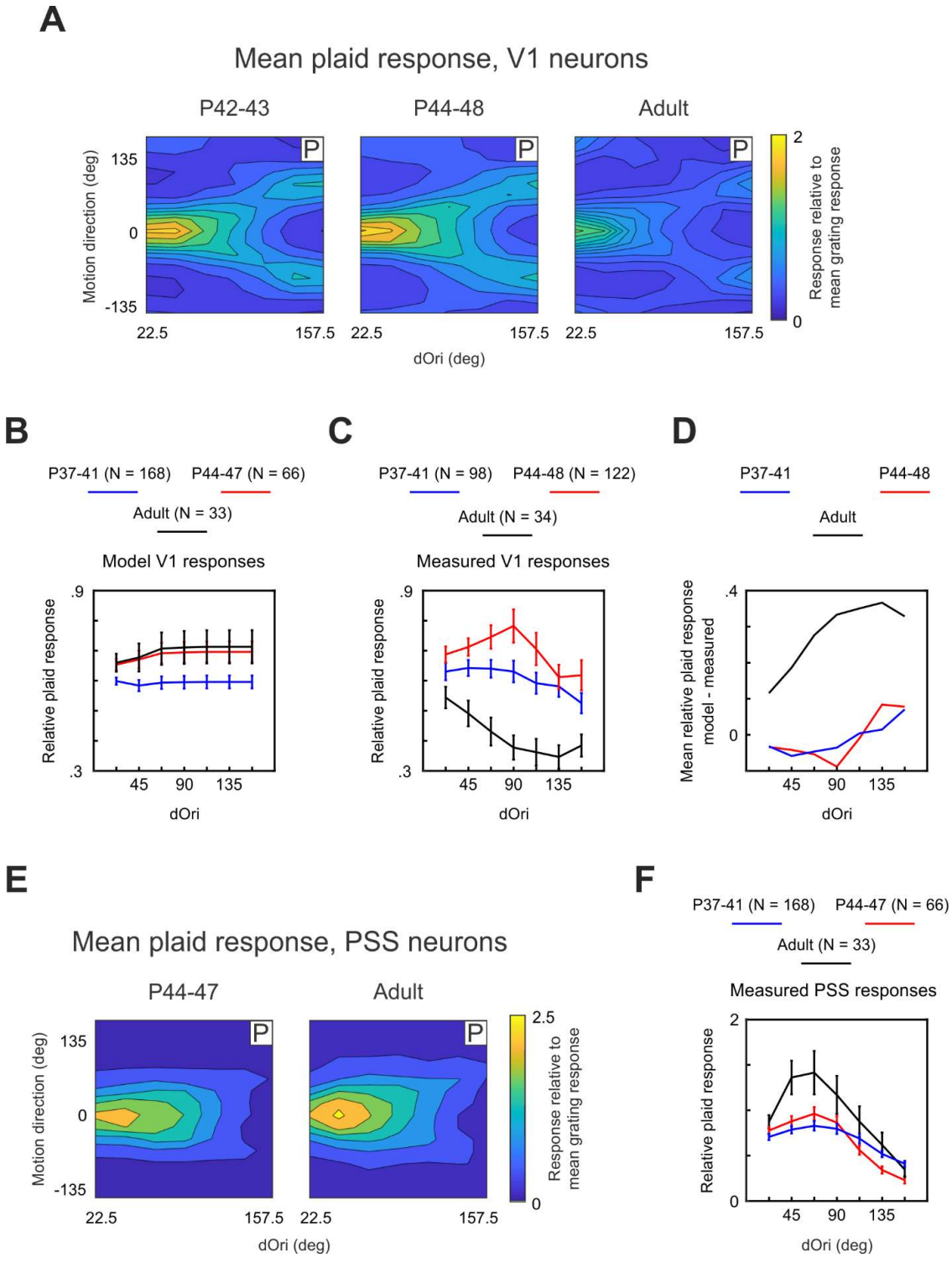
A
Mean plaid response, V1 neurons
P42-43
P44-48
Adult
P
Motion direction (deg)
135
0
-135
22.5
157.5
dOri (deg)
2
0
Response relative to mean grating response
B
P37-41 (N = 168)
P44-47 (N = 66)
Adult (N = 33)
Model V1 responses
Relative plaid response
.9
.3
45
90
135
dOri
C
P37-41 (N = 98)
P44-48 (N = 122)
Adult (N = 34)
Measured V1 responses
D
P37-41
P44-48
Adult
Mean relative plaid response model - measured
.4
0
E
Mean plaid response, PSS neurons
P44-47
Adult
2.5
F
P37-41 (N = 168)
P44-47 (N = 66)
Adult (N = 33)
Measured PSS responses
2
0

Figure 3.8: Comparison between predicted and measured developmental changes in relative plaid responses in V1 and PSS.
(A) Mean V1 plaid tuning profile at different ages. In these plots, the data from each cell was normalized by the mean grating response before averaging across cells. Same format as in Figure 3.4C.
(B) Relative plaid responses predicted based on the model V1 stage. Data is based on fitting the model to PSS data collected at different ages. Error bars: ± SEM.
(C) Measured V1 relative plaid responses at different ages. Error bars: ± SEM. Significance tests between data from different age groups can be found in Table 3.1.
(D) Difference between predicted and measured relative V1 plaid responses.
(E) Mean PSS plaid tuning profile at P44-P47 (left) and adults (right). Data shown here is normalized by the mean grating response for better comparison with the V1 data shown in (A), rather than the maximum response as in Figure 3.4.
(F) Measured PSS relative plaid responses at different ages. In contrast to Figure 3.5, data here is computed for all cells, and is based on the mean response to all plaids and the mean response to all gratings. Significance tests between data from different age groups can be found in Table 3.1.

3.8 - Results: Component motion responses temporarily decrease in V1 as PSS pattern motion responses increase.

To further analyze potential developmental changes in V1 motion responses that may be correlated with the emergence of pattern motion selectivity in PSS, pattern and component correlations were computed for V1 neurons as previously described for PSS. In all age groups, the majority of V1 neurons were classified as component cells (80-91%. Figure 3.9A). In addition, at all ages the V1 pattern index distribution was shifted to much lower values than those found in adult PSS (Figure 3.9B). Thus, V1 continuously maintained robust component motion tuning. Nonetheless, we observed significant developmental changes in the strength of V1 component responses. In particular, the V1 pattern index (Figure 3.9B) increased during the second week of visual experience (Median pattern index: P37-41 = -9.5, P44-48 = -6.17. Rank-sum test: $p < .001$). This is the same temporal window during which PSS pattern motion selectivity matured (See Figure 3.4). In addition, although pattern cells remained a minority of the V1 population, their number increased in this age group (12%. Figure 3.9A). These changes in pattern index distribution were temporary: The V1 pattern index distribution in adult animals (Figure 3.9B) was similar to that found at P37-41, and was shifted to significantly lower values than that at P44-48 (Median pattern index: Adult = -8.65. Rank-sum test: Adult vs P37-41 $p = .63$, adult vs P44-48 $p = .01$). Moreover, only one neuron in the adult V1 data set was classified as a pattern cell, combined with about 90% component cells (Figure 3.9A).

The observed developmental timeline for V1 suggests that component motion responses are reduced in V1 as pattern motion responses increase in PSS. To further test the

dependency between developmental changes in V1 and PSS, responses to plaids were recorded simultaneously in both areas at P37-41. We then determined whether the median PSS and V1 pattern indices were correlated in each animal (Figure 3.9C). Although this data was available for only a small group of animals, a significant correlation was found between pattern indices in PSS and V1 ($r = .88$. $P = .02$). This dependence suggests that more pattern-like responses in V1 may be involved in the development of pattern responses in PSS.

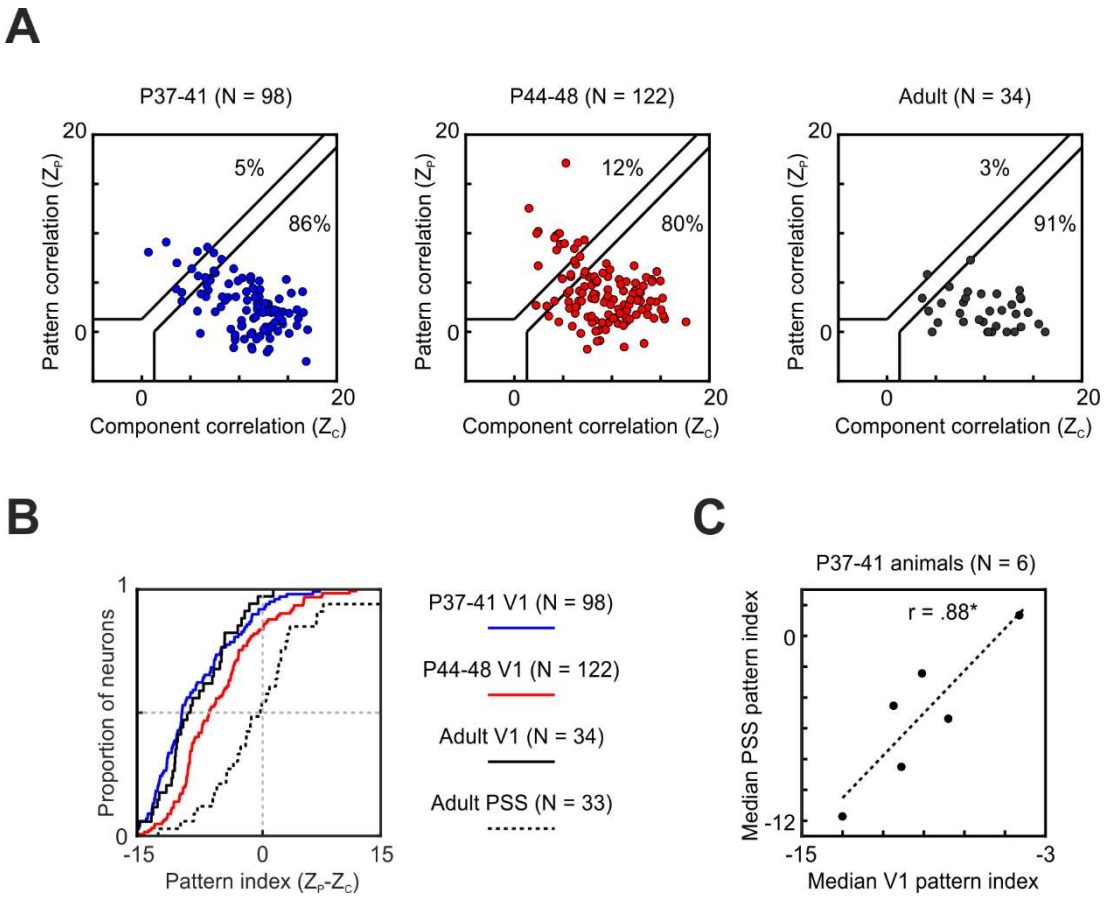

Figure 3.9: V1 plaid responses become more pattern-like as PSS pattern cells emerge between P37-41 and P44-48.
(A) Pattern versus component selectivity for V1 neurons in different age groups. Plot format as in Figure 3.2D.
(B) Cumulative V1 pattern index distribution for different age groups. For comparison, the pattern index distribution observed in adult PSS is also plotted (dashed black line). Note that while the distribution of V1 pattern indices changes across development, it is always shifted to more component (negative) values than that of adult PSS. Significance tests between data from different age groups can be found in Table 3.1.
(C) Relationship between the median pattern indices for V1 and PSS computed for 6 animals aged P37-41. Dashed line shows linear fit to the data. * = $p < 0.05$ for Pearson correlation coefficient (r).

3.9 - Results: PSS inactivation reverses the changes in V1 motion responses during the second week of visual experience.

The data presented so far indicate that V1 motion responses change during the second week after eye opening – the time period in which pattern responses emerge in PSS (Figure 3.4A and B) – in at least two ways: First, the responses to plaids relative to gratings increase (Figure 3.8A and 3.9C). Second, responses to plaids become more pattern-like (Figure 3.9A and 3.9B). Our data also suggest that the second change is correlated with the emergence of pattern responses in PSS (Figure 3.9C). Both observations could reflect independent changes in V1, or an effect of feedback from PSS to V1.

To answer this question, V1 responses to plaids and gratings were measured at P44-48 while inactivating PSS using muscimol. All recordings were done within 1 – 5 h after muscimol injection. Lack of visual responsiveness in PSS during this time period was confirmed by performing recordings either at the same time as V1 recordings or right after the last V1 recording (see methods). During PSS inactivation, the observed developmental changes in V1 pattern responses were reversed. Responses to plaid stimuli relative to gratings (Figure 3.10A) returned to similar, if not lower, values as those in P37-41 kits (2-way ANOVA dOri versus muscimol for animals age P44-48. Contribution of muscimol: $p < .001$). In addition, the pattern index distribution (Figure 3.10B) was shifted to similar values as those in younger kits and adults (Median pattern index: Muscimol = -8.29, P44-48 = -6.17. Rank-sum test: $p = .01$). Injection of ACSF solution without muscimol (Figure 3.10C and 3.10D) did not induce changes in V1 responses (Median pattern index: ACSF = -6.02. Rank-sum test: ACSF vs P44-48 $p = .66$. Plaid responses: 2-way ANOVA dOri versus ACSF for animals age P44-48. Contribution of ACSF: $p = .51$), confirming that PSS

inactivation, rather than other consequences of the injection procedure, was responsible for the observed effects. These results are consistent with a role of PSS feedback in the changes of V1 motion responses during the second week after eye opening, which in general raises the intriguing possibility that development of the motion pathway in part relies on feedback from higher processing stages shaping the responses of earlier stages.

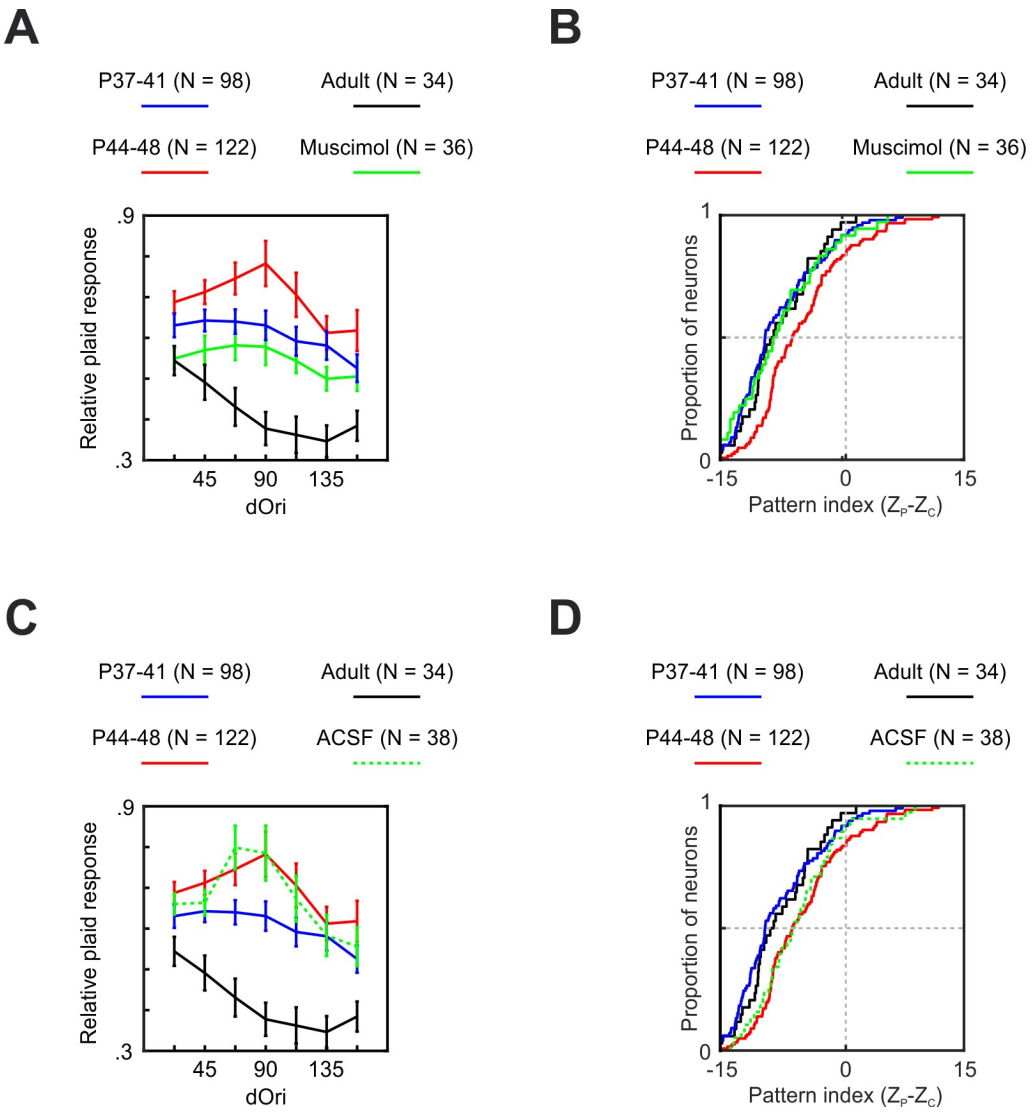

Figure 3.10: PSS inactivation decreases relative plaid responses and pattern indices in V1 at P44-48.
(A) Relative V1 plaid responses for animals in different age groups, as well as after PSS inactivation using muscimol at P44-48. Error bars: ± SEM. Significance tests between data from different groups can be found in Table 3.1.
(B) Cumulative V1 pattern index distribution for the same groups shown in (A). Significance tests between data from different groups can be found in Table 3.1.
(C) Relative V1 plaid responses for the same age groups shown in (A), as well as after injection of ACSF in PSS at P44-48. Error bars: ± SEM. Significance tests between data from different groups can be found in Table 3.1.
(D) Cumulative V1 pattern index distribution for the same data as shown in (C). Significance tests between data from different groups can be found in Table 3.1.

3.10 - Tables.

Table 3.1: Extended p values of statistical analysis.

Figure	*Experimental groups*	*Metric or variable*	*Test*	*p value*
3.1B	*All ages (P30-37)*	*DSI.* *Contribution of age.*	*One-way ANOVA*	*<.001*
3.1B	*P30-32 vs P33-34*	*DSI*	*Rank-sum*	*1*
3.1B	*P30-32 vs P35*	*DSI*	*Rank-sum*	*.63*
3.1B	*P30-32 vs P37*	*DSI*	*Rank-sum*	*.01*
3.1B	*P33-34 vs P35*	*DSI*	*Rank-sum*	*.49*
3.1B	*P33-34 vs P37*	*DSI*	*Rank-sum*	*<.001*
3.1B	*P35 vs P37*	*DSI*	*Rank-sum*	*.01*
3.1B	*P37 vs adult*	*DSI*	*Rank-sum*	*.69*
3.1B	*All ages (P30-37)*	*OCV.* *Contribution of age.*	*One-way ANOVA*	*.003*
3.1B	*P30-32 vs P33-34*	*OCV*	*Rank-sum*	*.19*
3.1B	*P30-32 vs P35*	*OCV*	*Rank-sum*	*<.001*
3.1B	*P30-32 vs P37*	*OCV*	*Rank-sum*	*.001*
3.1B	*P33-34 vs P35*	*OCV*	*Rank-sum*	*.02*
3.1B	*P33-34 vs P37*	*OCV*	*Rank-sum*	*.05*
3.1B	*P35 vs P37*	*OCV*	*Rank-sum*	*.36*
3.1B	*P35 vs adult*	*OCV*	*Rank-sum*	*.46*
3.2E	*P37-41 vs adult*	*Pattern index.* *Plaid dOri = 135deg.*	*Rank-sum*	*.005*

3.4B	*All ages (P37-48)*	*Z_c. Many dOri values. Contribution of age.*	*One-way ANOVA*	*<.001*
3.4B	*P37-41 vs P42-43*	*Z_c. Many dOri values.*	*Rank-sum*	*.002*
3.4B	*P37-41 vs P44-48*	*Z_c. Many dOri values.*	*Rank-sum*	*<.001*
3.4B	*P42-43 vs P44-48*	*Z_c. Many dOri values.*	*Rank-sum*	*.23*
3.4B	*P37-41 vs adult*	*Z_c. Many dOri values.*	*Rank-sum*	*<.001*
3.4B	*P42-43 vs adult*	*Z_c. Many dOri values.*	*Rank-sum*	*.60*
3.4B	*P44-48 vs adult*	*Z_c. Many dOri values.*	*Rank-sum*	*.66*
3.4B	*All ages (P37-48)*	*Z_P. Many dOri values. Contribution of age.*	*One-way ANOVA*	*<.001*
3.4B	*P37-41 vs P42-43*	*Z_P. Many dOri values.*	*Rank-sum*	*.02*
3.4B	*P37-41 vs P44-48*	*Z_P. Many dOri values.*	*Rank-sum*	*<.001*
3.4B	*P42-43 vs P44-48*	*Z_P. Many dOri values.*	*Rank-sum*	*.01*
3.4B	*P37-41 vs adult*	*Z_P. Many dOri values.*	*Rank-sum*	*<.001*
3.4B	*P42-43 vs adult*	*Z_P. Many dOri values.*	*Rank-sum*	*.07*
3.4B	*P44-48 vs adult*	*Z_P. Many dOri values.*	*Rank-sum*	*.68*
3.4B	*All ages (P37-48)*	*Pattern index. Many dOri values. Contribution of age.*	*One-way ANOVA*	*<.001*
3.4B	*P37-41 vs P42-43*	*Pattern index. Many dOri values.*	*Rank-sum*	*.002*
3.4B	*P37-41 vs P44-48*	*Pattern index. Many dOri values.*	*Rank-sum*	*<.001*
3.4B	*P42-43 vs P44-48*	*Pattern index. Many dOri values.*	*Rank-sum*	*.05*
3.4B	*P37-41 vs adult*	*Pattern index. Many dOri values.*	*Rank-sum*	*<.001*
3.4B	*P42-43 vs adult*	*Pattern index. Many dOri values.*	*Rank-sum*	*.23*
3.4B	*P44-48 vs adult*	*Pattern index. Many dOri values.*	*Rank-sum*	*.72*

3.5A	*P37-41*	*Pattern index vs plaid response relative to gratings*	*Pearson correlation*	*.003*
3.5A	*Adult*	*Pattern index vs plaid response relative to gratings*	*Pearson correlation*	*<.001*
3.5A	*P47-41 vs adult*	*Pattern index vs plaid response relative to gratings correlation*	*Correlation difference*	*.01*
3.5B	*All ages (P37-48). PSS pattern cells.*	*Relative plaid response. Contribution of age.*	*Two-way ANOVA.*	*<.001*
3.5B	*All ages (P37-48). PSS pattern cells.*	*Relative plaid response. Contribution of dOri.*	*Two-way ANOVA.*	*<.001*
3.5B	*All ages (P37-48). PSS pattern cells.*	*Relative plaid response. Contribution of interaction.*	*Two-way ANOVA.*	*.86*
3.5B	*P37-41 vs P42-43. Pattern cells.*	*Relative plaid response. Contribution of age.*	*Two-way ANOVA.*	*.11*
3.5B	*P37-41 vs P42-43. PSS pattern cells.*	*Relative plaid response. Contribution of dOri.*	*Two-way ANOVA*	*<.001*
3.5B	*P37-41 vs P42-43. PSS pattern cells.*	*Relative plaid response. Contribution of interaction.*	*Two-way ANOVA.*	*.95*
3.5B	*P42-43 vs P44-48. PSS pattern cells.*	*Relative plaid response. Contribution of age.*	*Two-way ANOVA.*	*.02*
3.5B	*P42-43 vs P44-48. PSS pattern cells.*	*Relative plaid response. Contribution of dOri.*	*Two-way ANOVA.*	*<.001*
3.5B	*P42-43 vs P44-48. PSS pattern cells.*	*Relative plaid response. Contribution of interaction.*	*Two-way ANOVA.*	*.46*
3.5B	*P44-48 vs adult. PSS pattern cells.*	*Relative plaid response. Contribution of age.*	*Two-way ANOVA.*	*.03*
3.5B	*P44-48 vs adult. PSS pattern cells.*	*Relative plaid response. Contribution of dOri.*	*Two-way ANOVA.*	*<.001*
3.5B	*P44-48 vs adult. PSS pattern cells.*	*Relative plaid response. Contribution of interaction.*	*Two-way ANOVA.*	*.81*

3.6C	*V4 vs ≥ V5*	*Pattern index*	*Rank-sum*	*.001*
3.6D	*P37 vs P40-41*	*Pattern index*	*Rank-sum*	*.28*
3.6F	*V4 vs ≥ V5. P38-40 animals.*	*Pattern index*	*Rank-sum*	*<.001*
3.7B	*P37-41 vs P42-43*	*Model correlation (r)*	*Rank-sum*	*<.001*
3.7B	*P37-41 vs P44-48*	*Model correlation (r)*	*Rank-sum*	*.51*
3.7B	*P37-41 vs adult*	*Model correlation (r)*	*Rank-sum*	*.71*
3.7B	*P42-43 vs P44-48*	*Model correlation (r)*	*Rank-sum*	*<.001*
3.7B	*P42-43 vs adult*	*Model correlation (r)*	*Rank-sum*	*.01*
3.7B	*P44-48 vs adult*	*Model correlation (r)*	*Rank-sum*	*.51*
3.7B	*P37-41 vs P44-48*	*Model variable T_{V1}*	*Rank-sum*	*.02*
3.7B	*P37-41 vs adult*	*Model variable T_{V1}*	*Rank-sum*	*.07*
3.7B	*P44-48 vs adult*	*Model variable T_{V1}*	*Rank-sum*	*.86*
3.7B	*P37-41 vs ≥P44*	*Model variable T_{V1}*	*Rank-sum*	*.006*
3.7B	*P37-41 vs P44-48*	*Model variable K_E*	*Rank-sum*	*.002*
3.7B	*P37-41 vs adult*	*Model variable K_E*	*Rank-sum*	*.31*
3.7B	*P44-48 vs adult*	*Model variable K_E*	*Rank-sum*	*.17*
3.7B	*P37-41 vs ≥P44*	*Model variable K_E*	*Rank-sum*	*.004*
3.7B	*P37-41 vs P44-48*	*Model metric W_{inh}*	*Rank-sum*	*.02*
3.7B	*P37-41 vs adult*	*Model metric W_{inh}*	*Rank-sum*	*.03*
3.7B	*P44-48 vs adult*	*Model metric W_{inh}*	*Rank-sum*	*.8*
3.7B	*P37-41 vs ≥P44*	*Model metric W_{inh}*	*Rank-sum*	*.005*
3.7B	*P37-41 vs P44-48*	*Model variable T_{PSS}*	*Rank-sum*	*.002*
3.7B	*P37-41 vs adult*	*Model variable T_{PSS}*	*Rank-sum*	*.33*

3.7B	*P44-48 vs adult*	*Model variable T_{PSS}*	*Rank-sum*	*.26*
3.7B	*P37-41 vs ≥P44*	*Model variable T_{PSS}*	*Rank-sum*	*.004*
3.8C	*P37-41 vs P44-48. V1 neurons.*	*Relative plaid responses. Contribution of age.*	*Two-way ANOVA.*	*<.001*
3.8C	*P37-41 vs P44-48. V1 neurons.*	*Relative plaid responses. Contribution of dOri.*	*Two-way ANOVA.*	*.005*
3.8C	*P37-41 vs P44-48. V1 neurons.*	*Relative plaid responses. Contribution of interaction.*	*Two-way ANOVA.*	*.81*
3.8C	*P44-48 vs adult. V1 neurons.*	*Relative plaid responses. Contribution of age.*	*Two-way ANOVA.*	*<.001*
3.8C	*P44-48 vs adult. V1 neurons.*	*Relative plaid responses. Contribution of dOri.*	*Two-way ANOVA.*	*.17*
3.8C	*P44-48 vs adult. V1 neurons.*	*Relative plaid responses. Contribution of interaction.*	*Two-way ANOVA.*	*.40*
3.8F	*P44-48 vs adult. PSS neurons.*	*Relative plaid responses. Contribution of age.*	*Two-way ANOVA.*	*<.001*
3.8F	*P44-48 vs adult. PSS neurons.*	*Relative plaid responses. Contribution of dOri.*	*Two-way ANOVA.*	*<.001*
3.8F	*P44-48 vs adult. PSS neurons.*	*Relative plaid responses. Contribution of interaction.*	*Two-way ANOVA.*	*.34*
3.9B	*P37-41 vs P44-48. V1 neurons.*	*Pattern index*	*Rank-sum*	*<.001*
3.9B	*P37-41 vs adult. V1 neurons.*	*Pattern index*	*Rank-sum*	*.63*
3.9B	*P44-48 vs adult. V1 neurons.*	*Pattern index*	*Rank-sum*	*.01*
3.9C	*P37-41 animals.*	*Median pattern index in PSS and V1.*	*Pearson correlation*	*.02*

3.10A	*Control vs muscimol.*	*Relative plaid responses. Contribution of muscimol.*	*Two-way ANOVA*	*<.001*
3.10A	*Control vs muscimol.*	*Relative plaid responses. Contribution of dOri.*	*Two-way ANOVA.*	*.24*
3.10A	*Control vs muscimol.*	*Relative plaid responses. Contribution of interaction.*	*Two-way ANOVA.*	*.99*
3.10 B	*Control vs muscimol.*	*Pattern index*	*Rank-sum*	*.01*
3.10C	*Control vs ACSF.*	*Relative plaid responses. Contribution of ACSF.*	*Two-way ANOVA.*	*.51*
3.10C	*Control vs ACSF.*	*Relative plaid responses. Contribution of dOri.*	*Two-way ANOVA.*	*.003*
3.10C	*Control vs ACSF.*	*Relative plaid responses. Contribution of interaction.*	*Two-way ANOVA.*	*.97*
3.10D	*Control vs ACSF.*	*Pattern index*	*Rank-sum*	*.66*

Table 3.2: Correlation coefficient (r) and p values for correlations between model parameters and pattern index in adult PSS neurons.

Model variable	Correlation coefficient (r)	p value
T_{V1}	-0.4	.02
K_E	-0.57	<.001
W_I	.16	.37
T_{PSS}	.67	<.001

Table 3.3 Number of animals and neurons for all experiments.

Figure	Experiment / Analysis	Experimental group	Animals	Neurons
3.1	Simple motion tuning.	PSS. P30-32.	4	16
3.1	Simple motion tuning.	PSS. P33-34.	2	31
3.1	Simple motion tuning.	PSS. P35,	2	22
3.1	Simple motion tuning.	PSS. P37.	3	37
3.1	Simple motion tuning.	PSS. Adult (>P90).	10	68
3.2C	Pattern cells direction selectivity.	PSS. P45-497.	9	15
3.2D,E	Classic 135dOri plaid pattern tuning.	PSS. P37-41.	7	14
3.2D,E	Classic 135dOri plaid pattern tuning.	PSS. Adult (>P90).	6	33
3.3, 3.5 & 3.7	Multiple dOri plaids.	PSS. P37-41.	30	168
3.3, 3.5 & 3.7	Multiple dOri plaids.	PSS. P42-43.	5	35
3.3, 3.5 & 3.7	Multiple dOri plaids.	PSS. P44-47.	68	66
3.3, 3.5 & 3.7	Multiple dOri plaids.	PSS. Adult (>P90).	7	33
3.6	Multiple dOri plaids.	PSS. V4.	4	37
3.6	Multiple dOri plaids.	PSS. ≥V5.	20	114
3.6	Multiple dOri plaids.	PSS. P37.	6	40
3.6	Multiple dOri plaids.	PSS. P40-41.	8	41
3.6	Multiple dOri plaids.	PSS. P38-40, V4.	2	13
3.6	Multiple dOri plaids.	PSS. P38-40, ≥V5.	18	103
3.8 & 3.9	Multiple dOri plaids.	V1. P37-41.	16	98
3.8 & 3.9	Multiple dOri plaids.	V1. P44-48.	16	122

3.8 & 3.9	Multiple dOri plaids	V1. Adult (>P90).	6	34
3.10	Multiple dOri plaids	V1. P44-48. Muscimol.	5	36
3.10	Multiple dOri plaids	V1. P44-48. ACSF.	3	38
Not shown	Contrast response function	V1. P45-100.	7	57

3.11 - Discussion.

By combining neuronal recordings in V1 and PSS across development with inactivation experiments and a computational model, we investigated how the multi-stage processing of the ferret motion pathway emerges. Here, we discuss proposed mechanisms for these developmental processes and their significance for the development of the multi-stage processing achieved by cortical pathways.

3.11.1 - Direction selectivity develops simultaneously in V1 and PSS.

Our data indicate that direction selectivity matures in PSS during the first week after eye opening, a similar temporal window as that observed for development of V1 direction selectivity (Clemens et al., 2012; Li et al., 2006). Similar results were reported for the emergence of direction selectivity in the cat visual system: in the cat, direction selectivity has been found to develop in higher-order motion area PMLS at the same time, if not before, as in V1 (Price et al., 1988). This is notable in particular because higher-order motion areas (PSS, MT and PMLS) are more direction-selective than V1 (Blakemore and Zumbroich, 1987; Dubner and Zeki, 1971; Philipp et al., 2006). Possible mechanisms behind this enhanced direction selectivity include threshold non-linearities and functionally biased input from V1 to motion areas, which has been shown in both PSS (Jarosiewicz et al., 2012) and MT (Movshon and Newsome, 1996). Our findings suggest that these mechanisms develop simultaneously, if not before, the emergence of direction selectivity in V1. In addition, the simultaneous emergence of direction selectivity in PSS and V1 opens the interesting possibility that, in addition to feed-forward input from V1 shaping the development of PSS, feedback input from PSS influences functional

development of V1. It has been shown that experience with moving stimuli can induce the early emergence of direction selectivity in V1 (Li et al., 2008). According to our findings, a similar protocol should induce direction selectivity in PSS as well. If these areas indeed need to interact bi-directionally for direction-selective signals to emerge, inactivation of either area should prevent the development of direction selectivity in the other area.

3.11.2 - Pattern responses remain immature in PSS after development of direction selectivity.

If the mechanisms required for computing pattern tuning developed in PSS before or at the same time as those required for direction selectivity, pattern responses would emerge simultaneously with direction selectivity. Contrary to this hypothesis, PSS pattern responses remained largely undeveloped after the maturation of direction selectivity (P37-41). This undeveloped state of plaid responses was confirmed using both classic and a more exhaustive 'streaming' stimulus paradigm. Therefore, the decreased proportion of pattern cells at P37-41 is not a consequence of a lack of responsiveness to a particular kind of plaid stimulus or the chosen presentation mode. In addition, our findings are consistent with previous studies in primates, which show that direction selectivity emerges during the first weeks after birth at least in V1 (Chino et al., 1997; Hatta et al., 1998). At the same age, pattern cells are absent in MT. They reach half of their mature proportion after about three months (Kiorpes and Movshon, 2014).

It could be hypothesized that before the emergence of pattern cells, PSS neurons integrate over V1 direction signals in an unorganized fashion, resulting in plaid responses that do not faithfully represent any motion signal. Yet, a relatively strong representation of

component motion is seen in PSS at P37-41, refuting this hypothesis. This finding suggests that PSS goes through a developmental stage at P37-41 that is characterized by the computation of local, component direction-selective signals similar to those computed in V1. The emergence of pattern responses then occurs during a subsequent stage of PSS development.

3.11.3 - Pattern tuning develops in PSS during the second week of visual experience in two distinct phases.

Pattern tuning, measured by the percentage of pattern cells and the pattern index distribution, developed during the second week of visual experience, reaching maturity at P44-48. We propose that the development of pattern cells occurs in two distinct phases. In the first phase, between P37-41 and P42-43, component responses are suppressed by increasing tuned inhibition in PSS. This is supported by a degradation of the PSS component responses between P37-41 and P42-43. In addition, our modeling efforts indicate that an increase in tuned inhibitory mechanisms in PSS is required to explain changes in plaid responses over development.

In the second phase, between P42-43 and adulthood, pattern responses become stronger. This is supported by two developmental changes observed in our data. First, pattern correlation values increased between P42-43 and P44-48. Second, the plaid responses of pattern cells increased relative to those for gratings between P42-43 and adulthood. The increase in relative plaid responses was mirrored by an increase in the correlation between pattern index and plaid response per cell in the adult. Stronger responses to pattern motion

than to simple motion in PSS could enhance the relative weight of pattern motion signals in the ferret motion pathway.

We propose that the increase in relative pattern responses in PSS is driven by a matching increase in the relative response to plaids versus gratings in V1. This change in V1 responses was predicted by the model, and was indeed observed in measured V1 data between P42-43 and P44-48. In addition to this change, plaid responses in V1 were shifted to be less component-like and more pattern-like during this period, which may also contribute to the stronger pattern responses in PSS.

In the adult, one of the model mechanisms that is most predictive of PSS pattern index is the range of motion directions that the PSS neuron integrates (see Chapter 2). This was also the case when applying a similar model to MT data (Rust et al., 2006). Interestingly, minimal changes in this mechanism were observed when fitting PSS responses across development. While it may seem unexpected, this result is consistent with our finding that PSS orientation tuning is similar before the emergence of pattern responses (P37-41) and in adults. If the range of motion directions that PSS neurons integrate changed radically across development, the orientation tuning of these neurons would be expected to change accordingly. Note that, even given a large change in integration, the direction selectivity index of PSS neurons would not be expected to decrease. This index compares the responses to the preferred and opposite motion directions which are not integrated to compute pattern responses.

It is important to consider that there are other mechanisms than the ones investigated here that could play a role in the emergence of pattern responses. In particular, we did not

investigate end-stopping in V1, which may play an important role in motion processing (see Chapter 1). In contrast to other V1 neurons, end-stopped V1 cells provide information about the motion of local cues or 'terminators' that is more closely related to the global motion of an object or pattern (Pack and Born, 2001; Pack et al., 2003; Shimojo et al., 1989; Tsui et al., 2010; Zarei Eskikand et al., 2016). Models other than the one discussed here have used this strategy to explain pattern responses in MT (Beck and Neumann, 2011; Zarei Eskikand et al., 2016). In addition, it appears that V1 neurons that project to PSS have stronger end-stopping than neurons that project elsewhere (Jarosiewicz et al., 2012), consistent with a role of end-stopped responses in the computation of pattern tuning in adult PSS. It is feasible that this mechanism could also play a role in the development of pattern responses. Experiments aimed at analyzing the functional development of the V1 input to PSS will be required to further test this hypothesis.

Overall, the developmental timelines of direction selectivity and pattern responses across V1 and PSS do not support the hypothesis that visual areas develop sequentially according to their hierarchy (Bourne and Rosa, 2006; Condé et al., 1996). A sequential development would suggest that response properties in lower-order visual areas mature first, followed by the emergence of simple and complex tuning in higher-order areas without further changes in lower-order structures. Instead, our data indicate that PSS develops direction selectivity during the first week of visual experience, the same time window for V1 direction selectivity development (Li et al., 2006). Moreover, changes in both V1 and PSS responses were observed during the emergence of pattern tuning, suggesting that both areas contribute to the development of this complex response property.

3.11.4 - Changes in V1 responses at P44-48 revert in the adult.

Surprisingly, both the increase in relative plaid responses and the increase in pattern-like responses in V1 between P37-41 and P44-48 were reversed in adult ferrets. They therefore represent a temporary developmental stage of V1 responses. In the mature visual system, V1 projects to many higher-order areas that are dedicated to the processing of different aspects of visual stimuli (Nassi and Callaway, 2009). The temporary nature of the changes in V1 might be important in this regard, as it would return V1 to a state in which information is represented (at least on average) in as unbiased a way as possible. In this case, the function of the temporary changes in V1 responses at P44-48 may be to assist in the emergence of complex responses in PSS, followed by a later recovery of a more 'neutral' V1 stimulus representation.

This finding raises an interesting question. How does PSS retain strong pattern responses as relative plaid responses decrease in V1 between P44-48 and adulthood? In fact, our data indicate that relative plaid responses increase in PSS during this period. These contradictory developmental changes in V1 and PSS are reflected by a discrepancy between measured and predicted relative plaid responses in adult V1 neurons. Given that the model fit adult PSS data with similar correlation values as for young kits, this result does not reflect a failure to explain PSS responses, but a failure to predict a developmental change in V1 given the opposite changes in PSS. A potential mechanism that could explain the high relative plaid responses in PSS in adult ferrets is a functionally biased input from V1 to PSS provided by V1 neurons with stronger plaid responses than the population average. Another possible alternative would be a late development of non-linear

mechanisms in PSS, such as synaptic facilitation. This mechanism could increase the response to plaid stimuli, which results from integrating two signals representing the two component motions of the plaid, relative to that of simple stimuli that do not require integration. Finally, input provided by other visual structures, such as thalamic nuclei or other visual areas, could support the stronger plaid responses observed in PSS. In the primate, MT has been shown to receive two inputs from thalamic regions that bypass V1. The first comes from superior colliculus through pulvinar (Berman and Wurtz, 2010; Felleman and Van Essen, 1991). The second goes directly from koniocellular neurons in LGN to MT (Sincich et al., 2004). Similar direct thalamic inputs have been shown in cat PMLS (Cleland et al., 1976; Hughes, 1980). Whether PSS receives direct thalamic input has not yet been investigated.

3.11.5 - A possible role for the bi-directional interaction between PSS and V1 in the emergence of pattern tuning.

Above, we discussed the potential role of a temporary increase in V1 relative plaid responses at P44-48 in the development of pattern responses in PSS. Suppressing PSS neuronal activity with muscimol at P44-48 decreased V1 relative plaid responses to values similar to those before the emergence of pattern responses (P37-41). PSS inactivation also reversed changes in V1 pattern index that occurred between P37-41 and P44-48. We therefore hypothesize that the temporary state of V1 responses at P44-48, which may assist the emergence of pattern responses in PSS, depends on, and may even be induced by, PSS feedback. The emergence of pattern responses at P44-48 could thus be, at least in part, the result of changes in the bi-directional interaction between PSS and V1. If our hypothesis is

correct, a lasting disruption of PSS feedback to V1 between P44 and P48 would affect V1 relative plaid responses and, in turn, prevent the development of pattern responses in PSS. While technically challenging, this prediction could be tested by optogenetic inactivation of PSS axons in V1 in animals age P44-48.

3.12 - Methods.

3.12.1 - Animal preparation and surgery.

All procedures adhered to the guidelines of the National Institute of Health and were approved by the Animal Care and Use Committee at Johns Hopkins University. Experiments were performed in both male and female sable ferrets (*Mustela putoris furo*) aged 30 - 652 days. Experiments were conducted in anesthetized ferrets, using the same procedures as described in Chapter 2. Briefly, animals were anesthetized during the experiments using isoflurane (during surgery: 1.5 – 3%, during recording: 0.5 – 2%), and paralyzed using pancuronium bromide (0.15 mg/kg/hr). A number of vital parameters (heart rate, SpO2, EKG, EtCO2 and the EEG) were monitored to ensure adequate anesthetic depth during the experiments. Neosynephrine and atropine were applied to the eyes to retract the nictitating membrane and dilate the pupil, and animals were fitted with contact lenses. Before recordings, craniotomies were made above either V1 or the posterior bank of the suprasylvian sulcus to reach PSS. We targeted central visual field regions in V1, and central and more peripheral visual field regions in PSS.

3.12.2 - Electrophysiology.

Neural signals were recorded using either custom-made tetrodes (12 μm nichrome wire, gold-plated to reach final impedances of 150-500 kΩ), or 64-channel silicon microprobes (Masmanides lab, UCLA; gold-plated to final impedances of 150-300 kΩ). Signals were amplified and recorded using a CerePlex Direct amplifier (Blackrock Microsystems) or a RHD2000 amplifier (intan Technologies). Raw data was acquired at either 30 or 20 kHz and filtered between 250 Hz and 5 kHz. Spike detection threshold was set manually for

each recording based on noise levels. Single unit isolation was performed off-line using MATLAB (MathWorks) custom-made software. Isolation was based on multiple waveform characteristics (e.g., spike amplitude peak, area under the waveform, repolarization phase slope) recorded on the four tetrode channels or on neighboring channels of the silicon probe. Quality of isolation was confirmed by inter-spike interval (ISI) analysis. Units that displayed ISIs below 1.2 ms were not included in further analyses.

3.12.3 - Muscimol injections.

PSS was inactivated at P44-48 by injecting muscimol (2.5mg/ml in ACSF) in multiple sites spanning the posterior bank of the suprasylvian sulcus. For control experiments, ACSF without muscimol was injected instead. To aid the visualization of injection location and spread, .05% fast green was added to both the muscimol and control solution. To inject the solution, we used glass pipettes pulled using a micropipette puller apparatus (Shutter instrument, model P-1000) and 5µl calibrated glass capillary tubes (VWR international). Infusion was performed at a rate of .1-.5µl/min. For each animal, injections were performed at 4 different locations along the posterior bank of the suprasylvian sulcus. At each location, .2-.4 µl of either muscimol or ACSF solution were infused at 4 depths spaced 200-300µm apart. In total, 4-5µl of either muscimol of ACSF solution were injected per animal. Recordings were made in V1 1-5 h after injection. For muscimol experiments, lack of PSS responsiveness was confirmed by extracellular recordings either during or right after the last V1 recording.

3.12.4 - Visual stimuli and experiment design.

Visual stimuli were generated using the Psychophysics Toolbox extensions for MATLAB (Brainard, 1997; Pelli, 1997) and displayed on a 24-inch LCD monitor with refresh rate of 120 Hz, placed 25 - 35 cm in front of the ferret. For a subset of experiments, a 43-inch LCD monitor with a refresh rate of 60 Hz was used instead. Monitors were gamma corrected using a SpectraScan 655 (PhotoResearch).

Measurements of direction selectivity: Experiments consisted of 5 repetitions of each stimulus condition (including a blank condition), presented in a pseudo-random sequence. Measurements of direction selectivity at and before P37 used square-wave gratings. In adults, either square-wave or sine-wave gratings were used. Grating spatial frequency was set to maximize responses in the recording location (range .05 - .1 cycles/deg), as was temporal frequency (range 2 - 6 Hz). Gratings were shown at 100% contrast and moved in 12 or 16 different directions. Stimuli were presented interspersed with presentation of a gray screen of equal mean luminance. Stimuli were presented for 1 s with inter stimulus intervals of 2 – 10 s, and had a size of 65 x 50 deg.

Measurements of contrast sensitivity curves: These experiments were performed to determine the correct values for the computational model (see below). Again, 5 repetitions of each stimulus condition were presented. Sine-wave gratings were shown at 5, 10, 15, 30, 50, 70 and 100% contrast and moved in 4 different directions. All other stimulus settings were identical to those described for the direction selectivity experiments.

Classic stimulus presentation using gratings and plaids: For plaid experiments, sine-wave gratings were shown at 50% contrast. Plaids were generated by superimposing two 50%

contrast sine-wave gratings of optimal spatial and temporal frequency at an intersection angle of 135 deg. Both gratings and plaids could move in 16 different directions. 5 repetitions of each stimulus condition were shown, similar to the other experiments. Stimulus sizes were optimized for each neuron. For most experiments, stimuli were shown in a circular aperture with radius 8 – 30 deg, but in a few adult plaid experiments, we used rectangular stimuli of 65 x 50 deg instead. Otherwise stimulus parameters were set as described above.

Streaming stimulus presentation: Each trial consisted of a 60 s long sequence of short stimulus presentations (3 - 4 stimuli/s). Each sequence was preceded and followed by a 2-4 s long presentation of a gray screen of equal luminance. Stimulus sequence was determined randomly by picking from all stimulus conditions with replacement. The following stimulus conditions were used: blank (uniform gray screen), 100% contrast sine-wave gratings moving in 16 directions, and plaids with 7 different component intersection angles (dOri; 22.5, 45, 67.4, 90, 112.5, 135 and 157.5 deg) moving in 16 directions. In a subset of experiments, we also included 50% contrast gratings moving in 16 directions. Spatial frequency (.05 - .15 cycles/deg), temporal frequency (3 – 6 Hz) and stimulus size (circular aperture of radius 10 – 35 deg) were optimized at each recording location. For each stimulus, the initial phase of each grating was chosen randomly from 4 possible values (0, 90, 180 and 270 deg). 30 or 45 trials were run for each experiment, which ensured that each stimulus was presented at least 10 times.

3.12.5 - Data analysis and inclusion criteria.

Classic stimulus presentations: For experiments using the classic stimulus presentation mode (Figures 3.1, 3.2 and contrast experiments), neuronal responses were calculated as the firing rate during stimulus presentation minus the firing rate during the last second of the pre-stimulus period. All neurons were then screened for general stimulus responsiveness. For direction selectivity measurements (Figure 3.1), we performed this test by using a one-way ANOVA to compare responses across all stimulus conditions (including the blank). Only cells that passed $p < .01$ for the ANOVA were included in further analyses. For contrast experiments, this test was conducted only for grating stimuli with 100% contrast. When both gratings and plaids were shown (Figure 3.2), a responsiveness test for each of the two stimuli classes was performed by using a one-way ANOVA to compare responses across all motion directions plus the blank condition. Cells that passed this test with $p < .05$ for both gratings and plaids were included in further analyses. In addition, neurons with a maximum mean response lower than 2 Hz for either grating or plaids were excluded. For all remaining neurons, tuning properties were then calculated from mean responses across stimulus repetitions.

Streaming stimulus presentation: Stimulus-evoked responses collected using the streaming stimulus paradigm were extracted after computing an optimal latency for every neuron, as described in Chapter 2. Cells were then screened for responsiveness using two criteria: For one, cells had to pass an ANOVA across all plaids with dOri = 90 deg and the blank with $p < .01$, using the optimal delay to compute responses. For the other, the responses to the

best grating had to be larger than 2 Hz and responses to the best plaid with dOri = 90 deg had to be larger than 1.5 Hz.

Analysis of direction and orientation selectivity: Direction selectivity was quantified using a direction index comparing responses between preferred and null directions, which was computed as

$$DSI = 1 - \frac{R(N)}{R(P)}$$

where R(P) is the response to the preferred direction, and R(N) is the response to the null direction. To quantify orientation tuning, we computed each neuron's circular variance (Batschelet, 1981; Mazurek et al., 2014; Ringach et al., 2002) as

$$CV = 1 - \frac{\sum_n \left(R(\theta_n) e^{2i\theta_n}\right)}{\sum_n R(\theta_n)}$$

where θ is the stimulus direction in circular space (0 to 360 deg).

We also computed an orientation selectivity index, which was used for cell selection in the plaid analysis (see below). This index was computed as

$$OSI = 1 - \frac{R(T)}{R(P)}$$

where R(P) is the response to the preferred direction, and R(T) is the mean response to the two gratings with an orientation orthogonal to the preferred.

Analysis of V1 contrast response functions: For each neuron, responses to 100% contrast gratings were first used to determine the preferred direction as the one that elicited the largest mean response. Responses to all contrasts were then calculated for this direction. Responses across contrast values were fit using a hyperbolic function of the form

$$R = \frac{c^N}{c^N + C_{50}^N}$$

where c represents the contrast value and R the neuron's response. C_{50} and N were variables fit to best explain responses for each neuron. This kind of function has been widely used to model contrast-response functions (Albrecht and Hamilton, 1982; Alitto and Usrey, 2004; Koch et al., 2016; Rathbun et al., 2016).

Analysis of plaid responses: When analyzing the development of PSS pattern responses, only neurons that were direction-selective (DSI > .7) were included, as pattern cells in this area are exclusively direction-selective (see Figure 3.2C). In addition, we limited the analysis of plaid responses for both V1 and PSS to neurons that were orientation selective (OSI > .7). This was to avoid including un-tuned neurons for which component and pattern predictions cannot reasonably be computed.

Classic stimulus presentations: We used standard methods to compute partial correlations between the measured plaids responses and pattern and component response predictions (Movshon et al., 1985). Partial correlations were then Z-transformed to stabilize the variance and allow comparisons across conditions. The Z-transform was computed as (Smith et al., 2005):

$$Z = \sqrt{N-3}\frac{1}{2}\ln\left(\frac{1+r}{1-r}\right)$$

where r is the partial correlation (either pattern or component), and N refers to the number of points in the correlation (here, 16). Cells were classified as pattern cells if they met $Z_P - Z_c > 1.28$ for $Z_C \geq 0$, and $Z_P > 1.28$ otherwise. Component cells had to meet the opposite criterion. We also computed a pattern index as Z_P-Z_C. As in the cell classification, any negative values (Z_P or Z_C) were set to 0 when computing the index.

Streaming stimulus presentation: Each neuron's pattern and component predictions were computed for the larger stimulus set in the following way: For the pattern prediction, we computed a direction tuning curve by averaging responses across all plaids with a shared pattern direction, as well as the gratings moving in the same direction. We also computed a dOri tuning curve, which was estimated by averaging across all stimuli with the same dOri. The complete pattern prediction was then computed as the product of the direction and dOri tuning curves. For the component prediction, we first estimated a direction tuning curve as a function of component direction by averaging across all plaid stimuli with a shared component direction (i.e. each plaid contributed twice), as well as the gratings moving in the same direction. This tuning curve was then transformed into a function of plaid direction by summing two copies of the component direction curve at each dOri, shifted relative to each other according to the dOri value. The resulting direction tuning curve was multiplied with the dOri tuning curve (identical to the one used for the pattern prediction) to generate a complete component prediction. We then computed partial correlations of each neuron's actual responses with the two predictions, and converted these values to Z-scores as before (with N set to 112 to account for the 7 dOri values and 16 directions involved in the computation).

3.12.6 - Image-computable motion-pathway model.

The model used here was developed as an extension of the model described in Chapter 2. More precisely, the model described in Chapter 2 was modified here in the following ways:

- *Contrast response function in the thalamic layer:* Two different versions of this stage were implemented. In the first version, C_{50} and N were set to constant values (.23 and 3.1, respectively). These values were chosen from amongst those sampled in the second model version were C_{50} and N are variable. In particular, values were chosen to best approximate the median C_{50} and N values measured for V1 neurons in animals older than 43 days (median C_{50}: .32; median N: 3.3). In the second version, T_{V1} remained constant (Figure 3.S1). In this model implementation, C_{50} and N remained free parameters as in the original model.
- *V1 non-linearity:* One modification of the model was the inclusion of a non-linearity in V1, which was applied to the output of each V1 direction channel. We implemented this nonlinearity as a half-wave rectification by setting all responses below a threshold T_{V1} to 0. In one model version, T_{V1} was a free parameter; in the other, it was set to a constant value of .125 (expressed as proportion of maximum response). This value was chosen from amongst those sampled in the version with variable T_{V1}. In particular, this value was chosen to prevent the variable C_{50} from taking extreme values when explaining PSS responses at any developmental stage.

In summary, the model had the following free parameters in the two implementations: In the fixed CRF implementation, free parameters were T_{V1}, K_E, K_I, I and T_{PSS} (referred to as

T in Chapter 2). In the fixed V1 threshold implementation, free parameters were C_{50}, N, K_E, K_I, I and T_{PSS}.

Model fitting: The stimulus set used for probing model responses was constructed as described previously, and replicated the entire set of conditions used in the streaming stimulus experiments (see Chapter 2). One million instances of the model were computed in both model implementations. Variables k_E, k_I, I and T_{PSS} could take 10 possible values in both implementations. For the constant T_{V1} implementation, C_{50} and N could also take 10 possible values. For the constant CRF implementation, the variable T_{V1} could take 100 possible values to keep the total number of possible relative plaid responses in V1 constant across model implementations. For each direction-selective PSS cell (DSI > .7), we then picked the model instance with the lowest mean square error.

3.13 - Supplementary figures.

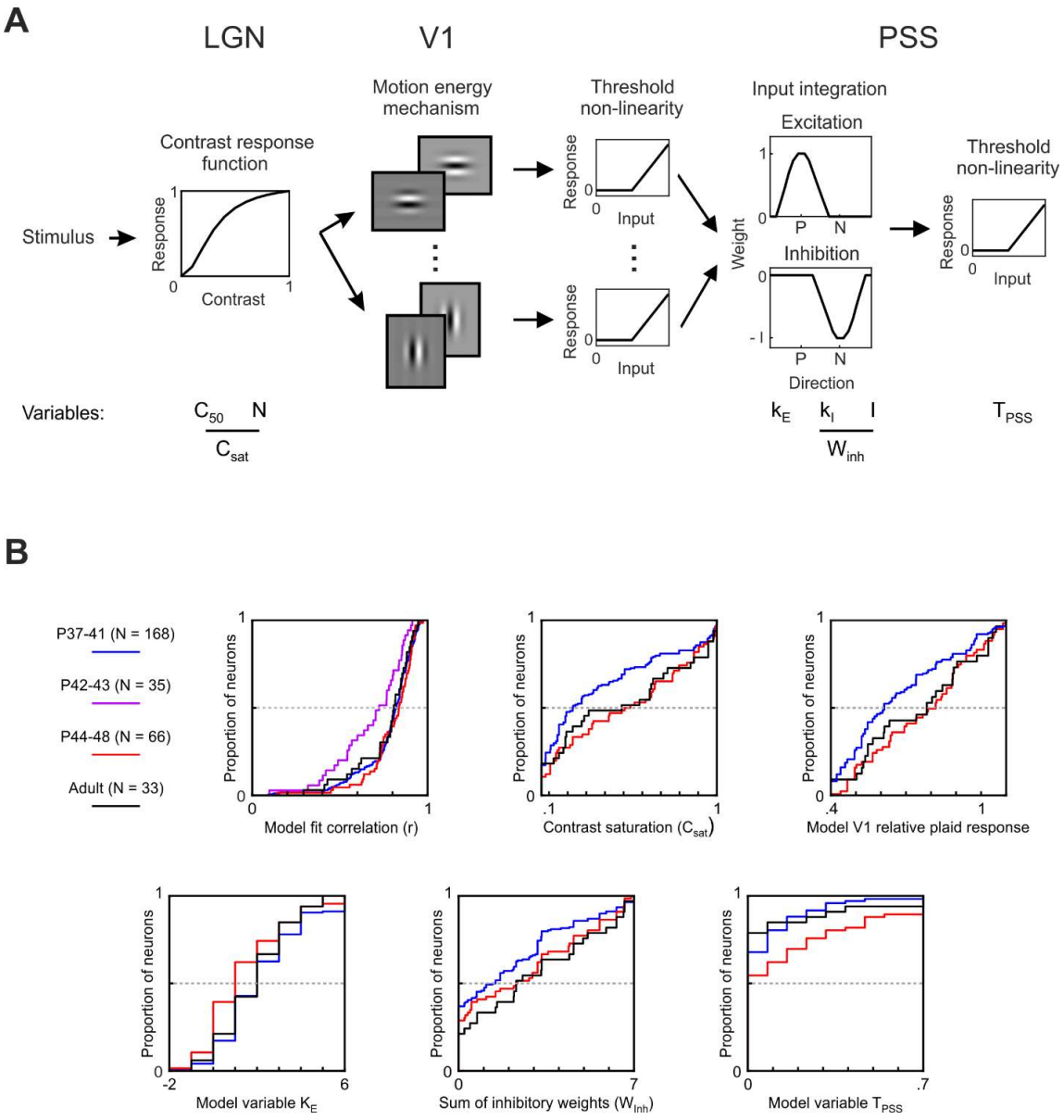

Figure 3.S1: Alternative model implementation with fixed T_{V1} and variable C_{50} and N.
(A) Diagram of the computational model as shown in Figure 3.7A, indicating the model variables for the implementation with fixed T_{V1} and variable C_{50} and N. C_{sat} represents the area under the curve of the contrast response function (CRF). This metric was computed to simplify further analysis. In this implementation, the variable T_{V1} was fixed to a value of .125 (expressed as proportion of maximum response, see Methods).
(B) Cumulative distributions of the model fit correlation and different model parameters at different ages. As was the case for the model implementation in Figure 3.7, model fit correlation values were lower for data at P42-43, and these data were excluded from further analyses.

Chapter 4: General discussion

My work presented in this thesis was done with the goal of establishing the ferret as a model for visual system development beyond V1. To this end, I performed extracellular single unit recordings in anesthetized ferrets to investigate complex motion processing in higher-order visual area PSS in adult animals. In addition, I analyzed the development of different tuning properties in this area. In Chapter 2, I show that pattern motion tuning, a key aspect of higher-order motion processing, is computed in PSS. This suggests an analogous relationship between information processing in ferret PSS and primate MT. This hypothesis is further supported by the finding that a feed-forward model similar to that used to explain complex motion responses in MT (Rust et al., 2006) can explain responses in PSS.

In Chapter 3, I describe the developmental timeline of direction selectivity and pattern responses in PSS. My data indicate that direction selectivity develops in PSS during the first week after eye opening, a similar temporal window as that reported for the emergence of direction selectivity in V1 (Clemens et al., 2012; Li et al., 2006). By the time direction selectivity matures in PSS (P37), pattern responses are still immature. Pattern cells emerge during the second week after eye opening and reach maturity at P44-48. Based on the results of applying a feed-forward model to plaid responses in PSS across development, I propose two possible mechanisms behind the emergence of pattern tuning. The first is a maturation of tuned inhibition in PSS. The second mechanism is an increase in V1 responses to plaids relative to gratings. Measured responses in V1 confirmed that relative

plaid responses indeed increase as pattern cells emerge in PSS. In addition to this change, I also observed that plaid responses in V1 were shifted to be less component-like and more pattern-like during this period. Both of these changes were temporary, as they were reversed in the adult. Importantly, inactivation of PSS at P44-48 reversed both temporary changes in V1 responses, i.e. relative plaid responses were reduced and became more component-like. This result suggests that a bi-directional interaction between V1 and PSS, executed by the feed-forward and feed-back connections between them, may play a role in the emergence of pattern responses in the ferret motion pathway.

In conclusion, my work presented in this thesis solidly stablishes ferrets as an animal model for studying development of higher-order cortex. In addition, it provides evidence that areas across the motion pathway do not develop sequentially, but instead interact and change simultaneously to support the emergence of complex stimulus representations. In the following paragraphs I discuss the impact of these findings on the fields of visual motion processing and development.

4.1 - PSS is a higher-order motion area in the ferret.

Preceding this thesis, a higher-order brain area that implements the computation of global pattern motion responses had not been described outside the primate. In mice, V1 plaid responses already show signs of motion integration, and do not represent the component directions as strongly as in primates and carnivores (Juavinett and Callaway, 2015; Muir et al., 2015; Palagina et al., 2017). In the cat, strong component responses were found in V1 (Movshon et al., 1985). Yet, no pattern cells were found in cat motion area PMLS (Movshon et al., 1985). Instead, pattern responses have been found in cat frontal cortex and pulvinar (Merabet et al., 1998; Scannell et al., 1995). Based on our findings in the ferret, however, it is likely that they can be found in other, as yet unstudied, higher-order motion areas.

The computation of pattern responses is believed to be a fundamental aspect of motion processing. It consequently has been the focus of many previous studies in primates (Jazayeri et al., 2012; Majaj et al., 2007; Pack and Born, 2010, 2001; Rodman and Albright, 1989; Rust et al., 2006; Smith et al., 2005; Wang and Movshon, 2016). The finding that this transformation occurs in PSS, a motion area in a non-primate mammal, supports this idea. In addition, the ability of similar feed-forward models to explain pattern tuning in both PSS and MT suggests that the neuronal mechanisms behind this computation are shared across species. These findings extend the similarities found between lower-order visual areas of primate and ferrets to higher-order motion processing. It also opens the door for further parallels between these species downstream of PSS.

The discovery of pattern responses in PSS puts the ferret in a unique position to serve as an animal model for studying multi-stage motion processing. Transgenic ferrets were recently established (Johnson et al., 2018; Sun et al., 2014) and may become more available in the near future. In addition, as will be discussed next, ferrets offer a unique opportunity to study the development of visual processing.

4.2 - Development of multi-stage motion processing in the ferret motion pathway.

The ferret offers a unique advantage for studying visual development due to its immature state at birth. Making use of this advantage, previous studies have focused on the development of visual processing in lower-order structures (Chapman and Stryker, 1993; Chapman et al., 1996; Sharma and Sur, 2014; White and Fitzpatrick, 2007). In this thesis, I extended this approach to study the development of higher-order motion processing in PSS. In particular, in a subset of PSS neurons the integration over local direction-selective signals present in V1 results in the computation of pattern motion. To understand how these multi-stage processes emerge in cortical pathways, we must investigate the development of multiple areas together within the same experimental model. By studying the emergence of pattern responses in PSS in concert with developmental changes in V1, I investigated potential mechanisms behind the emergence of multi-stage motion processing. Preceding this thesis, very few studies have investigated functional development across different areas. Similarly, little is currently known about the development of higher-order motion functions in general. Therefore, the mechanisms discussed here represent the first detailed working hypotheses for how multi-stage processes in the motion pathway develop.

Analyzing the development of direction selectivity in PSS revealed that these signals emerge simultaneously in PSS and V1 shortly after eye opening. Similar results have been observed in cat PMLS and V1 (Price et al., 1988). These results indicate that these higher-order motion areas interact with V1 as direction-selective signals emerge across the motion pathway. Therefore, the maturation of direction-selective signals cannot be studied

exclusively from the perspective of neuronal mechanisms in V1. Instead, to fully understand the development of motion processing, even for these simple signals, we must consider multiple areas and investigate how their interaction impacts the developmental processes that result in the computation of these responses.

The developmental timeline of pattern responses in PSS indicates that this more complex tuning property develops after the maturation of direction selectivity. This is consistent with findings for MT (Kiorpes and Movshon, 2014), where pattern cells emerge progressively for many months. These results might reflect a more general principle for the development of information processing stages in the motion pathway, in which basic motion signals, such as direction selectivity, mature before more complex tuning, like pattern responses. Interestingly, this developmental timeline reflects the order in which these signals are found across the motion pathway hierarchy. Direction selectivity is first observed in V1 while pattern tuning is only found in higher-order motion areas.

The feed-forward model used in Chapter 2 for explaining adult PSS responses was able to fit data across development with high correlation values. Yet, the variables controlling the contrast response function took extreme values when fitting data before the emergence of pattern cells (P37-41). One small modification to the model, which consisted of the addition of a threshold non-linearity in V1, was required to fix this issue. The ability of this modified model to fit plaid responses both in adult PSS and across development supports the validity and generality of the implemented mechanisms in this modified model. The modeling results suggest that changes in motion responses in V1, in addition to changes in neuronal mechanisms within PSS, could be responsible for the emergence of pattern

tuning. In PSS, the model suggests an increase in tuned inhibition centered on the null direction. This could be implemented at the neuronal level as an increased excitability of tuned inhibitory neurons or an increased strength of the synaptic connections of these neurons. In V1, the model predicts an increase in the responses to plaids relative to that of gratings. Multiple neuronal mechanisms could explain this change. In particular, changes in excitability, through changes in spiking threshold, are used in our model to explain changes in relative plaid responses. Alternatively, an increase in contrast saturation in V1 or earlier visual structures could explain this change (as tested in a different implementation of our model). Additionally, changes in divisive normalization mechanisms could explain these changes, and have been used in a similar model for MT (Rust et al., 2006).

The changes in V1 plaid responses predicted by the model were confirmed experimentally during the time window in which pattern cells emerge in PSS. In contrast to model predictions, this increase was temporary and receded in the adult. Along with their increase relative to gratings responses, plaid response also became more pattern-like as pattern responses emerged in PSS, and then recovered strong component tuning in the adult. Both of these temporary changes in V1 plaid responses were reversed by the inactivation of PSS. Together, these results suggest a possible mechanism by which the bi-directional interaction between PSS and V1 assists in the emergence of pattern cells. During the second week after eye opening (P37-44), V1 responses go through changes that make V1 input to PSS optimal for computing pattern responses. At least some of these changes may be induced by PSS feedback, indicating that PSS circuit maturation can regulate the timing of the changes in V1. Later, changes in V1 responses reverse to increase both the relative strength of basic motion responses and component tuning. This later change may be crucial

for the role of V1 in the mature visual system, as it feeds information to multiple visual processing pathways (Nassi and Callaway, 2009). Higher-order areas that process visual information not related to motion may require V1 input with strong component tuning that emphasizes fundamental signals that have not been contaminated in any way.

In the adult, PSS pattern responses must become independent of the temporary V1 responses that initially assisted their emergence. This could be achieved through the development of a functionally biased V1 input that sends optimal inputs for PSS to compute pattern tuning, while other local circuits in V1 change to better serve other visual pathways. Alternatively, the emergence of non-linear input integration mechanisms in PSS or changes in input to PSS from other visual structures could sustain strong pattern responses in adult animals. Indeed, multiple pathways connecting retina and MT bypassing V1 are known in the primate (Berman and Wurtz, 2010; Felleman and Van Essen, 1991; Sincich et al., 2004), but have yet to be investigated in the ferret.

In this thesis I focused on the development of a higher-order motion area to investigate how multi-stage information processing develops in the visual system. Yet, it has been suggested that motion areas, such as PSS, PMLS and MT, may develop considerably earlier than other higher-order areas (Bourne and Rosa, 2006; Condé et al., 1996). This raises the question whether the mechanisms described here for the development of motion processing also apply to other pathways. Ultimately, resolving this question requires extending developmental studies to other higher-order visual areas, such as those dedicated to representing stimulus shape.

4.3 - Future directions.

The body of work presented in this thesis establishes the ferret as a model for studying how a multi-stage cortical motion pathway performs complex motion processing. It also establishes developmental timelines and suggests potential mechanisms for the development of both basic and complex motion processing in this pathway. My work provides the necessary foundations for an extensive list of scientific investigations regarding the mechanisms behind multi-stage information processing and its development. What follows is a limited list of some future directions that could directly follow rom my research:

1- *Expanding our knowledge of motion processing in the ferret beyond PSS:*

The motion pathway has been studied in most detail in primates. This vast bibliography indicates that motion processing is implemented by a series of areas known as the 'dorsal pathway' (Freud et al., 2016). MT is the first of the higher-order areas in this pathway, and is followed by a number of other areas. From MT, complex motion signals are sent to areas such as MST, which analyzes more global motion stimuli such as optic flow patterns (Duffy, 1998; Ilg, 2008). Processed motion information is ultimately sent to frontal areas like the frontal eye fields (FEF) to control behaviors such as smooth pursuit eye movements (Vernet et al., 2014). In this thesis, I establish ferret PSS as an area highly similar to MT. Additional experiments are required to characterize further stages in the ferret motion pathway and investigate whether parallels with the primate extend to areas downstream of PSS. These include studies on the anatomical connectivity of PSS

to identify downstream areas and subsequent neuronal recordings to characterize their responses.

2- *Investigate the development of PSS connectivity with other visual areas:*

The work presented in this thesis focused on the development of PSS exclusively from the perspective of neuronal responses. Equally relevant to understanding how higher-order areas mature is to understand how their connectivity to both upstream and downstream areas develops. To resolve this question, anatomical studies involving the use of both retrograde and anterograde tracers need to be conducted in PSS across development. Additionally, the functional nature of these connections can also be investigated. In a previous study Jarosiewicz et al. combined retrograde tracing techniques with two-photon imaging to show that V1 neurons projecting to PSS might be functionally distinct from those projecting to other higher-order areas (Jarosiewicz et al., 2012). This can also be achieved by combining single cell recordings with opto-tagging. By extending these studies across development, we can study how the signals that PSS receives from other areas may contribute to the maturation of PSS responses. For example, the developmental timeline of the functionally biased input from V1 to PSS and its role in pattern cells emergence could be investigated.

3- *Study the mechanisms behind the simultaneous development of direction selectivity in V1 and PSS:*

Data presented in this thesis suggest that direction selectivity develops in PSS during the same temporal period as in V1. The simultaneous emergence of this property across V1 and PSS is notable considering that direction selectivity is

significantly stronger in PSS. Evidence in both PSS and primate MT suggests that this increased direction selectivity might be a result, at least in part, of a functionally-biased input from V1 (Jarosiewicz et al., 2012; Movshon and Newsome, 1996). Therefore, our result suggests that this functionally-biased input develops simultaneously, if not before, direction selectivity in V1. The developmental timeline of this biased input can be studied as described in item 2. In addition, the simultaneous emergence of direction selectivity in V1 and PSS suggests that the interaction between these areas may play a role in the development of this property. It has been shown that experience with moving stimuli can induce the emergence of direction selectivity in V1 within 4-8 hours (Li et al., 2008). If this property emerges simultaneously in V1 and PSS, this protocol should also induce the emergence of direction selectivity in PSS. Moreover, if the interaction between these areas is required for development, experience with moving stimuli should not induce the emergence of direction selectivity in V1 under inactivation of PSS.

4- *Further assess the role of visual experience in the development of pattern motion responses in PSS:*

In this thesis, I have shown that pattern responses are less developed in animals with 4 days of visual experience than animals of similar age but longer exposure to vision. This result suggests an important role of visual experience in the development of pattern cells. It has been shown that visual experience is required for the emergence of direction selectivity in V1 in both cats (Mower et al., 1981) and ferrets (Li et al., 2008). Does the development of pattern responses, which

occurs later than that of direction selectivity, require additional visual experience? To test this hypothesis, ferrets could be raised in the dark starting after the development of direction selectivity, but before the emergence of pattern cells (P37). If the emergence of pattern cells requires further visual experience, it is expected that the strong component responses seen at P37-41 will remain predominant at P44-48 under these rearing conditions. An additional approach to investigate the role of visual experience is to test the effects of prolonged, controlled visual stimulation in the emergence of pattern responses. This strategy was used by Li et al. to investigate what aspects of visual experience are required for the emergence of direction selectivity in V1 (Li et al., 2008). They concluded that experience with moving stimuli induces the emergence of direction selectivity, while static stimuli have no comparable effect. Does the emergence of pattern cells in PSS require experience with complex moving stimuli? Can visual experience induce the early emergence of these properties or do they require additional mechanisms independent of stimulation? By combining controlled visual stimulation with neuronal recordings in PSS we can address these issues.

5- *Investigate the role of the bi-directional interaction between V1 and PSS in the emergence of pattern responses:*

Research presented here indicates that one of the mechanisms that could contribute to the emergence of pattern cells in PSS is a temporary increase in the relative V1 response to plaids over gratings around P44-48. In addition, I have shown that this increase in plaid responses is reversed by inactivation of PSS at P44-48. Together, these results suggest that feedback from PSS to V1 may play an important role in

the development of PSS pattern responses. Testing this hypothesis would require a selective disruption of the feedback only while keeping each area intact. While technically challenging, this could be achieved by optogenetic inactivation of PSS axons in V1. This would disrupt PSS feedback to V1 without inactivation of PSS responses. If PSS feedback is essential for the emergence of pattern tuning, pattern responses should be suppressed in PSS at P44-48 as a consequence of this disruption.

Bibliography

Ackman, J.B., and Crair, M.C. (2014). Role of emergent neural activity in visual map development. Curr. Opin. Neurobiol. *24*, 166–175.

Adelson, E.H., and Bergen, J.R. (1985). Spatiotemporal energy models for the perception of motion. J. Opt. Soc. Am. A *2*, 284–299.

Adelson, E.H., and Movshon, J.A. (1982). Phenomenal coherence of moving visual patterns. Nature *300*, 523–525.

Albrecht, D.G., and Hamilton, D.B. (1982). Striate cortex of monkey and cat: contrast response function. J. Neurophysiol. *48*, 217–237.

Albright, T.D. (1984). Direction and orientation selectivity of neurons in visual area MT of the macaque. J. Neurophysiol. *52*, 1106–1130.

Albright, T.D., Desimone, R., and Gross, C.G. (1984). Columnar organization of directionally selective cells in visual area MT of the macaque. J. Neurophysiol. *51*, 16–31.

Alitto, H.J., and Usrey, W.M. (2004). Influence of contrast on orientation and temporal frequency tuning in ferret primary visual cortex. J. Neurophysiol. *91*, 2797–808.

Alonso, J.-M., Usrey, W.M., and Reid, R.C. (2001). Rules of Connectivity between Geniculate Cells and Simple Cells in Cat Primary Visual Cortex. J. Neurosci. *21*, 4002–4015.

Andersen, R.A. (1997). Neural mechanisms of visual motion perception in primates. Neuron *18*, 865–872.

Atkinson, J. (2017). The Davida Teller Award Lecture, 2016. J. Vis. *17*.

Baker, P.M., and Bair, W. (2016). A Model of Binocular Motion Integration in MT Neurons. J. Neurosci. *36*, 6563–6582.

Baker, G., Thompson, I., Krug, K., Smyth, D., and Tolhurst, D. (1998). Spatial-frequency tuning and geniculocortical projections in the visual cortex (areas 17 and 18) of the pigmented ferret. Eur. J. Neurosci. *10*, 2657–68.

Baker, J.F., Petersen, S.E., Newsome, W.T., and Allman, J.M. (1981). Visual response properties of neurons in four extrastriate visual areas of the owl monkey (Aotus trivirgatus): a quantitative comparison of medial, dorsomedial, dorsolateral, and middle temporal areas. J. Neurophysiol. *45*, 397–416.

Banton, T., Dobkins, K., and Bertenthal, B.I. (2001). Infant direction discrimination thresholds. Vision Res. *41*, 1049–1056.

Batschelet, E. (1981). Circular statistics in biology (London : Academic).

Beck, C., and Neumann, H. (2011). Combining Feature Selection and Integration—A Neural Model for MT Motion Selectivity. PLOS ONE *6*, e21254.

Berman, R.A., and Wurtz, R.H. (2010). Functional Identification of a Pulvinar Path from Superior Colliculus to Cortical Area MT. J. Neurosci. *30*, 6342–6354.

Blakemore, C., and Zumbroich, T.J. (1987). Stimulus selectivity and functional organization in the lateral suprasylvian visual cortex of the cat. J. Physiol. *389*, 569–603.

Blasdel, G.G., and Salama, G. (1986). Voltage-sensitive dyes reveal a modular organization in monkey striate cortex. Nature *321*, 579.

Bonhoeffer, T., and Grinvald, A. (1991). Iso-orientation domains in cat visual cortex are arranged in pinwheel-like patterns. Nature *353*, 429.

Bonin, V., Histed, M.H., Yurgenson, S., and Reid, R.C. (2011). Local Diversity and Fine-Scale Organization of Receptive Fields in Mouse Visual Cortex. J. Neurosci. *31*, 18506–18521.

Boothe, R.G., Kiorpes, L., Williams, R.A., and Teller, D.Y. (1988). Operant measurements of contrast sensitivity in infant macaque monkeys during normal development. Vision Res. *28*, 387–96.

Born, R.T., and Bradley, D.C. (2005). Structure and function of visual area MT. Annu. Rev. Neurosci. *28*, 157–189.

Borst, A., and Euler, T. (2011). Seeing things in motion: models, circuits, and mechanisms. Neuron *71*, 974–994.

Borst, A., Haag, J., and Reiff, D.F. (2010). Fly Motion Vision. Annu. Rev. Neurosci. *33*, 49–70.

Bourne, J.A., and Rosa, M.G.P. (2006). Hierarchical development of the primate visual cortex, as revealed by neurofilament immunoreactivity: early maturation of the middle temporal area (MT). Cereb. Cortex N. Y. N 1991 *16*, 405–414.

Braddick, O. (1993). Orientation- and motion-selective mechanisms in infants (Oxford University Press).

Braddick, O., and Atkinson, J. (2007). Development of brain mechanisms for visual global processing and object segmentation. Prog. Brain Res. *164*, 151–168.

Braddick, O., and Atkinson, J. (2011). Development of human visual function. Vision Res. *51*, 1588–1609.

Braddick, O., Atkinson, J., and Wattam-Bell, J. (2003). Normal and anomalous development of visual motion processing: motion coherence and "dorsal-stream vulnerability." Neuropsychologia *41*, 1769–1784.

Braddick, O., Birtles, D., Wattam-Bell, J., and Atkinson, J. (2005). Motion- and orientation-specific cortical responses in infancy. Vision Res. *45*, 3169–3179.

Brainard, D.H. (1997). The Psychophysics Toolbox. Spat. Vis. *10*, 433–436.

Burbridge, T.J., Xu, H.-P., Ackman, J.B., Ge, X., Zhang, Y., Ye, M.-J., Zhou, Z.J., Xu, J., Contractor, A., and Crair, M.C. (2014). Visual circuit development requires patterned activity mediated by retinal acetylcholine receptors. Neuron *84*, 1049–1064.

Cai, D., Deangelis, G.C., and Freeman, R.D. (1997). Spatiotemporal Receptive Field Organization in the Lateral Geniculate Nucleus of Cats and Kittens. J. Neurophysiol. *78*, 1045–1061.

Cantone, G., Xiao, J., and Levitt, J.B. (2006). Retinotopic organization of ferret suprasylvian cortex. Vis. Neurosci. *23*, 61–77.

Chaplin, T.A., Allitt, B.J., Hagan, M.A., Price, N.S.C., Rajan, R., Rosa, M.G.P., and Lui, L.L. (2017). Sensitivity of neurons in the middle temporal area of marmoset monkeys to random dot motion. J. Neurophysiol. *118*, 1567–1580.

Chapman, B., and Gödecke, I. (2000). Cortical cell orientation selectivity fails to develop in the absence of ON-center retinal ganglion cell activity. J. Neurosci. *20*, 1922–1930.

Chapman, B., and Stryker, M.P. (1993). Development of orientation selectivity in ferret visual cortex and effects of deprivation. J. Neurosci. *13*, 5251–5262.

Chapman, B., Stryker, M.P., and Bonhoeffer, T. (1996). Development of Orientation Preference Maps in Ferret Primary Visual Cortex. J. Neurosci. *16*, 6443–6453.

Chiao, C.-C., and Masland, R.H. (2002). Starburst Cells Nondirectionally Facilitate the Responses of Direction-Selective Retinal Ganglion Cells. J. Neurosci. *22*, 10509–10513.

Chino, Y.M., Smith, E.L., Hatta, S., and Cheng, H. (1997). Postnatal development of binocular disparity sensitivity in neurons of the primate visual cortex. J. Neurosci. *17*, 296–307.

Cleland, B.G., and Levick, W.R. (1974). Properties of rarely encountered types of ganglion cells in the cat's retina and on overall classification. J. Physiol. *240*, 457–492.

Cleland, B.G., Levick, W.R., Morstyn, R., and Wagner, H.G. (1976). Lateral geniculate relay of slowly conducting retinal afferents to cat visual cortex. J. Physiol. *255*, 299–320.

Clemens, J.M., Ritter, N.J., Roy, A., Miller, J.M., and Van Hooser, S.D. (2012). The laminar development of direction selectivity in ferret visual cortex. J. Neurosci. *32*, 18177–18185.

Condé, F., Lund, J.S., and Lewis, D.A. (1996). The hierarchical development of monkey visual cortical regions as revealed by the maturation of parvalbumin-immunoreactive neurons. Dev. Brain Res. *96*, 261–276.

Davis, Z.W., Chapman, B., and Cheng, H.-J. (2015). Increasing Spontaneous Retinal Activity before Eye Opening Accelerates the Development of Geniculate Receptive Fields. J. Neurosci. *35*, 14612–14623.

De Valois, R.L., Yund, E.W., and Hepler, N. (1982). The orientation and direction selectivity of cells in macaque visual cortex. Vision Res. *22*, 531–544.

De Valois, R.L., Cottaris, N.P., Mahon, L.E., Elfar, S.D., and Wilson, J.A. (2000). Spatial and temporal receptive fields of geniculate and cortical cells and directional selectivity. Vision Res. *40*, 3685–3702.

DeAngelis, G.C., Cumming, B.G., and Newsome, W.T. (1998). Cortical area MT and the perception of stereoscopic depth. Nature *394*, 677–680.

Dell, L.-A., Innocenti, G.M., Hilgetag, C.C., and Manger, P.R. Cortical and thalamic connectivity of temporal visual cortical areas 20a and 20b of the domestic ferret (Mustela putorius furo). J. Comp. Neurol. *0*.

Dobkins, K.R., Fine, I., Hsueh, A.C., and Vitten, C. (2004). Pattern motion integration in infants. J. Vis. *4*, 144–155.

Dubner, R., and Zeki, S.M. (1971). Response properties and receptive fields of cells in an anatomically defined region of the superior temporal sulcus in the monkey. Brain Res. *35*, 528–532.

Duffy, C.J. (1998). MST Neurons Respond to Optic Flow and Translational Movement. J. Neurophysiol. *80*, 1816–1827.

Felleman, D.J., and Van Essen, D.C. (1991). Distributed Hierarchical Processing in the Primate Cerebral Cortex. Cereb. Cortex *1*, 1–47.

Fennema, C.L., and Thompson, W.B. (1979). Velocity determination in scenes containing several moving objects. Comput. Graph. Image Process. *9*, 301–315.

Ferrera, V.P., and Wilson, H.R. (1991). Perceived speed of moving two-dimensional patterns. Vision Res. *31*, 877–893.

Freud, E., Plaut, D.C., and Behrmann, M. (2016). 'What' Is Happening in the Dorsal Visual Pathway. Trends Cogn. Sci. *20*, 773–784.

Gizzi, M.S., Katz, E., Schumer, R.A., and Movshon, J.A. (1990). Selectivity for orientation and direction of motion of single neurons in cat striate and extrastriate visual cortex. J. Neurophysiol. *63*, 1529–1543.

Grinvald, A., Lieke, E., Frostig, R.D., Gilbert, C.D., and Wiesel, T.N. (1986). Functional architecture of cortex revealed by optical imaging of intrinsic signals. Nature *324*, 361.

Hassenstein, B., and Reichardt, B.W. (1956). Systemtheoretische Analyse der Zeit-, Reihenfolgen- und Vorzeichenauswertung bei der Bewegungsperzeption des Rüsselkäfers Chlorophanus. Z. Für Naturforschung A.

Hatta, S., Kumagami, T., Qian, J., Thornton, M., Smith, E.L., and Chino, Y.M. (1998). Nasotemporal directional bias of V1 neurons in young infant monkeys. Invest. Ophthalmol. Vis. Sci. *39*, 2259–2267.

Homman-Ludiye, J., Manger, P.R., and Bourne, J.A. (2010). Immunohistochemical parcellation of the ferret (Mustela putorius) visual cortex reveals substantial homology with the cat (Felis catus). J. Comp. Neurol. *518*, 4439–4462.

Hubel, D.H., and Wiesel, T.N. (1962). Receptive fields, binocular interaction and functional architecture in the cat's visual cortex. J. Physiol. *160*, 106-154.2.

Hubel, D.H., and Wiesel, T.N. (1968). Receptive fields and functional architecture of monkey striate cortex. J. Physiol. *195*, 215–243.

Hubel, D.H., and Wiesel, T.N. (1969). Visual area of the lateral suprasylvian gyrus (Clare—Bishop area) of the cat. J. Physiol. *202*, 251–260.

Huberman, A.D., and Niell, C.M. (2011). What can mice tell us about how vision works? Trends Neurosci. *34*, 464–473.

Huberman, A.D., Speer, C.M., and Chapman, B. (2006). Spontaneous retinal activity mediates development of ocular dominance columns and binocular receptive fields in V1. Neuron *52*, 247–254.

Hughes, H.C. (1980). Efferent organization of the cat pulvinar complex, with a note on bilateral claustrocortical and reticulocortical connections. J. Comp. Neurol. *193*, 937–963.

Hupfeld, D., Distler, C., and Hoffmann, K.-P. (2007). Deficits of visual motion perception and optokinetic nystagmus after posterior suprasylvian lesions in the ferret (Mustela putorius furo). Exp. Brain Res. *182*, 509–23.

Ilg, U.J. (2008). The role of areas MT and MST in coding of visual motion underlying the execution of smooth pursuit. Vision Res. *48*, 2062–2069.

Jarosiewicz, B., Schummers, J., Malik, W.Q., Brown, E.N., and Sur, M. (2012). Functional Biases in Visual Cortex Neurons with Identified Projections to Higher Cortical Targets. Curr. Biol. *22*, 269–277.

Jazayeri, M., Wallisch, P., and Movshon, J.A. (2012). Dynamics of macaque MT cell responses to grating triplets. J. Neurosci. Off. J. Soc. Neurosci. *32*, 8242–8253.

Jin, J., Wang, Y., Swadlow, H.A., and Alonso, J.M. (2011). Population receptive fields of ON and OFF thalamic inputs to an orientation column in visual cortex. Nat. Neurosci. *14*, 232–238.

Johnson, M.B., Sun, X., Kodani, A., Borges-Monroy, R., Girskis, K.M., Ryu, S.C., Wang, P.P., Patel, K., Gonzalez, D.M., Woo, Y.M., et al. (2018). Aspm knockout ferret reveals an evolutionary mechanism governing cerebral cortical size. Nature *556*, 370–375.

Jones, H.E., Grieve, K.L., Wang, W., and Sillito, A.M. (2001). Surround Suppression in Primate V1. J. Neurophysiol. *86*, 2011–2028.

Juavinett, A.L., and Callaway, E.M. (2015). Pattern and Component Motion Responses in Mouse Visual Cortical Areas. Curr. Biol. CB *25*, 1759–1764.

Kiefer, W., Krüger, K., Strauß, G., and Berlucchi, G. (1989). Considerable deficits in the detection performance of the cat after lesion of the suprasylvian visual cortex. Exp. Brain Res. *75*, 208–212.

Kiorpes, L., and Movshon, J.A. (2004). Development of sensitivity to visual motion in macaque monkeys. Vis. Neurosci. *21*, 851–859.

Kiorpes, L., and Movshon, J.A. (2014). Neural limitations on visual development in primates: beyond striate cortex. In The New Visual Neurosciences, J. Werner, and J. Chalupa, eds. (Cambridge, MA: Massachusetts Institute of Technology), pp. 1423–1431.

Koch, E., Jin, J., Alonso, J.M., and Zaidi, Q. (2016). Functional implications of orientation maps in primary visual cortex. Nat. Commun. *7*, 13529.

Li, B., Li, B.W., Chen, Y., Wang, L.H., and Diao, Y.C. (2000). Response properties of PMLS and PLLS neurons to simulated optic flow patterns. Eur. J. Neurosci. *12*, 1534–44.

Li, B., Chen, Y., Li, B.W., Wang, L.H., and Diao, Y.C. (2001). Pattern and component motion selectivity in cortical area PMLS of the cat. Eur. J. Neurosci. *14*, 690–700.

Li, Y., Fitzpatrick, D., and White, L.E. (2006). The development of direction selectivity in ferret visual cortex requires early visual experience. Nat. Neurosci. *9*, 676–681.

Li, Y., Van Hooser, S.D., Mazurek, M., White, L.E., and Fitzpatrick, D. (2008). Experience with moving visual stimuli drives the early development of cortical direction selectivity. Nature *456*, 952–956.

Livingstone, M.S. (1998). Mechanisms of Direction Selectivity in Macaque V1. Neuron *20*, 509–526.

Lomber, S.G., Cornwell, P., Sun, J.S., MacNeil, M. a, and Payne, B.R. (1994). Reversible inactivation of visual processing operations in middle suprasylvian cortex of the behaving cat. Proc. Natl. Acad. Sci. U. S. A. *91*, 2999–3003.

MacNeil, M.A., Lomber, S.G., and Payne, B.R. (1996). Rewiring of transcortical projections to middle suprasylvian cortex following early removal of cat areas 17 and 18. Cereb. Cortex N. Y. N 1991 *6*, 362–376.

Majaj, N.J., Carandini, M., and Movshon, J.A. (2007). Motion Integration by Neurons in Macaque MT Is Local, Not Global. J. Neurosci. *27*, 366–370.

Manger, P., Nakamura, H., Valentiniene, S., and Innocenti, G. (2004). Visual areas in the lateral temporal cortex of the ferret (Mustela putorius). Cereb. Cortex *14*, 676–89.

Manny, R.E., and Fern, K.D. (1990). Motion coherence in infants. Vision Res. *30*, 1319–1329.

Marshel, J.H., Kaye, A.P., Nauhaus, I., and Callaway, E.M. (2012). Anterior-Posterior Direction Opponency in the Superficial Mouse Lateral Geniculate Nucleus. Neuron *76*, 713–720.

Mason, A.J.S., Braddick, O.J., and Wattam-Bell, J. (2003). Motion coherence thresholds in infants—different tasks identify at least two distinct motion systems. Vision Res. *43*, 1149–1157.

Maunsell, J.H., and Van Essen, D.C. (1983). Functional properties of neurons in middle temporal visual area of the macaque monkey. I. Selectivity for stimulus direction, speed, and orientation. J. Neurophysiol. *49*, 1127–1147.

Mazurek, M., Kager, M., and Van Hooser, S.D. (2014). Robust quantification of orientation selectivity and direction selectivity. Front. Neural Circuits *8*.

Merabet, L., Desautels, A., Minville, K., and Casanova, C. (1998). Motion integration in a thalamic visual nucleus. Nature *396*, 265–268.

Movshon, J.A., and Newsome, W.T. (1996). Visual Response Properties of Striate Cortical Neurons Projecting to Area MT in Macaque Monkeys. J. Neurosci. *16*, 7733–7741.

Movshon, J.A., Adelson, E., Gizzi, M.S., and Newsome, W.T. (1985). The analysis of moving visual patterns. In Pattern Recognition Mechanisms, C. Chagas, R. Gattass, and C. Gross, eds. pp. 117–151.

Mower, G.D., Berry, D., Burchfiel, J.L., and Duffy, F.H. (1981). Comparison of the effects of dark rearing and binocular suture on development and plasticity of cat visual cortex. Brain Res. *220*, 255–267.

Muir, D.R., Roth, M., Helmchen, F., and Kampa, B. (2015). Model-based analysis of pattern motion processing in mouse primary visual cortex. Front. Neural Circuits *9*.

Nassi, J.J., and Callaway, E.M. (2009). Parallel Processing Strategies of the Primate Visual System. Nat. Rev. Neurosci. *10*, 360–372.

Ohki, K., Chung, S., Kara, P., Hübener, M., Bonhoeffer, T., and Reid, R.C. (2006). Highly ordered arrangement of single neurons in orientation pinwheels. Nature *442*, 925–928.

Orban, G.A. (2008). Higher Order Visual Processing in Macaque Extrastriate Cortex. Physiol. Rev. *88*, 59–89.

Orban, G.A., Kennedy, H., and Bullier, J. (1986). Velocity sensitivity and direction selectivity of neurons in areas V1 and V2 of the monkey: influence of eccentricity. J. Neurophysiol. *56*, 462–480.

Pack, C.C., and Born, R. (2010). Cortical Mechanisms for the Integration of Visual Motion. Senses Compr. Ref. *2*, 189–218.

Pack, C.C., and Born, R.T. (2001). Temporal dynamics of a neural solution to the aperture problem in visual area MT of macaque brain. Nature *409*, 1040–1042.

Pack, C.C., Livingstone, M.S., Duffy, K.R., and Born, R.T. (2003). End-stopping and the aperture problem: two-dimensional motion signals in macaque V1. Neuron *39*, 671–680.

Palagina, G., Meyer, J.F., and Smirnakis, S.M. (2017). Complex Visual Motion Representation in Mouse Area V1. J. Neurosci. *37*, 164–183.

Paolini, M., and Sereno, M.I. (1998). Direction selectivity in the middle lateral and lateral (ML and L) visual areas in the California ground squirrel. Cereb. Cortex *8*, 362–371.

Pelli, D.G. (1997). The VideoToolbox software for visual psychophysics: transforming numbers into movies. Spat. Vis. *10*, 437–442.

Penn, A.A., Riquelme, P.A., Feller, M.B., and Shatz, C.J. (1998). Competition in Retinogeniculate Patterning Driven by Spontaneous Activity. Science *279*, 2108–2112.

Peterson, M.R., Li, B., and Freeman, R.D. (2004). The Derivation of Direction Selectivity in the Striate Cortex. J. Neurosci. *24*, 3583–3591.

Philipp, R., Distler, C., and Hoffmann, K.-P. (2006). A motion-sensitive area in ferret extrastriate visual cortex: an analysis in pigmented and albino animals. Cereb. Cortex *16*, 779–790.

Piscopo, D.M., El-Danaf, R.N., Huberman, A.D., and Niell, C.M. (2013). Diverse visual features encoded in mouse lateral geniculate nucleus. J. Neurosci. *33*, 4642–4656.

Popović, M., Stacy, A.K., Kang, M., Nanu, R., Oettgen, C.E., Wise, D.L., Fiser, J., and Hooser, S.D.V. (2018). Development of Cross-Orientation Suppression and Size Tuning and the Role of Experience. J. Neurosci. *38*, 2656–2670.

Price, D.J., and Morgan, J.E. (1987). Spatial properties of neurones in the lateral geniculate nucleus of the pigmented ferret. Exp. Brain Res. *68*, 28–36.

Price, D.J., Zumbroich, T.J., and Blakemore, C. (1988). Development of Stimulus Selectivity and Functional Organization in the Suprasylvian Visual Cortex of the Cat. Proc. R. Soc. Lond. B Biol. Sci. *233*, 123–163.

Priebe, N.J., Cassanello, C.R., and Lisberger, S.G. (2003). The neural representation of speed in macaque area MT/V5. J. Neurosci. *23*, 5650–5661.

Priebe, N.J., Lampl, I., and Ferster, D. (2010). Mechanisms of direction selectivity in cat primary visual cortex as revealed by visual adaptation. J. Neurophysiol. *104*, 2615–2623.

Qian, N., and Andersen, R.A. (1994). Transparent motion perception as detection of unbalanced motion signals. II. Physiology. J. Neurosci. *14*, 7367–7380.

Qian, N., Andersen, R.A., and Adelson, E.H. (1994). Transparent motion perception as detection of unbalanced motion signals. I. Psychophysics. J. Neurosci. *14*, 7357–7366.

Rathbun, D.L., Alitto, H.J., Warland, D.K., and Usrey, W.M. (2016). Stimulus Contrast and Retinogeniculate Signal Processing. Front. Neural Circuits *10*.

Rauschecker, J.P., Grunau, M. von, and Poulin, C. (1987). Centrifugal organization of direction preferences in the cat's lateral suprasylvian visual cortex and its relation to flow field processing. J. Neurosci. *7*, 943–958.

Ringach, D.L., Shapley, R.M., and Hawken, M.J. (2002). Orientation selectivity in macaque V1: diversity and laminar dependence. J. Neurosci. *22*, 5639–5651.

Ringach, D.L., Mineault, P.J., Tring, E., Olivas, N.D., Garcia-Junco-Clemente, P., and Trachtenberg, J.T. (2016). Spatial clustering of tuning in mouse primary visual cortex. Nat. Commun. *7*, 12270.

Ritter, N.J., Anderson, N.M., and Van Hooser, S.D. (2017). Visual stimulus speed does not influence the rapid emergence of direction selectivity in ferret visual cortex. J. Neurosci. 3365–16.

Rodman, H.R., and Albright, T.D. (1989). Single-unit analysis of pattern-motion selective properties in the middle temporal visual area (MT). Exp. Brain Res. *75*, 53–64.

Roy, A., Osik, J.J., Ritter, N.J., Wang, S., Shaw, J.T., Fiser, J., and Van Hooser, S.D. (2016). Optogenetic spatial and temporal control of cortical circuits on a columnar scale. J. Neurophysiol. *115*, 1043–1062.

Roy, A., Christie, I.K., Escobar, G.M., Osik, J.J., Popović, M., Ritter, N.J., Stacy, A.K., Wang, S., Fiser, J., Miller, P., et al. (2018). Does experience provide a permissive or instructive influence on the development of direction selectivity in visual cortex? Neural Develop. *13*, 16.

Rust, N.C., Mante, V., Simoncelli, E.P., and Movshon, J.A. (2006). How MT cells analyze the motion of visual patterns. Nat. Neurosci. *9*, 1421–1431.

van Santen, J.P., and Sperling, G. (1985). Elaborated Reichardt detectors. J. Opt. Soc. Am. A *2*, 300–321.

Saul, A.B., Carras, P.L., and Humphrey, A.L. (2005). Temporal Properties of Inputs to Direction-Selective Neurons in Monkey V1. J. Neurophysiol. *94*, 282–294.

Scannell, J.W., Blakemore, C., and Young, M.P. (1995). Analysis of connectivity in the cat cerebral cortex. J. Neurosci. *15*, 1463–1483.

Sceniak, M.P., Hawken, M.J., and Shapley, R. (2001). Visual spatial characterization of macaque V1 neurons. J. Neurophysiol. *85*, 1873–1887.

Sclar, G., and Freeman, R.D. (1982). Orientation selectivity in the cat's striate cortex is invariant with stimulus contrast. Exp. Brain Res. *46*, 457–461.

Sharma, J., and Sur, M. (2014). The Ferret as a Model for Visual System Development and Plasticity. In Biology and Diseases of the Ferret, (Editors JG Fox and RP Marini, John Wiley and Sons), pp. 711–734.

Sherk, H. (1986). Location and connections of visual cortical areas in the cat's suprasylvian sulcus. J. Comp. Neurol. *247*, 1–31.

Shimojo, S., Silverman, G.H., and Nakayama, K. (1989). Occlusion and the solution to the aperture problem for motion. Vision Res. *29*, 619–626.

Silies, M., Gohl, D.M., and Clandinin, T.R. (2014). Motion-detecting circuits in flies: coming into view. Annu. Rev. Neurosci. *37*, 307–327.

Simoncelli, E.P., and Heeger, D.J. (1998). A model of neuronal responses in visual area MT. Vision Res. *38*, 743–761.

Sincich, L.C., Park, K.F., Wohlgemuth, M.J., and Horton, J.C. (2004). Bypassing V1: a direct geniculate input to area MT. Nat. Neurosci. *7*, 1123–1128.

Smith, M.A., Majaj, N.J., and Movshon, J.A. (2005). Dynamics of motion signaling by neurons in macaque area MT. Nat. Neurosci. *8*, 220–228.

Snowden, R.J., Treue, S., Erickson, R.G., and Andersen, R.A. (1991). The response of area MT and V1 neurons to transparent motion. J. Neurosci. *11*, 2768–2785.

Solomon, S.S., Tailby, C., Gharaei, S., Camp, A.J., Bourne, J.A., and Solomon, S.G. (2011). Visual motion integration by neurons in the middle temporal area of a New World monkey, the marmoset. J. Physiol. *589*, 5741–5758.

Spear, P.D. (1991). Function of extrastriate visual cortex in non-primate species. Neural Basis Vis. Funct. *4*, 339–370.

Spear, P.D., and Baumann, T.P. (1975). Receptive-field characteristics of single neurons in lateral suprasylvian visual area of the cat. J. Neurophysiol. *38*, 1403–1420.

Spear, P.D., and Tong, L. (1980). Effects of monocular deprivation on neurons in cat's lateral suprasylvian visual area. I. Comparison of binocular and monocular segments. J. Neurophysiol. *44*, 568–584.

Spear, P.D., Tong, L., McCall, M.A., and Pasternak, T. (1985). Developmentally induced loss of direction-selective neurons in the cat's lateral suprasylvian visual cortex. Brain Res. *352*, 281–285.

Stellwagen, D., and Shatz, C.J. (2002). An Instructive Role for Retinal Waves in the Development of Retinogeniculate Connectivity. Neuron *33*, 357–367.

Stoner, G.R., Albright, T.D., and Ramachandran, V.S. (1990). Transparency and coherence in human motion perception. Nature *344*, 153–155.

Sun, W., Deng, Q., Levick, W.R., and He, S. (2006). ON direction-selective ganglion cells in the mouse retina. J. Physiol. *576*, 197–202.

Sun, X., Yan, Z., Liu, X., Olivier, A.K., and Engelhardt, J.F. (2014). Genetic Engineering in the Ferret. In Biology and Diseases of the Ferret, (John Wiley & Sons, Ltd), pp. 665–683.

Tavazoie, S.F., and Reid, R.C. (2000). Diverse receptive fields in the lateral geniculate nucleus during thalamocortical development. Nat. Neurosci. *3*, 608–616.

Thompson, K.G., Zhou, Y., and Leventhal, A.G. (1994a). Direction-sensitive X and Y cells within the A laminae of the cat's LGNd. Vis. Neurosci. *11*, 927–938.

Thompson, K.G., Leventhal, A.G., Zhou, Y., and Liu, D. (1994b). Stimulus dependence of orientation and direction sensitivity of cat LGNd relay cells without cortical inputs: a comparison with area 17 cells. Vis. Neurosci. *11*, 939–951.

Ts'o, D.Y., Frostig, R.D., Lieke, E.E., and Grinvald, A. (1990). Functional organization of primate visual cortex revealed by high resolution optical imaging. Science *249*, 417–420.

Tsui, J.M.G., Hunter, J.N., Born, R.T., and Pack, C.C. (2010). The Role of V1 Surround Suppression in MT Motion Integration. J. Neurophysiol. *103*, 3123–3138.

Van Essen, D.C., Maunsell, J., and Bixby, J. (1981). The Middle Temporal Visual Area in the Macaque: Myeloarchitecture, Connections, Functional Properties and Topographic Organization. J. Comp. Neurol. *199*, 293– 326.

Van Hooser, S.D., Li, Y., Christensson, M., Smith, G.B., White, L.E., and Fitzpatrick, D. (2012). Initial Neighborhood Biases and the Quality of Motion Stimulation Jointly Influence the Rapid Emergence of Direction Preference in Visual Cortex. J. Neurosci. *32*, 7258–7266.

Vaney, D.I., Sivyer, B., and Taylor, W.R. (2012). Direction selectivity in the retina: symmetry and asymmetry in structure and function. Nat. Rev. Neurosci. *13*, 194–208.

Vernet, M., Quentin, R., Chanes, L., Mitsumasu, A., and Valero-Cabré, A. (2014). Frontal eye field, where art thou? Anatomy, function, and non-invasive manipulation of frontal regions involved in eye movements and associated cognitive operations. Front. Integr. Neurosci. *8*.

Wang, H.X., and Movshon, J.A. (2016). Properties of pattern and component direction-selective cells in area MT of the macaque. J. Neurophysiol. *115*, 2705–2720.

Wattam-Bell, J. (1992). The development of maximum displacement limits for discrimination of motion direction in infancy. Vision Res. *32*, 621–630.

Wattam-Bell, J. (1996). Visual motion processing in one-month-old infants: preferential looking experiments. Vision Res. *36*, 1671–1677.

Wattam-Bell, J., Birtles, D., Nyström, P., von Hofsten, C., Rosander, K., Anker, S., Atkinson, J., and Braddick, O.J. (2010). Reorganization of global form and motion processing during human visual development. Curr. Biol. *20*, 411–5.

Weliky, M., Bosking, W.H., and Fitzpatrick, D. (1996). A systematic map of direction preference in primary visual cortex. Nature *379*, 725–728.

White, L.E., and Fitzpatrick, D. (2007). Vision and cortical map development. Neuron *56*, 327–338.

Wiesel, T.N., and Hubel, D.H. (1974). Ordered arrangement of orientation columns in monkeys lacking visual experience. J. Comp. Neurol. *158*, 307–318.

Wilson, D.E., Scholl, B., and Fitzpatrick, D. (2018). Differential tuning of excitation and inhibition shapes direction selectivity in ferret visual cortex. Nature *560*, 97.

Wright, M.J. (1969). Visual Receptive Fields of Cells in a Cortical Area remote from the Striate Cortex in the Cat. Nature *223*, 973–975.

Xu, H., Furman, M., Mineur, Y.S., Chen, H., King, S.L., Zenisek, D., Zhou, Z.J., Butts, D.A., Tian, N., Picciotto, M.R., et al. (2011). An instructive role for patterned spontaneous retinal activity in mouse visual map development. Neuron *70*, 1115–1127.

Xu, X., Ichida, J., Shostak, Y., Bonds, A.B., and Casagrande, V.A. (2002). Are primate lateral geniculate nucleus (LGN) cells really sensitive to orientation or direction? Vis. Neurosci. *19*, 97–108.

Zahs, K.R., and Stryker, M.P. (1985). The projection of the visual field onto the lateral geniculate nucleus of the ferret. J. Comp. Neurol. *241*, 210–24.

Zarei Eskikand, P., Kameneva, T., Ibbotson, M.R., Burkitt, A.N., and Grayden, D.B. (2016). A Possible Role for End-Stopped V1 Neurons in the Perception of Motion: A Computational Model. PLoS ONE *11*.

Zhao, X., Chen, H., Liu, X., and Cang, J. (2013). Orientation-selective responses in the mouse lateral geniculate nucleus. J. Neurosci. *33*, 12751–12763.

Zheng, J., Zhang, B., Bi, H., Maruko, I., Watanabe, I., Nakatsuka, C., Smith, E.L., and Chino, Y.M. (2007). Development of temporal response properties and contrast sensitivity of V1 and V2 neurons in macaque monkeys. J. Neurophysiol. *97*, 3905–16.

Curriculum Vitae

Name: Augusto Abel Lempel

Position: Graduate Student

Advisor: Dr. Kristina Nielsen

Affiliation: The Zanvyl Krieger Mind/Brain Institute. The Johns Hopkins University. Maryland, US.

Contact information:
Cell phone (preferred): 443-529-5965
Work phone: 410-516-5827
E-Mail: aguslempel@gmail.com

Education:

Institution	Degree	Completion Date	Field of study
Universidad de Buenos Aires. Buenos Aires, Argentina.	Licenciatura	08/2012	Biology
Johns Hopkins University School of Medicine, Maryland, US.	Ph.D.	05/2019	Neuroscience

Short summary:

I grew up in Buenos Aires, Argentina. For my undergraduate studies, I attended the Biology program at "Universidad de Buenos Aires" and specialized in animal physiology. During this time, I performed research in the lab of Dr. Osvaldo Uchitel. My research focused on studying the effects of the anti-epileptic drug Pregabalin on the development of newborn neurons in the adult hippocampus of mice. My work resulted in a published undergraduate thesis work and a first author publication in J. Neurochem. (Lempel et al., 2016).
In August 2012, I joined the Neuroscience PhD program at the Johns Hopkins University School of Medicine. In contrast to the molecular and cellular background that I received during my undergraduate education, I focused on acquiring skills in systems neuroscience and programing. For my graduate thesis work, I joined the lab of Dr. Kristina Nielsen to work on characterizing the physiology and development of higher order motion processing in the ferret visual system. My research has yielded relevant insights on the representation of complex motion stimuli in a higher order visual area (PSS) in adult ferrets (Lempel and Nielsen, 2019). In addition, I have made several advances in studying the functional

development of complex motion representation in ferret visual cortex, as well as the role of visual experience in this process (Manuscript in preparation). Finally, I have been serving as a mentor for undergraduate students at the Johns Hopkins School of Arts and Science to study the anatomical development of inhibitory neurons in different visual areas in the ferret following eye opening and effects of visual experience.
My main scientific interest is to understand how dynamic cortical circuits develop to implement the information processing mechanisms required for perception.

Research experience:

2009-2012: Universidad de Buenos Aires, Undergraduate Thesis. Advisors: Dr. Joaquin Piriz and Dr. Osvaldo Uchitel.
2012-2019: Johns Hopkins University School of Medicine, Doctoral Thesis. Advisor: Dr. Kristina Nielsen.

Meetings and Presentations:

2016: *Ferret visual area PSS: A model for studying functional development of higher order motion processing*. Poster presentation at the annual meeting of the Society for Neuroscience, San Diego, CA

2017: *Development of simple and complex motion processing in ferret higher order visual area PSS.* Poster presentation at the annual meeting of the Society for Neuroscience, Washington, DC

2017: *Development of motion processing in ferret area PSS*. Research talk at the 3rd Ferret Brain Meeting, Johns Hopkins University, Baltimore, MD

2018: *Development of motion integration in ferret visual area PSS: Effects of visual stimulation.* Poster presentation at the annual meeting of the Society for Neuroscience, San Diego, CA

Publications:

Lempel, A. A., Coll, L., Schinder, A. F., Uchitel, O. D. and Piriz, J. (2017), *Chronic pregabalin treatment decreases excitability of dentate gyrus and accelerates maturation of adult-born granule cells*. J. Neurochem., 140: 257–267.

Lempel, A.A., Nielsen, K.J. (2019), *Ferrets as a Model for Higher-Level Visual Motion Processing*. Curr. Biol. 29, 179-191.

Skills:

- Multi-channel extracellular electrophysiology in anesthetized animals.
- Two-photon imaging in anesthetized large animals (ferrets and macaque monkeys).
- Whole cell patch clamp in brain slices (current and voltage clamp configurations).
- Survival surgical procedures for stereotaxic virus injection in mice and ferrets.
- Perfusion for tissue fixation in mice and ferrets.
- Immunohistochemistry and other histochemical techniques frequently used in brain tissue.
- Microscopy: Confocal, wide-field fluorescence, bright field.
- MATLAB programing including custom-made analysis of multi-channel electrophysiology data.
- Development and implementation of descriptive mathematical models of neural data.
- Experience mentoring undergraduate and high school students.

Professional references:

Dr. Kristina Nielsen

Affiliation: The Zanvyl Krieger Mind/Brain Institute. The Johns Hopkins University. Maryland, US.

Contact information:

Phone number: 410-516-5833

E-Mail: knielse4@jhu.edu

Dr. James Knierim

Affiliation: The Zanvyl Krieger Mind/Brain Institute. The Johns Hopkins University. Maryland, US.

Contact information:

Phone number: 410-516-5170

E-Mail: jknierim@jhu.edu

Dr. Charles E. Connor

Affiliation: The Zanvyl Krieger Mind/Brain Institute. The Johns Hopkins University. Maryland, US.

Contact information:

Phone number: 410-516-7342

E-Mail: connor@jhu.edu